SISSA
Scuola
Internazionale
Superiore di
Studi Avanzati

Physics Area – PhD course in

Theory and Numerical Simulation of Condensed Matter

Dissipation effects in driven quantum many-body systems

Candidate:
Luca Arceci

Advisor:
Prof. Giuseppe E. Santoro

Academic Year 2018-2019

Publications

The present thesis is based on the following manuscripts, published or under review in international peer-reviewed journals:

- L. Arceci, S. Barbarino, R. Fazio and G. E. Santoro, "Dissipative Landau-Zener problem and thermally assisted quantum annealing", Phys. Rev. B **96** (5), 054301 (2017)

- L. Arceci, S. Barbarino, D. Rossini and G. E. Santoro, "Optimal working point in dissipative quantum annealing", Phys. Rev. B **98** (6), 064307 (2018)

- L. Arceci, A. Russomanno, G. E. Santoro, "Thermally assisted Thouless pumping in the Rice-Mele model", arXiv:1905.08808 (2019)

During my PhD, I have also contributed to the following papers, not discussed in this thesis:

- G. B. Mbeng, L. Privitera, L. Arceci, G. E. Santoro, "Dynamics of simulated quantum annealing in random Ising chains", Phys. Rev. B **99** (6), 064201 (2019)

- G. B. Mbeng, L. Arceci, G. E. Santoro, "Optimal working point in digitized quantum annealing", arXiv:1909.00817 (2019)

Contents

Chapter 1

Introduction

The rapid advances in the experimental control of quantum systems over the last decades paved the way to what has been called the *second quantum revolution* [1], that is the possibility to engineer exotic quantum states in the laboratory with unprecedented precision. This promises to generate new technologies based on purely quantum phenomena, as can be seen for example from the quantum technologies roadmap [2] sponsored by the European Quantum Flagship [3].

Remarkable new directions of research were opened by the so-called *quantum simulators* [4], that is the realization of Feynman's pioneering idea of quantum devices that could simulate other quantum systems [5]. Several experimental platforms can already serve for this purpose, such as ultracold atoms in optical lattices [6], trapped ions [7] and arrays of cavities [8]. These technologies allow for the investigation of new phenomena that are not found in Nature spontaneously, as physicists can now engineer theoretical models in the laboratory with a high degree of control. Because of this, there is now great interest in the behaviour of quantum systems which are *driven out of equilibrium*, usually as a consequence of quenches, ramps or periodic drivings [9], since they can show the emergence of physics that has never been observed before. Equilibrium can be lost also through interaction with an external reservoir, and the emerging physics is intriguing even for a static two-level system [10].

The interplay between driving and dissipation can lead to even more interesting and surprising phenomena, such as dissipative phase transitions [11, 12, 13]. Furthermore, one can also assume a different perspective and think of *engineering dissipation* cleverly, so to exploit it as a resource [14, 15, 16]. It is indeed possible to prepare interesting quantum states as steady states of a dissipative time-evolution [17, 18, 19, 20]: in some cases, it might be easier to reach the steady-state of an open system rather than preparing the ground state of a closed one [21].

From the *quantum computation* side, despite the ambitious long-term goal of a universal quantum computer is still very far, there are already prototypes that are being tested and used. They are still at an early stage so that the quality of the qubits

is not good enough for ensuring the unitary dynamics one would need. According to John Preskill's definition [22], we currently are in the *Noisy Intermediate-Scale Quantum* (NISQ) technology era: we already have — or are going to have within five or ten years — devices whose behaviour is not fully quantum coherent, but can nevertheless lead to deep insights into complex physical problems. Since dissipation effects enter crucially in the performance of these devices, understanding the behaviour of driven open quantum systems has become of primary importance for their development.

All these reasons motivate the research activity on driven-dissipative quantum systems described in this thesis, which can be divided into two main branches: the first is related to dissipation in Quantum Annealing (QA) — *alias* Adiabatic Quantum Computation (AQC) —, while the second regards dissipation effects in topological pumping. Both topics will be introduced in the following sections. After that, an overview of the theoretical methods to compute the dissipative dynamics is provided.

1.1 Dissipation in Quantum Annealing

At the intersection between quantum simulators and quantum computers lies a very interesting class of devices called *quantum annealers* [23, 24, 25, 26, 27]. They aim to solve optimization problems by applying a strategy named Quantum Annealing (QA), often also called Adiabatic Quantum Computation (AQC). The protocol works as follows. Assume to encode the solution of a given problem in the ground state of a suitable Hamiltonian. The goal is to find such a state by performing an adiabatic connection with another Hamiltonian, typically describing a much simpler physical system. To be more concrete, suppose that the optimization problem is encoded in the following (classical) *target* spin Hamiltonian:

$$\widehat{H}_T = \sum_p \sum_{i_1, i_2 \dots i_p} J_{i_1, i_2 \dots i_p} \hat{\sigma}^z_{i_1} \hat{\sigma}^z_{i_2} \dots \hat{\sigma}^z_{i_p} \,, \tag{1.1}$$

where, for each site, we used the Pauli matrices, $\hat{\boldsymbol{\sigma}} = (\hat{\sigma}^x, \hat{\sigma}^y, \hat{\sigma}^z)$. There are in general p-body interactions, but all the operators commute, so we can regard $\widehat{H}_T$ as describing a classical system. We now introduce another much simpler Hamiltonian that *does not commute* with the target one, for example

$$\widehat{H}_D = -\sum_i \hat{\sigma}^x_i \,, \tag{1.2}$$

which we call *driving* Hamiltonian. We interpolate between target and driving Hamiltonian through a controllable time-dependent parameter $s(t) \in [0, 1]$, with

$t \in [0, \tau]$, τ being the total evolution time (or annealing time), so that

$$\widehat{H}(t) = (1 - s(t))\, \widehat{H}_D + s(t)\widehat{H}_T \ , \tag{1.3}$$

where we impose $s(0) = 0$ and $s(\tau) = 1$. Therefore, at the beginning the ground state of $\widehat{H}(0)$ is very easy to prepare — simply all the spins are aligned along the $\hat{\sigma}^x$ direction:

$$|\Psi_{\rm gs}(0)\rangle = \bigotimes_i |\uparrow\rangle_{i,x} \ , \tag{1.4}$$

with $|\uparrow\rangle_{i,x}$ being the eigenstate of $\hat{\sigma}_i^x$ with positive eigenvalue. Then, one changes $s(t)$ adiabatically to remain close to the instantaneous ground state of $\widehat{H}(t)$, exploiting the adiabatic theorem [28, 27]. If adiabaticity holds throughout the whole dynamics, one eventually reaches the desired ground state of $\widehat{H}_T$ and therefore can read the solution of the optimization problem. The success of this procedure can be estimated through the overlap between the final time-evolved state $|\psi(\tau)\rangle$ and the true final ground state $|\Psi_{\rm gs}(\tau)\rangle$:

$$P_{\rm gs} = |\langle\psi(\tau)|\Psi_{\rm gs}(\tau)\rangle|^2 \ . \tag{1.5}$$

Big companies have invested much in building the prototypes of quantum annealers. The most popular one belongs to D-Wave®, which claims to currently have 2000 superconducting flux qubits available in their D-Wave 2000Q machine. However, earlier versions of this machine had qubits exhibiting a strongly incoherent dynamics. Indeed, Ref.s [29, 30] study the behaviour of a single D-Wave® qubit that undergoes a Landau-Zener transition, demonstrating that the experimental data match well with the theoretical predictions found by assuming incoherent dynamics. Therefore, it is clear that superconducting flux qubits in D-Wave®'s machine suffer from interaction with their surroundings and the non-unitary dynamics induced by dissipation must be accounted for.

With the long-term goal of understanding dissipation in these complex devices, the QA-related research activity described in this thesis tackles two problems on prototypical simplified models, see Ref.s [31, 32]. The first is the **dissipative Landau-Zener model**, which describes two quantum states undergoing an avoided crossing in the presence of thermal noise. Despite its apparent simplicity, there are still theoretical open questions related to it. There are two main reasons to investigate the driven-dissipative dynamics in this model. First, it models a simple non-trivial driving scheme applied to a qubit: it is very unlikely that one can understand dissipation in many-qubits systems without having a clear idea of what happens to just one of them. Secondly, the Landau-Zener model captures the frequent situation in which the ground and first excited states of a many-body driven system anti-cross. It can thus be related to QA problems. Following this argument, the theoretical analysis of the dissipative Landau-Zener model in Ref. [33] concluded that interaction

with a thermal bath might enhance the QA final ground state probability over the corresponding coherent value. This phenomenon has been defined as *thermally assisted AQC*. Although other works on the same model showed no evidence for such improvement, a recent paper from the D-Wave® group [34] remarkably reported experimental evidence for the environment improving the QA performance: the authors implemented QA on a 16-qubit Hamiltonian, whose parameters were tuned so to have a spectrum with ground state energy always well separated from the other levels, except for one point in which there was a Landau-Zener anti-crossing. The experiment, tailored to test the theoretical prediction of Ref. [33], seemed to confirm the possibility of thermally assisted AQC. In our study, we revisit this issue, finding evidence for such a mechanism only in the cases of coupling directions which are *transverse* to the driving field. For the cases with purely longitudinal couplings, like the model in Ref. [33], we observe no improvement in all the cases studied.

During any non-trivial QA dynamics, it can also happen that one encounters some kind of phase transition, be it a second-order critical point or a first-order transition, where the gap protecting the ground state — in principle non-zero, for a finite system — vanishes as the size of the system goes to infinity [35, 36, 37]. In this case, the adiabaticity condition can never be perfectly fulfilled. Our second work, discussed in Chapter 4 and presented in Ref. [32], studies dissipation in QA when crossing the second-order quantum phase transition in the quantum spin-1/2 **Ising chain in transverse field**. The density of defects is, in this case, the natural estimator of the final ground state probability in Eq. (1.5), with zero defects corresponding to perfect annealing. In the absence of dissipation, it is known that the density of defects follows a Kibble-Zurek scaling law, $n_{\mathrm{def}}(\tau) \simeq \tau^{-1/2}$, where τ is the annealing time and plays the role of the adiabatic parameter. Interaction with a thermal bath modifies this scenario considerably. One can argue that an environment will likely have an opposite effect on the density of defects [38]: at some large enough τ, the system will start to thermalize, leading to an increase of $n_{\mathrm{def}}(\tau)$ over the coherent value. Our work aims to address the following question: under interaction with a thermal bath, is it always possible to find an Optimal Working Point (OWP), that is an optimal annealing time for which the density of defects is minimized? Although all the previous studies in the literature seemed to point at a positive answer, we find that this is not always the case, depending on the bath temperature and the interaction strength. In particular, we predict the absence of OWP in the regime of temperatures the current quantum annealers seem to work at.

1.2 Dissipation in topological pumping

Since the pioneering explanation of the integer quantum Hall effect [39], the study of topological phenomena in condensed matter physics has become a quite intense

field of research, the so-called topological insulators [40]. These materials have a finite energy gap between the highest occupied electronic band and the lowest empty band — like ordinary band insulators —, but they also show quantization of some observables and the emergence of gapless edge states protected by time-reversal symmetry [40]. These peculiar effects happen because these systems present a non-trivial Berry curvature in the Hamiltonian parameter space [41, 42]. Of particular interest is *topological adiabatic transport*, first studied by Thouless [43], who showed that certain periodically-driven models, despite being band insulators, can move charge in a quantized fashion [42]. Topological adiabatic pumps — also called Thouless pumps — have gained much attention after they have been realized in two different experiments employing ultracold atoms in optical lattices [44, 45]. In both cases, the experiment can be modelled by a periodically-driven Rice-Mele model [46], which is one of the simplest examples of topological adiabatic pumps.

Charge quantization is expected to be robust against several unavoidable experimental factors, like noise in the driving scheme or small disorder in the lattice. One can as well wonder about the impact of dissipation due to the interaction with an external environment. In our third work, discussed in Chapter 5 and presented in Ref. [47], we investigate how weak dissipation from a thermal bath can affect pumped charge quantization in the **periodically-driven Rice-Mele model**. A former study of the same (non-dissipative) model [48] for small but finite driving frequencies ω — adiabaticity corresponds to $\omega \to 0$ — showed that the pumped charge deviates from the quantized value quadratically in ω. Here we remarkably find that a bath at low enough temperature can fight such deviations, leading to a pumped charge which can be much closer to perfect quantization. We call this effect *thermally assisted Thouless pumping*, and we analyse it within the Floquet formalism.

1.3 Methods for computing dissipative dynamics

There are different approaches to model theoretically the time evolution of the state of a system which is not isolated from its surroundings. All of them must treat such a state within the density matrix formalism since decoherence makes any time-evolved state more and more mixed. A common approach is to write a Markovian quantum master equation (QME) in Lindblad form [49, 50, 51],

$$\frac{d}{dt}\hat{\rho}_{\mathrm{S}} = -\frac{i}{\hbar}\left[\widehat{H}_{\mathrm{S}}, \hat{\rho}_{\mathrm{S}}\right] + \sum_{ij}\gamma_{ij}\left(\hat{L}_i\hat{\rho}_{\mathrm{S}}\hat{L}_j^{\dagger} - \frac{1}{2}\left\{\hat{L}_j^{\dagger}\hat{L}_i, \hat{\rho}_{\mathrm{S}}\right\}\right) , \tag{1.6}$$

with $\hat{L}_i$ the so-called Lindblad operators that characterize the dissipation channels and γ_{ij} components of the so-called dampening matrix [52]. For time-independent systems and dissipations, a necessary and sufficient condition for positivity preser-

vation of the density matrix is that the dampening matrix is positive semidefinite [49, 50, 51, 52]. This condition remains unaltered even if the dampening matrix is time-dependent, with the proviso that its positive semidefiniteness holds for all times [53]. It is very common in the scientific literature on open systems to start directly from a Lindblad equation in the form of Eq. (1.6) and choose appropriate Lindblad operators that provide the dissipation channels one looks for [54, 55]. The advantage of this approach is that, as we said, positivity can be preserved and the structure of the equation is rather simple; as a drawback, however, one might lose intuition about the physical sources of dissipation.

Another approach — the one we will adopt throughout this thesis — is to consider the system under study in interaction with its environment. Already in the 80s, Caldeira and Leggett proved that one can model *weak* dissipation by simply coupling the system to a set of harmonic oscillators, with an interaction linear in the oscillator coordinates [56, 57]. This is often called the *Caldeira-Leggett bath*. Numerical methods exist to solve the resulting dynamics of the system alone in this setting. We mention here the Quasi-Adiabatic Path Integral (QUAPI) technique [58, 59, 60], which computes the time evolution of both system and bath, taking into account also a (properly truncated) memory kernel able to capture non-Markovian dynamics. A more recent approach exploits the exact mapping between the bath of bosons and semi-infinite discrete chains [61]: one can use methods like tensor networks to compute the overall dynamics, by properly truncating the size of the chains [62]. Both approaches are computationally heavy, but they are reliable also at non-Markovian and strong coupling regimes. Another interesting technique able to reach the strong coupling regime is the so-called Hierarchy of Equations [63, 64], where one derives and solves a set of nested differential equations to obtain the system dynamics. However, the number of differential equations — and the ensuing computational cost — increases as the coupling becomes stronger.

Starting from a Caldeira-Leggett bath, under weak coupling and Born-Markov approximations, one can also derive the so-called Bloch-Redfield quantum master equation (QME) [65, 66, 52, 67], as will be discussed in Chapter 2. Unfortunately, this equation cannot ensure positivity preservation because, in general, it cannot be written in Lindblad form, like Eq. (1.6). However, as will be detailed, in some specific limits it can be recast in such a form after applying the so-called Rotating-Wave Approximation (RWA) [66, 52]. The advantage then would be to have a master equation whose terms are reminiscent of the microscopic details of the system-bath interaction and the bath Hamiltonian. The QME can be solved by direct integration, for example through Runge-Kutta methods (and this is the approach we will follow in this thesis).

Alternatively, there exist several approaches to simulate the density matrix dynamics using tensor networks [68, 21]. One possible way is to use Matrix Product Density Operators (MPDO) [69], which extend the notion of Matrix Product States

(MPS) to generic density matrices. By construction, this *Ansatz* guarantees the positivity of the system's reduced density matrix at all times. To simulate the dynamics, one can for example map an MPDO (of dimension $L \times L$) to an MPS in "superket" form (a vector of dimension L^2) through Choi isomorphism [70, 71]. One can then solve the dissipative time-evolution of the superket according to a Schrödinger-like equation where, instead of the Hamiltonian, there is a Liouvillian superoperator [68]. Another approach that ensures positivity consists in evolving the purification of the reduced density matrix, instead of the reduced density matrix itself [72]. One can otherwise resort to quantum trajectories methods [73, 74, 75, 76]: instead of propagating the full density matrix in time, one reconstructs it statistically by averaging over many independent time evolutions of pure states subject to random interactions induced by the Lindblad operators. The advantage is that pure states require much fewer variables for their description compared to mixed states, so one can tackle systems with bigger Hilbert spaces. However, since many repetitions are required, this technique is not ideal for small Hilbert spaces.

1.4 Overview

We start in Chapter 2 with a derivation of the Bloch-Redfield Quantum Master Equation (QME), which is the starting point of all the calculations in this thesis. Different variants of QME will be derived, depending on the approximations used. Next, the basic mechanisms of dephasing (or decoherence) and relaxation are illustrated in the context of a static two-level system in interaction with a thermal bath, the so-called spin-boson model. We then move to discuss original research results. The dissipative Landau-Zener problem and the issue of thermally assisted QA are discussed in Chapter 3. The following Chapter 4 is then devoted to dissipation effects in the QA of the quantum Ising chain in a transverse field. In Chapter 5 we discuss the effects of dissipation in topological pumping. We conclude with some final remarks and future research perspectives.

Chapter 2

Quantum master equations for driven-dissipative systems

This chapter introduces the tool that will be used to compute the dissipative dynamics of a generic system in (weak) interaction with one or more Caldeira-Leggett baths. Sec. 2.1 introduces the setting of the Caldeira-Leggett bosonic reservoir. Then, under the assumptions of weak coupling and Born-Markov approximation, in Sec. 2.2 we derive the well-known Bloch-Redfield Quantum Master Equation (QME). In Sec. 2.3 we describe how to obtain a Lindblad QME from the Bloch-Redfield one, employing the so-called Rotating-Wave Approximation (RWA). In Sec. 2.4, we apply the previously derived equations to compute the dissipative dynamics of a static two-level system. We highlight the thermalization process on this system, showing how the mechanisms of relaxation and dephasing (or decoherence) take place in this setting.

2.1 Systems in interaction with thermal bosonic baths

Suppose that we have a system in interaction with its environment and we want to write the total Hamiltonian that describes both. Then, a general expression for the system plus environment can be [66, 52]

$$\widehat{H}_{\mathrm{tot}}(t) = \widehat{H}_{\mathrm{S}}(t) + \widehat{H}_{\mathrm{SB}} + \widehat{H}_{\mathrm{B}} \ , \tag{2.1}$$

where $\widehat{H}_{\mathrm{S}}(t)$ is the system Hamiltonian (that can be time-dependent), $\widehat{H}_{\mathrm{B}}$ is the environment Hamiltonian and $\widehat{H}_{\mathrm{SB}}$ describes the interaction between the two. When the interaction is weak, a good description for the environment Hamiltonian is to consider one or more sets of harmonic oscillators with different frequencies [56, 57],

$$\widehat{H}_{\mathrm{B}} = \sum_{\nu} \sum_{l} \hbar \omega_{l\nu} \hat{b}^{\dagger}_{l\nu} \hat{b}_{l\nu} \tag{2.2}$$

where ν identifies the set of harmonic oscillators and l indicates their modes. The $\hat{b}^\dagger_{l\nu}$ operator creates an excitation of energy $\hbar\omega_{l\nu}$. We will refer later to a set of harmonic oscillators also as a *bath of bosons*. The interaction between system and environment can be conveniently modelled as [56, 57]

$$\widehat{H}_{\rm SB} = \sum_\nu \hat{A}_\nu \otimes \hat{B}_\nu \ , \tag{2.3}$$

$\hat{A}_\nu$ and $\hat{B}_\nu$ acting respectively on the system and on the bath Hilbert space. $\hat{B}_\nu$ is taken to describe creation and annihilation of bosons in the bath, according to the operator

$$\hat{B}_\nu = \sum_l \lambda_{l\nu}\left(\hat{b}^\dagger_{l\nu} + \hat{b}_{l\nu}\right) \ . \tag{2.4}$$

The $\hat{A}_\nu$ operator can be whatever operator would be suitable to describe the action of the bath on the system. It can even be time-dependent and, without loss of generality, it is usually chosen to be Hermitean [52].[1] The parameters $\lambda_{l\nu}$ are real and related to the bath spectral function:

$$J_\nu(\omega) = \sum_l \lambda^2_{l\nu}\delta(\omega - \omega_{l\nu}) \, . \tag{2.5}$$

In a nutshell, $\lambda^2_{l\nu}$ gives the (unnormalized) probability that a process involving the ν^{th} bath and exchanging energy $\hbar\omega_{l\nu}$ can take place. In general, one has a continuum of modes for each bath, so that Eq. (2.5) is usually defined in the continuum limit. A very common choice is the so-called *ohmic* spectral function, which has the form

$$J_\nu(\omega) = 2\,\hbar^2\,\alpha_\nu\,\omega\,\mathrm{e}^{-\omega/\omega_{c,\nu}} \ , \tag{2.6}$$

with α_ν a *dimensionless* coupling constant and $\omega_{c,\nu}$ a cutoff frequency. Eq. (2.6) is plotted in Fig.2.1: we observe that the maximum of the function is at $\omega = \omega_{c,\nu}$, with value $J(\omega_{c,\nu}) = 2\,\hbar^2\alpha_\nu\omega_{c,\nu}/\mathrm{e}$. Therefore, one first sets the cutoff frequency to determine the range of frequencies that come more probably into play. Then, one adjusts the coupling strength by tuning α_ν. Although we mostly adopt ohmic spectral functions throughout this work, it is worth to mention that slight generalizations of Eq. (2.6) exist. They are defined as

$$J_\nu(\omega) = 2\,\hbar^2\,\alpha_\nu\,\omega^{s_\nu}\omega_{c,\nu}^{1-s_\nu}\,\mathrm{e}^{-\omega/\omega_{c,\nu}} \ , \tag{2.7}$$

and are called sub-ohmic ($s_\nu < 1$) and super-ohmic ($s_\nu > 1$), where the frequencies in the spectral function do not grow linearly with ω, but sub or super-linearly,

[1] If $\hat{A}_\nu$ is not Hermitean, it can always be expressed as a combination of two Hermitean operators, for example $\tilde{A}_{\nu,1} = \left(\hat{A}_\nu + \hat{A}^\dagger_\nu\right)/2$ and $\tilde{A}_{\nu,2} = i\left(\hat{A}_\nu - \hat{A}^\dagger_\nu\right)/2$, so that $\hat{A}_\nu \otimes \hat{B}_\nu = \tilde{A}_{\nu,1} \otimes \hat{B}_\nu + \tilde{A}_{\nu,2} \otimes \hat{B}_\nu$.

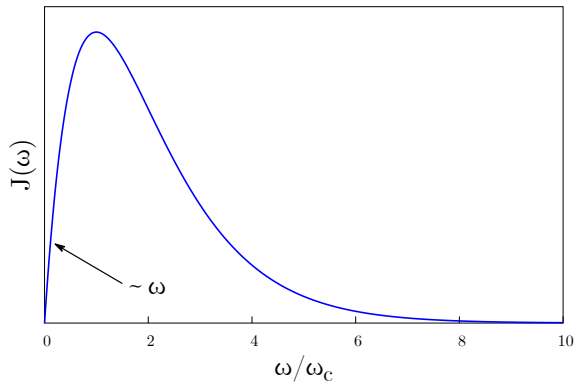

Figure 2.1: Ohmic spectral function.

respectively.

The system and the bath are initially uncorrelated, as we are assuming to put them in contact only at the beginning of the evolution,

$$\hat{\rho}_{\rm tot}(0) = \hat{\rho}_{\rm S}(0) \otimes \hat{\rho}_{\rm B} \ , \tag{2.8}$$

with the bath taken to be at thermal equilibrium,

$$\hat{\rho}_{\rm B} = \frac{{\rm e}^{-\beta \widehat{H}_{\rm B}}}{{\rm Tr}\{{\rm e}^{-\beta \widehat{H}_{\rm B}}\}} \ , \tag{2.9}$$

with $\beta = (k_B T)^{-1}$, k_B the Boltzmann constant and T the bath temperature. As will be clear in Sec. 2.2, within the perturbative Bloch-Redfield approach the state of the bath can be regarded as unaffected by the interaction with the system, so that it remains at equilibrium at all times t, $\hat{\rho}_{\rm B}(t) \equiv \hat{\rho}_{\rm B}$.

It is also very useful to define correlation functions that quantify the degree of correlation between processes that happen at different times [52]. Consider two different baths, denoted by indices ν and ν'. In general, their correlation function is given by

$$C_{\nu\nu'}(t) \equiv \langle \hat{B}_{\nu {\rm I}}(t) \hat{B}_{\nu' {\rm I}}(0) \rangle_{\rm eq} \tag{2.10}$$

where, since the $\hat{B}_\nu$ operators are Hermitean, it follows that $C^*_{\nu\nu'}(t) = C_{\nu'\nu}(-t)$. The Fourier transform of the correlation function,

$$\gamma_{\nu\nu'}(\omega) = \int_{-\infty}^{+\infty} dt \ {\rm e}^{i\omega t} C_{\nu\nu'}(t) \, . \tag{2.11}$$

will also turn out to be of crucial importance in the following. Notice that $C^*_{\nu\nu'}(t) = C_{\nu'\nu}(-t)$ implies immediately that $\gamma_{\nu\nu'}(\omega) = \gamma^*_{\nu'\nu}(\omega)$, hence the diagonal terms

for $\nu' = \nu$ must be real. A direct computation of correlation functions and their respective Fourier transforms for uncorrelated baths and Ohmic spectral functions can be found in Appendix A. In the derivation of the Bloch-Redfield QME, we will encounter also one-sided Fourier transforms of $C_{\nu\nu'}(t)$,

$$\Gamma_{\nu\nu'}(\omega) = \int_0^\infty dt\, \mathrm{e}^{i\omega t} C_{\nu\nu'}(t) \;, \tag{2.12}$$

which is in general complex. Employing the inverse Fourier transform of Eq. (2.11) and using it to substitute $C_{\nu\nu'}(t)$ in the expression for $\Gamma_{\nu\nu'}(\omega)$, one can show that[2]

$$\Gamma_{\nu\nu'}(\omega) = \frac{1}{2}\gamma_{\nu\nu'}(\omega) + i\sigma_{\nu\nu'}(\omega) \;, \tag{2.13}$$

where we have introduced the Hilbert transform of $\gamma_{\nu\nu'}(\omega)$,

$$\sigma_{\nu\nu'}(\omega) = \mathcal{P}\int_{-\infty}^{+\infty} \frac{d\omega'}{2\pi} \frac{\gamma_{\nu\nu'}(\omega')}{\omega - \omega'} \;, \tag{2.14}$$

which is also an Hermitean matrix, $\sigma_{\nu\nu'}(\omega) = \sigma^*_{\nu'\nu}(\omega)$.

2.2 The Bloch-Redfield quantum master equation

We derive here the main tool we will employ throughout this work to compute the dissipative dynamics of quantum systems: the Bloch-Redfield Quantum Master Equation (QME) [66, 52, 67].

As a first step, we need to move to the interaction picture, to focus just on the evolution induced by the interaction between system and environment. Given the "non-interacting" Hamiltonian $\widehat{H}_0(t) = \widehat{H}_{\mathrm{S}}(t) + \widehat{H}_{\mathrm{B}}$, the corresponding free evolution operator is

$$\widehat{U}_0(t,0) = \mathcal{T}\exp\left(-\frac{i}{\hbar}\int_0^t dt'\; \widehat{H}_0(t')\right) = \widehat{U}_{0\mathrm{S}}(t,0) \otimes \widehat{U}_{0\mathrm{B}}(t,0) \;, \tag{2.15}$$

[2] To compute the integral, define $\omega^+ = \omega + i\epsilon$, where ϵ is an infinitesimal imaginary part added to ensure convergence of the integral. Then,

$$\begin{aligned}
\Gamma_{\nu\nu'}(\omega^+) &= \int_0^\infty dt\, \mathrm{e}^{i(\omega+i\epsilon)t} \int_{-\infty}^{+\infty} \frac{d\omega'}{2\pi}\, \mathrm{e}^{-i\omega' t}\gamma_{\nu\nu'}(\omega') = i\int_{-\infty}^{+\infty} \frac{d\omega'}{2\pi}\, \frac{\gamma_{\nu\nu'}(\omega')}{\omega - \omega' + i\epsilon} = \\
&= i\,\mathcal{P}\int_{-\infty}^{+\infty} \frac{d\omega'}{2\pi}\, \frac{\gamma_{\nu\nu'}(\omega')}{\omega - \omega'} + \frac{1}{2}\int_{-\infty}^{+\infty} d\omega'\, \gamma_{\nu\nu'}(\omega')\delta(\omega - \omega') = \\
&= \frac{1}{2}\gamma_{\nu\nu'}(\omega) + i\sigma_{\nu\nu'}(\omega) \;,
\end{aligned}$$

Notice that, in the first step, we made use of $\int_0^\infty dt\, \mathrm{e}^{i(\omega-\omega'+i\epsilon)t} = i/(\omega - \omega' + i\epsilon)$, while in the second step we employed the standard relation $1/(\omega - \omega' + i\epsilon) = \mathcal{P}(1/(\omega - \omega')) - i\pi\delta(\omega - \omega')$, where $\mathcal{P}$ denotes the Cauchy principal value.

where $\mathcal{T}\text{exp}$ stands for the time-ordered exponential and $\widehat{U}_{0\mathrm{S}}(t,0)$ and $\widehat{U}_{0\mathrm{B}}(t,0)$ are the non-interacting propagators for the system and the bath respectively. The second equality holds simply because the system and bath Hamiltonians belong to different Hilbert spaces and therefore commute. The density matrix in the interaction representation,

$$\hat{\rho}_{\mathrm{tot},I}(t) = \widehat{U}_0^\dagger(t,0)\hat{\rho}_{\mathrm{tot}}(t)\widehat{U}_0(t,0)\,, \tag{2.16}$$

obeys a Liouville-von Neumann equation,

$$\frac{d}{dt}\hat{\rho}_{\mathrm{tot},I}(t) = -\frac{i}{\hbar}\left[\widehat{H}_{\mathrm{SB,I}}(t), \hat{\rho}_{\mathrm{tot},I}(t)\right]\,, \tag{2.17}$$

where $\widehat{H}_{\mathrm{SB,I}}(t) = \widehat{U}_0^\dagger(t,0)\widehat{H}_{\mathrm{SB}}(t)\widehat{U}_0(t,0)$ is the system-bath Hamiltonian in interaction representation. Integrating Eq. (2.17) in the interval $(0,t)$ we have

$$\hat{\rho}_{\mathrm{tot},I}(t) = \hat{\rho}_{\mathrm{tot},I}(0) - \frac{i}{\hbar}\int_0^t dt_1 \left[\widehat{H}_{\mathrm{SB,I}}(t_1), \hat{\rho}_{\mathrm{tot},I}(t_1)\right]\,. \tag{2.18}$$

We can then iterate Eq. (2.18) to express $\hat{\rho}_{\mathrm{tot},I}(t_1)$ on the r.h.s., to get

$$\begin{aligned}\hat{\rho}_{\mathrm{tot},I}(t) = \hat{\rho}_{\mathrm{tot},I}(0) &- \frac{i}{\hbar}\int_0^t dt_1 \left[\widehat{H}_{\mathrm{SB,I}}(t_1), \hat{\rho}_{\mathrm{tot},I}(0)\right] \\ &- \frac{1}{\hbar^2}\int_0^t dt_1 \int_0^{t_1} dt_2 \Big[\widehat{H}_{\mathrm{SB,I}}(t_1), \Big[\widehat{H}_{\mathrm{SB,I}}(t_2), \hat{\rho}_{\mathrm{tot},I}(t_2)\Big]\Big]\,.\end{aligned} \tag{2.19}$$

At this point, we make the crucial assumption of **weak coupling**. To go on, we exploit the fact that we can always isolate a scalar α out of the interaction Hamiltonian, so to quantify the coupling strength. In our case, we can redefine $\widehat{H}_{\mathrm{SB,I}} \to \alpha\widehat{H}_{\mathrm{SB,I}}$, with $\alpha \ll 1$. Then, each occurrance of $\widehat{H}_{\mathrm{SB,I}}$ in Eq. (2.19) would yield a factor α in front. Moreover, the system's state can be perturbatively expanded in α, so that $\hat{\rho}_{\mathrm{tot},I}(t_2) = \hat{\rho}_{\mathrm{tot},I}(0) + O(\alpha)$ for $t_2 \in [0,t]$. We can thus write Eq. (2.19) up to second order in α as

$$\begin{aligned}\hat{\rho}_{\mathrm{tot},I}(t) = \hat{\rho}_{\mathrm{tot},I}(0) &- \frac{i\alpha}{\hbar}\int_0^t dt_1 \left[\widehat{H}_{\mathrm{SB,I}}(t_1), \hat{\rho}_{\mathrm{tot},I}(0)\right] \\ &- \frac{\alpha^2}{\hbar^2}\int_0^t dt_1 \int_0^{t_1} dt_2 \Big[\widehat{H}_{\mathrm{SB,I}}(t_1), \Big[\widehat{H}_{\mathrm{SB,I}}(t_2), \hat{\rho}_{\mathrm{tot},I}(0)\Big]\Big] + O(\alpha^3)\,.\end{aligned} \tag{2.20}$$

To obtain a master equation in differential form, we take a time derivative and trace out the bath degrees of freedom, to get an evolution equation for the system alone, $\hat{\rho}_{\mathrm{S}}(t) = \mathrm{Tr}_{\mathrm{B}}\{\hat{\rho}_{\mathrm{tot}}\}$. After this, we obtain

$$\frac{d}{dt}\hat{\rho}_{\mathrm{S,I}}(t) = -\frac{\alpha^2}{\hbar^2}\int_0^t dt_2 \mathrm{Tr}_B\Big[\widehat{H}_{\mathrm{SB,I}}(t), \Big[\widehat{H}_{\mathrm{SB,I}}(t_2), \hat{\rho}_{\mathrm{tot},I}(0)\Big]\Big] + O(\alpha^3)\,. \tag{2.21}$$

where the first correction in α, after tracing out the bath, is null due to the assumption that $\mathrm{Tr_B}\{\hat{\rho}_\mathrm{B}\hat{B}_{\nu\mathrm{I}}(t)\} = 0$. We can calculate the trace by using Eq. (2.3) and assuming that the system and the bath start in a separable state as in Eq. (2.8), so that

$$\frac{d}{dt}\hat{\rho}_{\mathrm{S,I}}(t) = -\frac{\alpha^2}{\hbar^2}\sum_\nu \left(\left[\hat{A}_{\nu\mathrm{I}}(t), \widehat{S}_{\nu,\mathrm{I}}(t)\hat{\rho}_{\mathrm{S,I}}(0)\right] + \mathrm{H.c.}\right) + O(\alpha^3)\,, \tag{2.22}$$

where we defined the convoluted and integrated system operators

$$\begin{aligned}\widehat{S}_{\nu,\mathrm{I}}(t) &\equiv \sum_{\nu'}\int_0^t dt'\; C_{\nu\nu'}(t-t')\;\hat{A}_{\nu'\mathrm{I}}(t') = \\ &= \sum_{\nu'}\int_0^t d\tau\; C_{\nu\nu'}(\tau)\;\hat{A}_{\nu'\mathrm{I}}(t-\tau)\,.\end{aligned} \tag{2.23}$$

In the second equality we simply made the change of variable $t - t' = \tau$, to get an expression that will be useful later on. Since, up to zero order in α, $\hat{\rho}_{\mathrm{S,I}}(t) = \hat{\rho}_{\mathrm{S,I}}(0) + O(\alpha)$, Eq. (2.22) can be equivalently rewritten, in "closed" differential form, as

$$\frac{d}{dt}\hat{\rho}_{\mathrm{S,I}}(t) = -\frac{\alpha^2}{\hbar^2}\sum_\nu \left(\left[\hat{A}_{\nu\mathrm{I}}(t), \widehat{S}_{\nu,\mathrm{I}}(t)\hat{\rho}_{\mathrm{S,I}}(t)\right] + \mathrm{H.c.}\right) + O(\alpha^3)\,, \tag{2.24}$$

which is still valid up to second order in α. This is the so-called **Bloch-Redfield quantum master equation** in the interaction representation. Going back to the Schrödinger picture, Eq. (2.24) becomes

$$\frac{d}{dt}\hat{\rho}_\mathrm{S}(t) = -\frac{i}{\hbar}\left[\widehat{H}_\mathrm{S}(t), \hat{\rho}_\mathrm{S}(t)\right] - \frac{\alpha^2}{\hbar^2}\sum_\nu \left(\left[\hat{A}_\nu, \widehat{S}_\nu(t)\hat{\rho}_\mathrm{S}(t)\right] + \mathrm{H.c.}\right) + O(\alpha^3)\,, \tag{2.25}$$

where the convoluted operator in the Schrödinger picture now looks

$$\widehat{S}_\nu(t) \equiv \widehat{U}_0(t,0)\widehat{S}_{\nu,\mathrm{I}}(t)\widehat{U}_0^\dagger(t,0) = \sum_{\nu'}\int_0^t dt'\; C_{\nu\nu'}(t-t')\;\widehat{U}_0(t,t')\hat{A}_{\nu'}\widehat{U}_0^\dagger(t,t')\,. \tag{2.26}$$

Notice that, as a result of the approximations done on $\hat{\rho}_{\mathrm{tot},I}(t)$ and $\hat{\rho}_{\mathrm{S,I}}(t)$ to lowest order in α, we now have an equation that considers the evolution of the system disregarding completely the evolution of the bath, which is kept unchanged in time. Therefore, this approach is consistent with the application of the so-called *Born approximation* [66], *i.e.* neglecting the build-up of correlations between system and bath in time:

$$\hat{\rho}_{\mathrm{tot},I}(t) \simeq \hat{\rho}_{\mathrm{S,I}}(t) \otimes \hat{\rho}_\mathrm{B}\,. \tag{2.27}$$

Moreover, notice that the QME only depends on the system's state at time t and not

on previous times. This lack of memory is usually called *first Markov approximation*. But this does not mean that Eq.s (2.24) and (2.25) describe a truly Markovian interaction. Indeed, the non-Markovian nature of such equations is hidden in the fact that the operator $\widehat{S}_\nu(t)$ appearing in Eq. (2.26) *depends on the past* through the integral over t'. However, in many physical situations, it is possible to perform a further simplifying assumption, called the *second Markov approximation* [66, 52]. Suppose one can define a characteristic time-scale of the bath τ_B, after which the bath correlation functions go to zero, $C_{\nu\nu}(t > \tau_B) \simeq 0$. Then, one often assumes that the system's dynamics is much slower than the bath one, so that $t \gg \tau_B$ in Eq. (2.26). This means that the system's dynamics is insensible to the short memory of the bath, leading to an effective Markovian system's dynamics. In this setting, for all $t \gg \tau_B$ Eq. (2.26) can be approximated with

$$\widehat{S}_\nu(t) \simeq \widehat{S}^\infty_\nu(t) = \sum_{\nu'} \int_0^\infty d\tau \; C_{\nu\nu'}(\tau) \; \widehat{U}_0(t, t-\tau) \hat{A}_{\nu'} \widehat{U}_0^\dagger(t, t-\tau) \; , \tag{2.28}$$

where we performed the change of variables $t - t' = \tau$ and sent the upper limit of the integral to infinity. Within this approximation, we can now regard Eq. (2.25) as describing a Markovian dynamics.

A very important property of Eq. (2.25) is that *it preserves the trace of the density matrix*. Indeed,

$$\frac{d}{dt} \mathrm{Tr}_\mathrm{S} \left\{ \hat{\rho}_\mathrm{S}(t) \right\} = \mathrm{Tr}_\mathrm{S} \left\{ \frac{d}{dt} \hat{\rho}_\mathrm{S}(t) \right\} = 0 \, , \tag{2.29}$$

the last equality coming from the fact that in Eq. (2.25) only commutators appear and their trace must be zero because of the cyclic property of the trace. Moreover, observe that the right-hand side of Eq. (2.25) is manifestly Hermitean, which implies that *the Hermitean nature of $\hat{\rho}_\mathrm{S}(t)$ is evidently preserved* during the evolution. Unfortunately, the *positivity* of the system's density matrix *is not a priori preserved* by the Bloch-Redfield quantum master equation. However, there are some special cases in which one can write the Bloch-Redfield QME in Lindblad form, thus guaranteeing positivity preservation. This topic is discussed in the upcoming Sec. 2.3.

2.3 Lindblad equations from the Bloch-Redfield QME

Under further specific approximations, it is possible to cast the Bloch-Redfield QME Eq. (2.25) in Lindblad form, thus ensuring positivity preservation. For example, as shown in Sec. 2.3.1, a bath with no memory at all, *i.e.* $\tau_B \to 0$, leads almost straightforwardly to a Lindblad QME. However, this is an extreme limit and we will not use it in the rest of the work. On the other hand, one can also recover the Lindblad form by applying the so-called **Rotating-Wave Approximation**

(RWA) [66, 52]. Despite some similarities, there may be different ways to perform the RWA, which lead to different equations. For systems with sufficiently slow drivings (or simply with static Hamiltonians), one may employ the RWA by looking at the system energy levels [77], as detailed in Sec 2.3.2. In the different setting of periodic drivings, one can exploit the Floquet representation of states and perform the RWA according to the system's quasi-energies [78, 79], see Sec. 2.3.3.

To achieve these last two results, it will be convenient to fix a basis of states $\{|a\rangle\}$ — let it be generic, for now — to re-express some terms in the Bloch-Redfield QME in the interaction picture. Specifically, we can add identities $\mathbb{1} = \sum_a |a\rangle\langle a|$ to get

$$\hat{A}_{\nu\mathrm{I}}(t-\tau) = \sum_{ab} \widehat{U}^{\dagger}_{0\mathrm{S}}(t-\tau,0)|a\rangle\langle a|\hat{A}_\nu|b\rangle\langle b|\widehat{U}_{0\mathrm{S}}(t-\tau,0)\ . \tag{2.30}$$

2.3.1 Lindblad QME for memoryless baths

Suppose that each process occurring in our baths is completely uncorrelated with what happened before, that is

$$C_{\nu\nu'}(t) \longrightarrow D_{\nu\nu'}\,\delta(t)\ . \tag{2.31}$$

This implies that the convoluted operator $\widehat{S}_\nu(t)$ of Eq. (2.26) becomes

$$\widehat{S}_\nu(t) \longrightarrow \frac{1}{2}\sum_{\nu'} D_{\nu\nu'}\hat{A}_{\nu'}\ , \tag{2.32}$$

where the $1/2$ comes from integrating the delta function only at positive times. By substituting Eq. (2.32) into Eq. (2.25), it is easy to see that

$$\frac{d}{dt}\hat{\rho}_{\mathrm{S}}(t) = -\frac{i}{\hbar}\left[\widehat{H}_{\mathrm{S}}(t),\hat{\rho}_{\mathrm{S}}(t)\right] + \frac{\alpha^2}{\hbar^2}\sum_{\nu\nu'} D_{\nu\nu'}\Big(\hat{A}_{\nu'}\hat{\rho}_{\mathrm{S}}(t)\hat{A}_\nu - \frac{1}{2}\Big\{\hat{A}_\nu\hat{A}_{\nu'},\hat{\rho}_{\mathrm{S}}(t)\Big\}\Big) + O(\alpha^3)\,, \tag{2.33}$$

where we exploited the fact that, since the bath operators $\hat{B}_\nu$ are Hermitean, $D^*_{\nu\nu'} = D_{\nu'\nu}$. This equation can be brought to Lindblad form by a simple unitary transformation: since the matrix $\mathbf{D}$, formed by the $D_{\nu\nu'}$ as components, is a positive matrix, it can be diagonalized by a unitary transformation $\mathbf{U}$ such that $\mathbf{U}^\dagger\,\mathbf{D}\,\mathbf{U} = \mathrm{diag}(d_\mu)$, where $\mathrm{diag}(d_\mu)$ is a diagonal matrix with the positive eigenvalues of $\mathbf{D}$, $d_\mu > 0$. Then, we can define the *Lindblad operators* as follows

$$\hat{L}_\mu = \sqrt{d_\mu}\sum_\nu U^*_{\nu\mu}\hat{A}_\nu\ , \tag{2.34}$$

so that we eventually obtain the QME explicitly in Lindblad form [49]:

$$\frac{d}{dt}\hat{\rho}_{\rm S}(t) = -\frac{i}{\hbar}\left[\widehat{H}_{\rm S}(t), \hat{\rho}_{\rm S}(t)\right] + \frac{\alpha^2}{\hbar^2}\sum_{\mu}\left(\hat{L}_{\mu}\hat{\rho}_{\rm S}(t)\hat{L}_{\mu}^{\dagger} - \frac{1}{2}\left\{\hat{L}_{\mu}^{\dagger}\hat{L}_{\mu}, \hat{\rho}_{\rm S}(t)\right\}\right) + O(\alpha^3)\,. \tag{2.35}$$

2.3.2 Rotating-wave approximation for adiabatic drivings

We will consider here a time-dependent system with *adiabatic* driving and show how we can get a Lindblad QME with the RWA [77]. The treatment for time-independent Hamiltonians is just a sub-case of what we will present and it is more standard and rigorous [66, 52].

Following Ref. [77], where the problem has been analysed first, we impose a strict adiabatic approximation, in the sense that the time evolution operator for the system is approximated up to zero-order in the adiabatic parameter,

$$\widehat{U}_{0\rm S}(t,0) = \widehat{U}_{0\rm S}^{\rm ad}(t,0) + O\left(\frac{\xi}{\Delta_{min}^2 t_f}\right)\,, \tag{2.36}$$

where $\xi/(\Delta_{min}^2 t_f) \ll 1$ is the adiabatic parameter, with Δ_{min} the smallest gap between ground state and first excited state, t_f the total evolution time and, defining $\{|a(t)\rangle\}$ as the eigenbasis of $\widehat{H}_{\rm S}(t)$, $\xi = \max_{t,a,b}|\langle a(t)|\partial_t \widehat{H}_{\rm S}(t)|b(t)\rangle|$ [77]. Furthermore, assuming that the characteristic time-scale of the bath τ_B is much smaller than the time-scale associated to the system's dynamics, we can regard the system Hamiltonian as *time-independent within times of the order of* τ_B, so that we can carry out the following approximation:

$$\widehat{U}_{0\rm S}(t, t-\tau) = \mathcal{T}\exp\left(-\frac{i}{\hbar}\int_{t-\tau}^{t} dt' \widehat{H}_{\rm S}(t')\right) \simeq \exp\left(-\frac{i}{\hbar}\widehat{H}_{\rm S}(t)\tau\right) \tag{2.37}$$

Consider now Eq. (2.30) again, where the basis $\{|a\rangle\} = \{|a(t)\rangle\}$ is chosen to be the *system Hamiltonian eigenbasis* at time t, $\widehat{H}_{\rm S}(t)|a(t)\rangle = E_a(t)|a(t)\rangle$. Then, exploiting the fact that $\widehat{U}_{0\rm S}^{\dagger}(t-\tau,0) = \widehat{U}_{0\rm S}^{\dagger}(t,0)\widehat{U}_{0\rm S}(t,t-\tau)$, we have

$$\hat{A}_{\nu\rm I}(t-\tau) = \sum_{ab} {\rm e}^{i\mu_{ab}(t,0)}\, {\rm e}^{-i\Delta_{ab}(t)\tau} A_{\nu,ab}(t)\hat{L}_{ab}(0)\,, \tag{2.38}$$

where $\mu_{ab}(t,0) = \mu_a(t,0) - \mu_b(t,0)$, with $\mu_a(t,0)$ being the dynamical plus Berry phase accumulated during the adiabatic dynamics of the eigenstate $|a(t)\rangle$. Moreover, $\Delta_{ab}(t) = (E_a(t) - E_b(t))/\hbar$, and we defined

$$A_{\nu,ab}(t) = \langle a(t)|\hat{A}_{\nu}|b(t)\rangle \tag{2.39}$$

$$\hat{L}_{ab}(t) = |a(t)\rangle\langle b(t)| \tag{2.40}$$

We can apply this to the Bloch-Redfield QME in interaction picture, Eq. (2.24), to obtain

$$\frac{d}{dt}\hat{\rho}_{\mathrm{S,I}}(t) = -\frac{\alpha^2}{\hbar^2}\sum_{\nu\nu'}\sum_{abcd}\Bigg(\mathrm{e}^{i(\mu_{ab}(t,0)+\mu_{cd}(t,0))}A_{\nu,ab}(t)A_{\nu',cd}(t)\Gamma_{\nu\nu'}(\Delta_{dc}(t)) \times \\ \times\left[\hat{L}_{ab}(0),\hat{L}_{cd}(0)\hat{\rho}_{\mathrm{S,I}}(t)\right] + \mathrm{H.c.}\Bigg) . \tag{2.41}$$

Let us take a look at the exponential for a *time-independent* system first: in this case, we would have only the dynamical phase, *i.e.* $\mathrm{e}^{i(\mu_{ab}(t,0)+\mu_{cd}(t,0))} = \mathrm{e}^{i(E_a-E_b+E_c-E_d)t/\hbar}$. If t is large enough, so that $(E_a - E_b + E_c - E_d)\,t/\hbar \gg 1$, the corresponding factor in the master equation would experience very fast oscillations, which would average out during the evolution. Therefore, it would be legitimate to neglect these terms, performing the so-called **Rotating-Wave Approximation** (RWA), alias secular approximation [66, 52]. For a *time-dependent* system, the application of the RWA is in general *"far from rigorous"*, quoting Ref. [77]. Indeed, the phase in the exponential is an integral over time, where the dynamical and Berry phase vary in time. Nevertheless, we can guess that the RWA should still retain a good degree of reliability whenever the system energies and eigenstates do not change remarkably in time during the whole evolution. Let us suppose that the oscillatory terms are indeed negligible and impose

$$\mathrm{e}^{i(\mu_{ab}(t,0)+\mu_{cd}(t,0))} \xrightarrow{\mathrm{RWA}} \delta_{\mu_{ab}(t,0),\mu_{dc}(t,0)} . \tag{2.42}$$

In particular, it is crucial that $\Delta_{ab}(t) = \Delta_{dc}(t)$, therefore we require that the dynamical and Berry contributions vanish independently. Then, starting from Eq. (2.41), using Eq. (2.13) and exchanging some summation indices, we finally arrive at the following *Lindblad QME* for *adiabatically-driven* systems *under RWA*:

$$\frac{d}{dt}\hat{\rho}_{\mathrm{S,I}}(t) = -\frac{i}{\hbar}\left[\widehat{H}_{\mathrm{LS,I}}(t),\hat{\rho}_{\mathrm{S,I}}(t)\right] + \\ + \sum_{abcd}\gamma_{abcd}(t)\left(\hat{L}_{ab}(0)\,\hat{\rho}_{\mathrm{S,I}}(t)\,\hat{L}^{\dagger}_{dc}(0) - \frac{1}{2}\left\{\hat{L}^{\dagger}_{dc}(0)\,\hat{L}_{ab}(0),\hat{\rho}_{\mathrm{S,I}}(t)\right\}\right) , \tag{2.43}$$

where we have defined:

$$\gamma_{abcd}(t) = \frac{\alpha^2}{\hbar^2}\sum_{\nu\nu'}\delta_{\mu_{ab}(t,0),\mu_{dc}(t,0)}\,A_{\nu,cd}\,A_{\nu',ab}\,\gamma_{\nu\nu'}(\Delta_{cd}(t)) , \tag{2.44}$$

$$\widehat{H}_{\mathrm{LS,I}}(t) = \frac{\alpha^2}{\hbar}\sum_{\nu\nu'}\sum_{abc}\delta_{\mu_{ab}(t,0),\mu_{dc}(t,0)}\,A_{\nu,ab}(t)A_{\nu',bc}(t)\sigma_{\nu\nu'}(\Delta_{ab}(t))\hat{L}_{ac}(0) . \tag{2.45}$$

We can now rewrite Eq. (2.43) in the Schrödinger representation by using the free time evolution operator $\widehat{U}_{0\mathrm{S}}(t,0)$, so that

$$\frac{d}{dt}\hat{\rho}_{\mathrm{S}}(t) = -\frac{i}{\hbar}\Big[\widehat{H}_{\mathrm{S}}(t), \hat{\rho}_{\mathrm{S}}(t)\Big] + \widehat{U}_{0\mathrm{S}}(t,0)\frac{d}{dt}\hat{\rho}_{\mathrm{S,I}}(t)\widehat{U}^{\dagger}_{0\mathrm{S}}(t,0) \; .$$

Eventually, the **Bloch-Redfield QME** in **Lindblad form** and in the **Schrödinger picture** looks

$$\frac{d}{dt}\hat{\rho}_{\mathrm{S}}(t) = -\frac{i}{\hbar}\left[\widehat{H}_{\mathrm{S}}(t) + \widehat{H}_{\mathrm{LS}}(t), \hat{\rho}_{\mathrm{S}}(t)\right] + \tag{2.46}$$

$$+ \sum_{abcd} \gamma_{abcd}(t)\left(\hat{L}_{ab}(t)\,\hat{\rho}_{\mathrm{S}}(t)\,\hat{L}^{\dagger}_{dc}(t) - \frac{1}{2}\left\{\hat{L}^{\dagger}_{dc}(t)\,\hat{L}_{ab}(t), \hat{\rho}_{\mathrm{S}}(t)\right\}\right) , \tag{2.47}$$

where now the Lamb shift Hamiltonian has the Lindblad operator computed at time t:

$$\widehat{H}_{\mathrm{LS}}(t) = \frac{\alpha^2}{\hbar}\sum_{\nu\nu'}\sum_{abc}\delta_{\mu_{ab}(t,0),\mu_{dc}(t,0)}\,A_{\nu,ab}(t)A_{\nu',bc}(t)\sigma_{\nu\nu'}(\Delta_{ab}(t))\hat{L}_{ac}(t) \; . \tag{2.48}$$

This QME can be brought to the standard Lindblad form by diagonalizing the matrix of $\gamma_{ab,cd} = \gamma_{\alpha,\beta}$ components, as we did to get Eq. (2.34) [52]. If we assume that there are *no degenerate spectral differences*, we can further write

$$\delta_{\mu_{ab}(t,0),\mu_{dc}(t,0)} = \delta_{a,b}\,\delta_{c,d} + \delta_{a,d}\,\delta_{b,c}\,(1-\delta_{a,b}) \; , \tag{2.49}$$

i.e. we keep only the terms corresponding to 1) $a=b$ & $c=d$ and 2) $a=d$ & $b=c$, where the factor $(1-\delta_{a,b})$ on the r.h.s. prevents us from counting twice the terms with $a=b=c=d$. As a consequence, the QME in Lindblad form for **non-degenerate spectral differences** becomes

$$\begin{aligned}\frac{d}{dt}\hat{\rho}_{\mathrm{S}}(t) = & -\frac{i}{\hbar}\left[\widehat{H}_{\mathrm{S}}(t) + \widehat{H}_{\mathrm{LS}}(t), \hat{\rho}_{\mathrm{S}}(t)\right] + \\ & + \sum_{ab,a\neq b}\gamma_{abba}(t)\left(\hat{L}_{ab}(t)\,\hat{\rho}_{\mathrm{S}}(t)\,\hat{L}^{\dagger}_{ab}(t) - \frac{1}{2}\left\{\hat{L}^{\dagger}_{ab}(t)\,\hat{L}_{ab}(t), \hat{\rho}_{\mathrm{S}}(t)\right\}\right) + \\ & + \sum_{ab}\gamma_{aabb}(t)\left(\hat{L}_{aa}(t)\,\hat{\rho}_{\mathrm{S}}(t)\,\hat{L}^{\dagger}_{bb}(t) - \frac{1}{2}\left\{\hat{L}^{\dagger}_{bb}(t)\,\hat{L}_{aa}(t), \hat{\rho}_{\mathrm{S}}(t)\right\}\right) .\end{aligned} \tag{2.50}$$

Notice that $\gamma_{aabb}(t)$ is a sum of terms proportional to $\gamma_{\nu\nu'}(0)$, therefore it is only responsible for the so-called pure dephasing. The $\gamma_{abba}(t)$ is instead responsible for transitions between energy levels, since we assume $a \neq b$. Furthermore, it can be shown that Eq. (2.50) brings to a decoupling of the dynamics of populations and

coherences of the density matrix [52], in the form of classical rate equations for the populations.

2.3.3 Rotating-wave approximation for periodic drivings

We derive here a QME in Lindblad form for the specific case of periodically-driven systems of period τ. In order to do so, we employ the instantaneous *Floquet basis* relative to the *non-dissipative* system's dynamics [78, 79]. Let us thus introduce the Floquet states [80, 81, 82, 83] for the unitary dynamics, which are solutions to the time-dependent Schrödinger equation, as

$$|\psi_a(t)\rangle = \mathrm{e}^{-i\epsilon_a t/\hbar}|u_a(t)\rangle \,, \tag{2.51}$$

which are labelled by a, and where ϵ_a is the associated quasi-energy and $|u_a(t)\rangle$ is the Floquet mode, which is periodic, *i.e.* $|u_a(t+\tau)\rangle = |u_a(t)\rangle$.

The Floquet states form a basis for the system's Hilbert space for any time t, so we can use them to get more insight into the QME. For any operator $\hat{A}_{\nu\mathrm{I}}(t')$ we can use the basis of states in Eq. (2.51), $|a\rangle = |\psi_a(t')\rangle$. Exploiting the fact that for Floquet states $\widehat{U}_{0\mathrm{S}}(t_2,t_1)|\psi_a(t_1)\rangle = |\psi_a(t_2)\rangle$, we can easily write Eq. (2.30) as

$$\begin{aligned}\hat{A}_{\nu\mathrm{I}}(t') &= \sum_{ab} \mathrm{e}^{i(\epsilon_a-\epsilon_b)t'/\hbar}\langle u_a(t')|\hat{A}_\nu|u_b(t')\rangle|\psi_a(0)\rangle\langle\psi_b(0)| = \\ &= \sum_{ab}\sum_{k} \mathrm{e}^{i\Delta_{ab,k}t'} A^k_{\nu,ab}|\psi_a(0)\rangle\langle\psi_b(0)| \,,\end{aligned} \tag{2.52}$$

where, in the second equality, we exploited the periodicity of $\langle u_a(t')|\hat{A}_\nu|u_b(t')\rangle$ to write it as a Fourier series,

$$\langle u_a(t')|\hat{A}_\nu|u_b(t')\rangle = \sum_k \mathrm{e}^{-i\Omega k t'} A^k_{\nu,ab} \,, \tag{2.53}$$

with $\Omega = 2\pi/\tau$. Here, we defined the quantity $\Delta_{ab,k} = (\epsilon_a - \epsilon_b)/\hbar - \Omega k$. Using this in the Bloch-Redfield QME in the interaction picture, Eq. (2.24), we can carry out a calculation very similar to the one in the previous section, to get

$$\begin{aligned}\frac{d}{dt}\hat{\rho}_{\mathrm{S,I}}(t) = \frac{\alpha^2}{\hbar^2}\sum_{\nu\nu'}\sum_{abcd}\sum_{kk'}\Bigg(&\mathrm{e}^{i(\Delta_{ab,k}+\Delta_{cd,k'})t}\,\Gamma_{\nu\nu'}(-\Delta_{cd,k'})\,A^k_{\nu,ab}\,A^{k'}_{\nu',cd}\times \\ &\times\Big[\hat{L}_{ab}(0),\hat{L}_{cd}(0)\hat{\rho}_{\mathrm{S,I}}(t)\Big] + \mathrm{H.c.}\Bigg) \,,\end{aligned} \tag{2.54}$$

with

$$\hat{L}_{ab}(t) = |\psi_a(t)\rangle\langle\psi_b(t)| \,. \tag{2.55}$$

Again, we see that there are potential rapidly-oscillating terms as the evolution time

t increases. Indeed, we can treat the factor $\mathrm{e}^{i(\Delta_{ab,k}+\Delta_{cd,k'})t}$ as in the previous section and perform a **RWA** according to the coherent dynamics quasi-energies:

$$\mathrm{e}^{i(\Delta_{ab,k}+\Delta_{cd,k'})t} \xrightarrow{\text{RWA}} \delta_{\Delta_{ab,k},\Delta_{dc,-k'}} \simeq \delta_{\Delta_{ab,k},\Delta_{dc,k}} \cdot \delta_{k,-k'} \ . \tag{2.56}$$

Applying the RWA, using Eq. (2.13), we get the following QME in *Lindblad form* in the Schrödinger representation

$$\frac{d}{dt}\hat{\rho}_{\mathrm{S}}(t) = -\frac{i}{\hbar}\left[\widehat{H}_{\mathrm{S}}(t) + \widetilde{H}_{\mathrm{LS}}(t), \hat{\rho}_{\mathrm{S}}(t)\right] + \tag{2.57}$$

$$+ \sum_{abcd} \widetilde{\gamma}_{abcd}\left(\hat{L}_{ab}(t)\,\hat{\rho}_{\mathrm{S}}(t)\,\hat{L}^{\dagger}_{dc}(t) - \frac{1}{2}\left\{\hat{L}^{\dagger}_{dc}(t)\,\hat{L}_{ab}(t), \hat{\rho}_{\mathrm{S}}(t)\right\}\right) , \tag{2.58}$$

where we defined

$$\widetilde{H}_{\mathrm{LS}}(t) = \frac{\alpha^2}{\hbar}\sum_{\nu\nu'}\sum_{abc}\sum_{k} \delta_{\Delta_{ab,k},\Delta_{dc,k}}\, A^{k}_{\nu,ab}\left(A^{k}_{\nu',cb}\right)^{*} \sigma_{\nu\nu'}(\Delta_{ab,k})\hat{L}_{ac}(t) \tag{2.59}$$

$$\widetilde{\gamma}_{abcd} = \frac{\alpha^2}{\hbar^2}\sum_{\nu\nu'}\sum_{k} \delta_{\Delta_{ab,k},\Delta_{dc,k}}\, A^{k}_{\nu,cd}\left(A^{k}_{\nu',ba}\right)^{*} \gamma_{\nu\nu'}(\Delta_{ba,k}) \ . \tag{2.60}$$

Notice how this equation formally looks very similar to Eq. (2.43) for the adiabatic driving case, although we have very different Lindblad operators and coefficients.

If there are no degeneracies in the quasi-energies spectrum, we can also set $a = b$ & $c = d$ and $a = d$ & $b = c$, being careful of not over-counting the $a = b = c = d$ case, *i.e.*

$$\delta_{\Delta_{ab,k},\Delta_{dc,k}} = \delta_{a,b}\,\delta_{c,d} + \delta_{a,d}\,\delta_{b,c}\,(1 - \delta_{a,b}) \ , \tag{2.61}$$

analogously to Eq. (2.49). Then, Eq. (2.57) for the case of **no degenerate quasi-energies differencies** becomes

$$\begin{aligned}\frac{d}{dt}\hat{\rho}_{\mathrm{S}}(t) = &-\frac{i}{\hbar}\left[\widehat{H}_{\mathrm{S}}(t) + \widetilde{H}_{\mathrm{LS}}(t), \hat{\rho}_{\mathrm{S}}(t)\right] + \\ &+ \sum_{ab,a\neq b} \widetilde{\gamma}_{abba}\left(\hat{L}_{ab}(t)\,\hat{\rho}_{\mathrm{S}}(t)\,\hat{L}^{\dagger}_{ab}(t) - \frac{1}{2}\left\{\hat{L}^{\dagger}_{ab}(t)\,\hat{L}_{ab}(t), \hat{\rho}_{\mathrm{S}}(t)\right\}\right) + \\ &+ \sum_{ab} \widetilde{\gamma}_{aabb}\left(\hat{L}_{aa}(t)\,\hat{\rho}_{\mathrm{S}}(t)\,\hat{L}^{\dagger}_{bb}(t) - \frac{1}{2}\left\{\hat{L}^{\dagger}_{bb}(t)\,\hat{L}_{aa}(t), \hat{\rho}_{\mathrm{S}}(t)\right\}\right) .\end{aligned} \tag{2.62}$$

Notice, again, the analogy with Eq. (2.50) for the adiabatic case. It is thus not surprising that also Eq. (2.62) leads to a decoupling of the dynamics of coherences and populations, but this time in the Floquet basis. It can be shown that the coherences modules go to zero in the stationary limit so that one is left with simple rate equations for the Floquet stationary populations.

2.4 Thermalization in static systems

Let us start our journey among the open quantum systems from the simplest setting we can think of: a spin-1/2 coupled to a bosonic reservoir. This is known as the *spin-boson model* and has been thoroughly studied [10, 84, 85]. Despite its apparent simplicity, the spin-boson model exhibits quite interesting physics depending on the details of the interaction Hamiltonian (like coupling strength, bath temperature or spectral density) [10]. In this chapter, we review it in the weak coupling regime utilizing the Bloch-Redfield QME, Eq. (2.25), to illustrate the basic mechanisms of dephasing and relaxation, which are very clear in this time-independent setting.

2.4.1 The spin-boson model

The spin-boson model describes a *time-independent* two-level system coupled to one thermal bath. The total Hamiltonian has the form of Eq. (2.1), where the system Hamiltonian is

$$\widehat{H}_{\mathrm{S}} = \frac{\epsilon}{2}\hat{\sigma}^z + \frac{\Delta}{2}\hat{\sigma}^x \ , \tag{2.63}$$

with $\hat{\sigma}^\nu$, $\nu = x, y, z$ the usual Pauli matrices. The eigenstates of $\hat{\sigma}^z$ can be thought as two macroscopic states, with energy difference ϵ, coupled by a tunnelling term Δ. The bath Hamiltonian is as in Eq. (2.2) with only one value of ν in the sum since we have only one reservoir. The interaction is modelled by Eq. (2.3), with $\hat{B}$ describing the emission/absorption of bosons from/in the bath, and

$$\hat{A} = \hat{\sigma}^z \tag{2.64}$$

describes how the interaction affects the system state [10, 85]. Notice that the coupling along $\hat{\sigma}^z$ is general enough: if we had another operator, we simply could apply a unitary transformation to go back to Eq. (2.63) with a proper renormalization of ϵ and Δ. It is more interesting to look at the problem in the system energy basis. We can introduce a new set of Pauli matrices $\hat{\tau}^\nu$, corresponding to this basis, and we can rewrite the total Hamiltonian as

$$\widehat{H}^{\mathrm{eig}}_{\mathrm{tot}} = \frac{\Delta E}{2}\hat{\tau}^z + (\sin\theta\ \hat{\tau}^x + \cos\theta\ \hat{\tau}^z) \otimes \hat{B} + \widehat{H}_{\mathrm{B}} \ , \tag{2.65}$$

where ΔE is the gap between the two system's eigenstates, while θ tunes the coupling direction with respect to the system energy basis.

We are interested in the dynamics of the system starting from a generic initial state $\hat{\rho}_{\mathrm{S}}(0)$. Several techniques can be employed to achieve this goal: under weak coupling approximation, for example, we can use a suitable QME among the ones provided in the previous chapter. A well-established result in the literature is that two different time-scales govern the system's time-evolution [85]. On the one hand,

we have the so-called *dephasing* or *decoherence*, *i.e.* the off-diagonal elements of the density matrix in the system energy eigenbasis tend to zero after a characteristic dephasing time-scale. This means that the system tends to become a purely mixed state, losing the quantum superposition between the energy eigenstates. On the other hand, the populations of the density matrix, again in the system energy eigenbasis, tend to acquire a Boltzmann distribution depending on the bath temperature. This phenomenon is denominated *relaxation* and it also takes place within a proper relaxation time-scale. The interplay of relaxation and dephasing leads the system to reach a thermal steady state after a transient,

$$\hat{\rho}_{\mathrm{S}}(t \to \infty) = \frac{\mathrm{e}^{-\beta \widehat{H}_{\mathrm{S}}}}{\mathrm{Tr}\{\mathrm{e}^{-\beta \widehat{H}_{\mathrm{S}}}\}} \,, \tag{2.66}$$

where β is the bath inverse temperature. Notice that $\hat{\rho}_{\mathrm{S}}(t \to \infty)$, written in the system energy eigenbasis, is diagonal. A very peculiar case happens whenever the system coupling operator $\hat{A}$ commutes with the system Hamiltonian $\widehat{H}_{\mathrm{S}}$: in that case, the system energies must be conserved, hence interactions with the bath cannot change them. Therefore, relaxation does not occur, but we still have dephasing. This setting is thus called *pure-dephasing*.

2.4.2 Visualizing dephasing and relaxation

It is instructive to visualize the processes of dephasing and relaxation on the Bloch sphere. We express the system density matrix in the energy eigenbasis as

$$\hat{\rho}_{\mathrm{S}}^{\mathrm{eig}}(t) = \frac{1}{2}\left(\mathbb{1} + \mathbf{r}(t) \cdot \hat{\boldsymbol{\tau}}\right) \,, \tag{2.67}$$

where $\mathbf{r}(t) = (r_x(t), r_y(t), r_z(t)) \in \mathbb{R}^3$ and $\hat{\boldsymbol{\tau}} = (\hat{\tau}^x, \hat{\tau}^y, \hat{\tau}^z)$. By using the Bloch-Redfield QME written in Appendix B, one finds that the dynamics of populations and coherences is decoupled, giving

$$r_{\pm}(t) = r_x(t) \pm i r_y(t) \sim \mathrm{e}^{-t/\tau_\varphi} \,, \tag{2.68}$$

$$r_z(t) - r_z^{eq} \sim \mathrm{e}^{-t/\tau_{\mathrm{R}}} \,, \tag{2.69}$$

where $r_z^{eq} = \tanh(\beta \Delta E/2)$ characterizes the thermal equilibrium for the populations, while τ_φ and τ_{R} are respectively the dephasing and relaxation time-scales, associated to the following corresponding rates

$$\gamma_{\mathrm{R}} = \frac{1}{\tau_{\mathrm{R}}} = \sin^2\theta \, \frac{S_X(\Delta E/\hbar)}{\hbar^2} \,, \tag{2.70}$$

$$\gamma_\varphi = \frac{1}{\tau_\varphi} = \frac{1}{2}\gamma_{\mathrm{R}} + \cos^2\theta \, \frac{S_X(0)}{\hbar^2} \,, \tag{2.71}$$

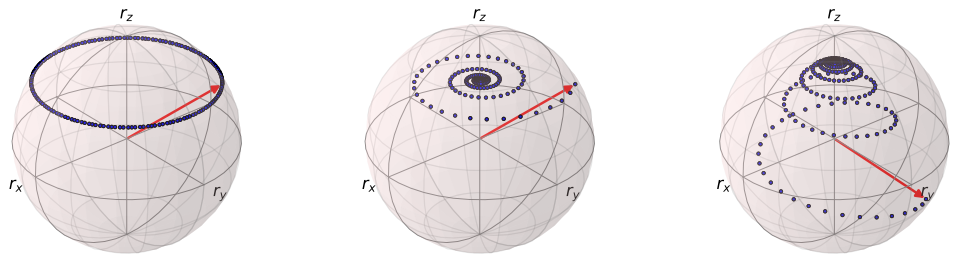

(a) (b) (c)

Figure 2.2: Dynamics of a spin-1/2 under the spin-boson Hamiltonian for (a) no dissipation, (b) pure-dephasing and (c) relaxation plus decoherence. In (a), the spin oscillates coherently. In (b), the coherences of the density matrix go to zero, but the populations do not change. Plots realized using the Qutip package [86, 87].

with $S_X(\omega) = \gamma(\omega) + \gamma(-\omega)$ being the Fourier transform of the symmetrized bath correlation function [85]. These results are illustrated in Fig. 2.2, where we show the dissipative dynamics of the Bloch vector $\mathbf{r}(t)$, starting from a generic initial pure state, indicated by the red arrows. Recall that pure states correspond to vectors that point at the surface of the Bloch sphere while, if the state becomes mixed, the associated vector points inside the sphere. Panel (a) shows non-dissipative dynamics: the state is always pure and thus the Bloch vector always points at the surface of the sphere, precessing at fixed frequency $\Delta E/\hbar$. Panel (b) illustrates the peculiar pure-dephasing case: the coherent oscillations of the previous case are damped in time, as the Bloch vector tends to dig deeper and deeper inside the sphere; however, the value of $r_z(0)$ never changes, because populations cannot be modified by the interaction with the bath. Panel (c) eventually displays a generic relaxation plus dephasing process, where now also r_z relaxes to the equilibrium value r_z^{eq}.

Whenever the system Hamiltonian is time-dependent, the phenomena of dephasing and relaxation still occur, but in general it is more difficult to disentangle them. On the one hand, their time-scales are no more constant and the dynamics is more complicated than a pure exponential; on the other hand, the energy eigenbasis also depends on time.

Chapter 3

The dissipative Landau-Zener model

We present here results contained in our first paper [31], in which we analyse how interaction with a bosonic reservoir at thermal equilibrium can affect the dynamics of a two-level quantum system described by the Landau-Zener Hamiltonian. In particular, we shed light upon the mechanism by which dissipation can remarkably *enhance* the final ground state probability over the coherent evolution. We interpret this in the context of Quantum Annealing (QA) — *alias* Adiabatic Quantum Computation (AQC) —, in analogy with what has been called "thermally assisted AQC" [33].

There have been many studies on the dissipative Landau-Zener model over the years. However, almost all of them focused on a coupling to the environment which is *purely longitudinal* — *i.e.* along the same direction — with respect to the driving. By purely longitudinal we mean that, if the Landau-Zener Hamiltonian is written as $\widehat{H}_{\text{LZ}} = \epsilon(t)\hat{\sigma}^z + \Delta\hat{\sigma}^x$, the coupling would be proportional to the $\hat{\sigma}^z$ operator only. The reason for neglecting transverse coupling directions, as discussed in Ref. [10], is probably due to the fact that longitudinal coupling is definitely the dominant noise mechanism when one deals with a macroscopic two-level system — such as a qubit in a quantum annealer —, because any transverse coupling would be proportional to the "exponentially small" (overlap-related) tunnelling matrix element between the two states that undergo the avoided crossing.

Some analytic results are known for some limiting cases and a *purely longitudinal* system-bath interaction: at fast sweeps, for low temperatures or strong couplings, the dissipative dynamics is expected to be identical to the coherent one [88, 89, 90, 91, 92]; at very high temperatures and slow sweeps, the system is expected to reach equal populations at the end of the dynamics [88, 89]. This partial understanding of the model has been then supplemented by numerical approaches, such as the weak-coupling Bloch-Redfield QME and the numerically-exact Quasi-

Adiabatic Path Integral (QUAPI) technique [58, 59], which have given answers to all the remaining regimes under the choice of an ohmic bath spectral function [93, 94]. In particular, they highlighted a non-monotonic dependence of the final ground state probability as a function of the driving speed in the adiabatic region. Importantly, none of these results showed that such an interaction can improve the final ground state probability over the one corresponding to the coherent case, *i.e.* either this dissipation is detrimental or it does not affect the dynamics.

On the other hand, another study on the very same model in the context of AQC-QA [33], using again a standard Bloch-Redfield QME, claimed that dissipation might enhance the final ground state probability, at least in some regimes of ohmic or super-ohmic bath spectral functions. This phenomenon is known in the literature as "thermally assisted AQC" [33]. The authors, however, do not integrate the evolution equations for the Landau-Zener model to support their claim, but rather study numerically QA on much more complicated models with 12, 16 and 20 qubits. In the super-ohmic case, their data report thermal improvement. Our analysis does not support their conclusions.

These are all results related to purely longitudinal interaction. However, a coupling along the *transverse* direction might as well realize an interesting thermal improvement, since it couples to the tunnelling term that causes transitions (the $\hat{\sigma}^x$ operator in the Landau-Zener Hamiltonian). Notice that a transverse interaction might be relevant for Landau-Zener processes happening in AQC-QA. Although the longitudinal coupling is dominant for a single qubit in the D-Wave machine, when the Landau-Zener physics emerges from the two lowest-lying eigenstates of a complex multi-qubit Hamiltonian, one would expect that an appropriate model to describe the dissipation should include couplings to the transverse directions. At zero temperature, the dissipative Landau-Zener model has been exactly solved for generic coupling directions [90, 91], finding an analytic formula for the final ground state probability that generalizes the famous Landau-Zener formula for the coherent case. Very interestingly, if the coupling has some transverse component, in some cases the final ground state probability can be larger than its coherent counterpart, realizing again a dissipative enhancement in the spirit of Ref. [33]. The same problem has also been tackled numerically at finite temperature and for an ohmic spectral function [95], utilizing Bloch-Redfield QME (with RWA) and QUAPI: the study, however, does not investigate the non-adiabatic region, where we do find the most interesting physics.

In this chapter, we revisit the issue of thermally assisted QA using the Bloch-Redfield QME, benchmarked against the exact results at zero temperature in Ref.s [90, 91] and against the numerically-exact QUAPI technique at finite temperature. In Sec. 3.1 the physics of the Landau-Zener model is introduced, while Sec. 3.2 describes how we model dissipation. In Sec. 3.3 we present our results: first, we benchmark the validity of the QME, with and without RWA; next, we investigate the effect of

both longitudinal and transverse couplings at all temperatures. As we will show, thermal dissipation can enhance the final ground state probability — *i.e.* the QA performance — whenever the system-bath coupling possesses at least a certain degree of transverse component. This effect is prominent at high temperatures and fast sweeps, although it appears also at low temperatures. To understand more intuitively this phenomenon, we present a simple model based on a bath made of a single harmonic oscillator. In Sec. 3.4 we try to make contact with the experiment in Ref. [34], where the authors reported thermally assisted QA on a 16-qubit Hamiltonian with the annealing dynamics dominated by a unique Landau-Zener crossing.

3.1 The Landau-Zener problem

The Landau-Zener model, conceived and solved almost a century ago [96, 97, 98, 99], describes two quantum states that undergo an avoided crossing as a consequence of driving. The Hamiltonian that captures this physics can be written as

$$\widehat{H}_{\mathrm{S}}(t) = \frac{vt}{2}\hat{\sigma}^z + \frac{\Delta}{2}\hat{\sigma}^x \,, \tag{3.1}$$

with v the *driving speed* and Δ the smallest gap through the evolution. Notice that Eq. 3.1 reminds of the spin-boson Hamiltonian in Eq. (2.63) in Sec. 2.4, with ϵ now replaced by a time-dependent $\epsilon(t) = vt$. At the extreme times $t = \pm\infty$, the Hamiltonian eigenstates are equal to the $\hat{\sigma}^z$ eigenstates — the so-called *diabatic basis* —, which we denote by $\{|\uparrow\rangle, |\downarrow\rangle\}$. If $\Delta = 0$, these states would be eigenstates of the Hamiltonian for the whole dynamics, but they would change their energies linearly in time: as can be seen from Fig. 3.1, the initial ground (excited) state would become the final excited (ground) state, following the dotted lines that represent the two uncoupled energy levels. A non-zero Δ opens a gap in the spectrum, with the energies given by

$$E_{\pm}(t) = \pm\sqrt{(vt)^2 + \Delta^2} \tag{3.2}$$

and time-dependent eigenstates $\{|\psi_{\mathrm{gs}}(t)\rangle, |\psi_{\mathrm{ex}}(t)\rangle\}$ that form the so-called *adiabatic basis*. The presence of Δ, proportional to $\hat{\sigma}^x$ in Eq. (3.1), opens up the possibility of *tunnelling* between the two diabatic basis states.

The problem now is to understand the interplay of driving speed and tunnelling in determining the final state at the end of the time-evolution, given a certain initial state. Let us thus start from the ground state at $t = -\infty$, *i.e.* $|\psi(-\infty)\rangle = |\downarrow\rangle$, and let the system's state $|\psi(t)\rangle$ evolve unitarily according to

$$|\psi(t)\rangle = \widehat{U}(t, -\infty)|\downarrow\rangle \,, \tag{3.3}$$

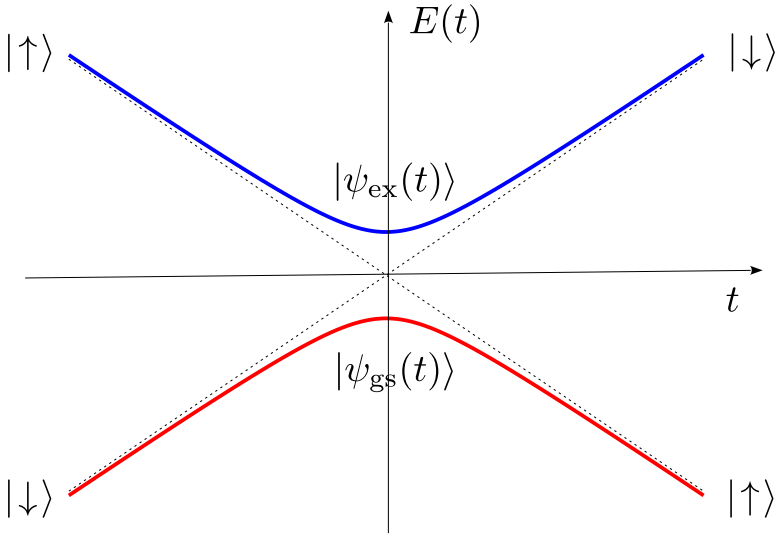

Figure 3.1: Energy bands of the Landau-Zener model, corresponding to the adiabatic states, plotted versus time. The avoided crossing takes place at $t = 0$, where the (minimum) gap is equal to Δ.

where the time-propagator is written as a time-ordered exponential,

$$\widehat{U}(t, t_0) = \mathcal{T}\exp\left(-\frac{i}{\hbar}\int_{t_0}^{t} dt' \widehat{H}_{\rm S}(t')\right) . \tag{3.4}$$

From the adiabatic theorem [28] we know that, if the condition for adiabaticity $\hbar v \ll \Delta^2$ is satisfied, we will be able to follow the instantaneous ground state at any time. If instead adiabaticity is broken, tunnelling between the diabatic states influences less the dynamics and the state will stay closer to the initial diabatic state. One can see this by computing the instantaneous ground state probability

$$\mathrm{P}_{\rm gs}^{\rm LZ}(t) = |\langle\psi_{\rm gs}(t)|\psi(t)\rangle|^2 , \tag{3.5}$$

which also depends on the adiabatic parameter $\hbar v/\Delta^2$. Of particular interest is the ground state probability well after the avoided crossing, ideally at $t = +\infty$, that we define as

$$P_{\rm gs}^{\rm LZ}(v/\Delta^2) = \mathrm{P}_{\rm gs}^{\rm LZ}(t = +\infty) . \tag{3.6}$$

This quantity has been exactly calculated, giving what is usually called the *Landau-*

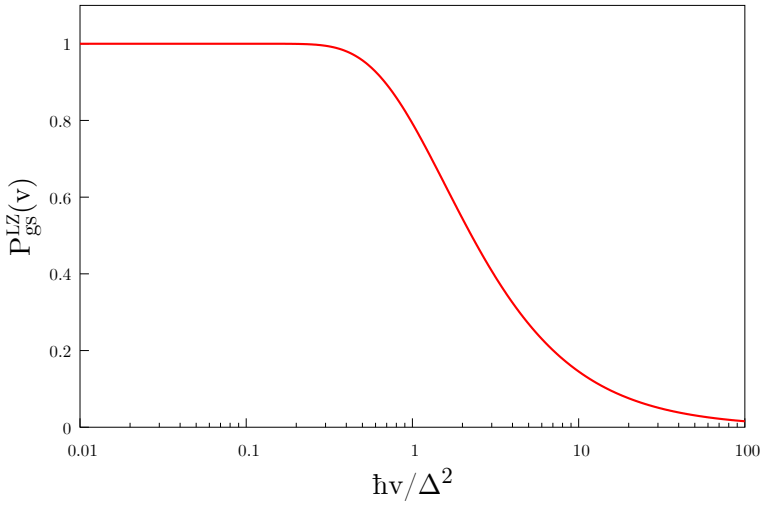

Figure 3.2: Plot of the final ground state probability in Eq. (3.7) as a function of the adiabatic parameter $\hbar v/\Delta^2$. For slow drivings the initial state follows very closely the instantaneous ground state and eventually reaches the final ground state with very high fidelity (adiabatic region, $\hbar v/\Delta^2$). For $\hbar v/\Delta^2 > 1$ we enter the non-adiabatic regime, where $P_{\rm gs}^{\rm LZ}(v/\Delta^2)$ decreases as tunnelling becomes less effective.

Zener formula [96, 97]:

$$P_{\rm gs}^{\rm LZ}(v/\Delta^2) = 1 - \exp\left\{-\frac{\pi\Delta^2}{2\hbar v}\right\} . \tag{3.7}$$

The plot of Eq. 3.7 is shown in Fig. 3.2. A high overlap with the final ground state can be achieved only through an adiabatic driving, $\hbar v \ll \Delta^2$, as expected. If we instead sweep faster, we partly follow the diabatic state up to the final excited state $|\uparrow\rangle$, since we do not spend enough time in the tunnelling region to be able to follow perfectly the instantaneous ground state.

All this theory is well-known and established. However, things can remarkably change when dissipation is added, as we will discuss in the rest of this chapter.

3.2 Dissipation in the Landau-Zener model

We model dissipation in the Landau-Zener problem following previous works already present in the literature [10, 100, 89, 84, 66, 78]. The system Hamiltonian in Eq. (3.1) is subject to interaction with one thermal bosonic reservoir at equilibrium with temperature T, so that the total Hamiltonian is a sum of system, bath and system-bath interaction terms, $\widehat{H}_{\rm tot}(t) = \widehat{H}_{\rm S}(t) + \widehat{H}_{\rm B} + \widehat{H}_{\rm SB}$, as in Eq. (2.1). The bath

Hamiltonian is

$$\widehat{H}_{\rm B} = \sum_l \hbar\omega_l \hat{b}_l^\dagger \hat{b}_l \ , \tag{3.8}$$

while we choose the interaction to be modelled by

$$\widehat{H}_{\rm SB} = \frac{1}{2}\left(\cos\theta\,\hat{\sigma}^z + \sin\theta\,\hat{\sigma}^x\right) \otimes \hat{B} \ , \tag{3.9}$$

where $\theta \in [0, \pi/2]$ and $\hat{B} = \sum_l \lambda_l(\hat{b}_l^\dagger + \hat{b}_l)$, given by Eq. (2.4) specialized for a single bath. Choosing $\theta = 0$ realizes a coupling *longitudinal* to the driving direction, while $\theta > 0$ provides a *transverse* component.

It is worth stressing here the importance of the coupling direction chosen by θ. In Sec. 2.4.1, regarding the spin-boson model, we said that a coupling purely along $\hat{\sigma}^z$ was enough to capture all the physics, since for generic directions one can always choose a unitary transformation to bring the coupling along $\hat{\sigma}^z$, at the cost of a renormalization of the system Hamiltonian parameters. However, the situation is different in the present time-dependent setting: to align the coupling along $\hat{\sigma}^z$, one would need a time-dependent unitary transformation so that the renormalization of the parameters would imply a different non-trivial driving scheme with respect to Eq. (3.1). So, different coupling directions can lead to the emergence of different physics, as we will observe in Sec. 3.3. Notice that Eq. (3.9) is not in the most general form since the $\hat{\sigma}^y$ direction is missing. We made this choice for the sake of simplicity and in analogy with some previous literature. Both longitudinal and transverse couplings are in any case guaranteed by our simple choice. Another point to highlight is that we choose a *common bath* for both longitudinal and transverse couplings, while in principle one might as well take two different baths, even correlated between them. We studied the effect of two different independent baths on the same model, but we did not find any regime in which results are interestingly different from what we present in the following for a single common bath.

In our model, the coupling to the environment is captured, in the limit of a continuous distribution of frequencies, by an *ohmic* bath spectral function — see Eq. (2.6) — which in this setting looks

$$J(\omega) = 2\,\hbar^2\,\alpha\,\omega\,\mathrm{e}^{-\omega/\omega_c} \ , \tag{3.10}$$

with a cut-off frequency ω_c and an overall dimensionless coupling constant α, which encodes the coupling strength between the system and the environment. We will set $\omega_c = 10\Delta/\hbar$ from now on, since we have verified that our results are not qualitatively affected by the choice of the cut-off frequency.

In the spirit of the Landau-Zener problem discussed in Sec. 3.1, we start our numerical calculation at some large negative time $t_0 = -t_a$ — which we select such that $vt_a \gg \Delta$, so that the initial ground state $|\psi_{\rm gs}(t_0)\rangle$ is very close to being a $\hat{\sigma}^z$-eigenstate — and we assume the system and the bath to be decoupled and

defined by the state $\hat{\rho}_{\rm tot}^{in} = |\psi_{\rm gs}(t_0)\rangle\langle\psi_{\rm gs}(t_0)| \otimes \hat{\rho}_{\rm B}$, where $\hat{\rho}_{\rm B} = {\rm e}^{-\beta \widehat{H}_{\rm B}}/Z$ is the bath thermal equilibrium density matrix at temperature T, with $Z = {\rm Tr}({\rm e}^{-\beta \widehat{H}_{\rm B}})$ the bath partition function and $\beta = 1/(k_B T)$. The ensuing unitary dynamics is captured by the full evolution operator

$$\hat{\mathcal{U}}(t, t_0) = \mathcal{T}\exp\left(-\frac{i}{\hbar}\int_{t_0}^{t} dt'\ \widehat{H}_{\rm tot}(t')\right)\ , \tag{3.11}$$

where $\mathcal{T}$exp is the time-ordered exponential. Information on the two-level system — *e.g.* a qubit — is fully encoded in its reduced density matrix

$$\hat{\rho}_{\rm S}(t) = {\rm Tr}_{\rm B}\left(\hat{\mathcal{U}}(t, t_0)\hat{\rho}_{\rm tot}^{in}\hat{\mathcal{U}}^{\dagger}(t, t_0)\right) \tag{3.12}$$

and we can extract the probability that the qubit can be found in its (instantaneous) ground state $|\psi_{\rm gs}(t)\rangle$ at time t by computing the *ground state probability* as

$${\rm P}_{\rm gs}(t) = {\rm Tr}_{\rm S}\Big(\hat{\rho}_{\rm S}(t)\ |\psi_{\rm gs}(t)\rangle\langle\psi_{\rm gs}(t)|\Big)\ , \tag{3.13}$$

which generalizes Eq. (3.5) to density matrices. From the probability ${\rm P}_{\rm gs}(t)$ calculated at a large positive time $t_{\rm f} = -t_0 = t_a$, we obtain the quantity that effectively generalizes the LZ formula in Eq. (3.7),

$$P_{\rm gs}(v, T) \equiv {\rm P}_{\rm gs}(t_{\rm f})\ , \tag{3.14}$$

which turns out to be effectively independent of the value of t_a, provided $vt_a \gg \Delta$. In practice, choosing $vt_a = 200\Delta$ is enough to guarantee convergence to the infinite-time limit; this is the value used throughout this chapter, unless otherwise stated.

3.3 Numerical results

In this section, we present the main results of our paper [31] and bring evidence for the enhancement over the Landau-Zener probability due to a dissipative dynamics. Our data have been obtained through the Bloch-Redfield QME with and without RWA — see the differential equations computed in App. B.3 —, which have been tested against QUAPI data in several regimes, revealing the regimes of reliability. The differential equations have been solved by means of a standard IV order Runge-Kutta method. Notice that all the data from QME presented here are related to the differential equations obtained without RWA.

We start the section from a discussion of the zero temperature case, Sec. 3.3.1, where we find excellent agreement with the exact results of Ref.s [90, 91], at least at weak coupling. We anticipate here that the QME turned out to be surprisingly accurate for a purely-transverse coupling, even for strong interactions and very fast

drivings, as we will discuss. We then move to finite temperatures in Sec. 3.3.2. We benchmark again the QME against the numerically-exact QUAPI and interpret the results we obtain. We illustrate the thermal enhancement of the Landau-Zener probability, which constitutes the main finding of our work [31]. After that, in Sec. 3.3.3 we also discuss a simple single-oscillator-bath model, in terms of which the effect of finite temperature for a $\hat{\sigma}^x$-coupling becomes physically very transparent. Finally, in Sec. 3.3.4 we also test the impact of performing the RWA on the Bloch-Redfield QME.

3.3.1 Zero temperature

Let us start by discussing our results at zero-temperature. In this regime, we have a perfect benchmark for our QME approach given by the exact predictions by Hänggi and coworkers [90, 91], who showed that, in presence of a bath at $T = 0$ and for an evolution starting at $t_0 = -\infty$ and ending at $t_{\rm f} = +\infty$, the exact generalization of the Landau-Zener formula reads

$$P_{\rm gs}(v, T = 0) = 1 - {\rm e}^{-\frac{\pi W_\theta^2}{2\hbar v}} , \tag{3.15}$$

where W_θ, effectively replacing the tunnelling matrix element Δ in the standard Landau-Zener formula, for our ohmic bath choice is

$$W_\theta^2 = \left|\Delta - \alpha\hbar\omega_c \sin 2\theta\right|^2 + 2\alpha(\hbar\omega_c)^2 \sin^2\theta \, . \tag{3.16}$$

According to Eq. (3.16), the bath has no effect when acting only along $\hat{\sigma}^z$ since $W^2_{\theta=0} = \Delta^2$; on the contrary, it effectively increases the bare tunnelling amplitude Δ when, for instance, it acts along $\hat{\sigma}^x$ since $W^2_{\theta=\pi/2} = \Delta^2 + 2\alpha\omega_c^2$. (Incidentally, an identical enhancement would hold for a bath coupling along $\hat{\sigma}^y$.) This effective increase of the tunnelling amplitude leads to a definite *enhancement* of the probability to remain in the ground state $P_{\rm gs}(v, T = 0)$: we illustrate this in Fig. 3.3(a), where the exact predictions of Refs. [90, 91] reported in Eq. (3.15) are compared to the evolution data coming from the QME without RWA for two relatively weak values of the coupling α. The agreement is almost perfect at weak coupling and, as shown in Fig. 3.3(b), it also persists in a remarkable and puzzling fashion all the way *up to the strong coupling regime*. Therefore, our QME is extremely good for a pure transversal noise, $\theta = \pi/2$, even in the strong coupling regime. This excellent agreement diminishes, or even disappears, if the noise has a longitudinal component, as shown in Fig. 3.4, where the probability $P_{\rm gs}(v, T = 0)$ is plotted, for fixed driving velocities v, $v$ersus the noise coupling direction θ and for different coupling strengths α. The reason for this great reliability is still unclear to us, but we speculate that it might be linked to the fact that the system's dynamics is Markovian for a purely transversal coupling, while non-Markovian effects are more pronounced for a purely

longitudinal noise [53]. Indeed, we have checked the behaviour in time of the trace distance between pairs of random initial states both for $\theta = 0$ and $\theta = \pi/2$: in the former case, we have found non-monotonic trends, hinting that the dynamics must be non-Markovian [53]; in the latter case, we have found that the trace distance always monotonically decreases, as expected for Markovian dynamics [53].

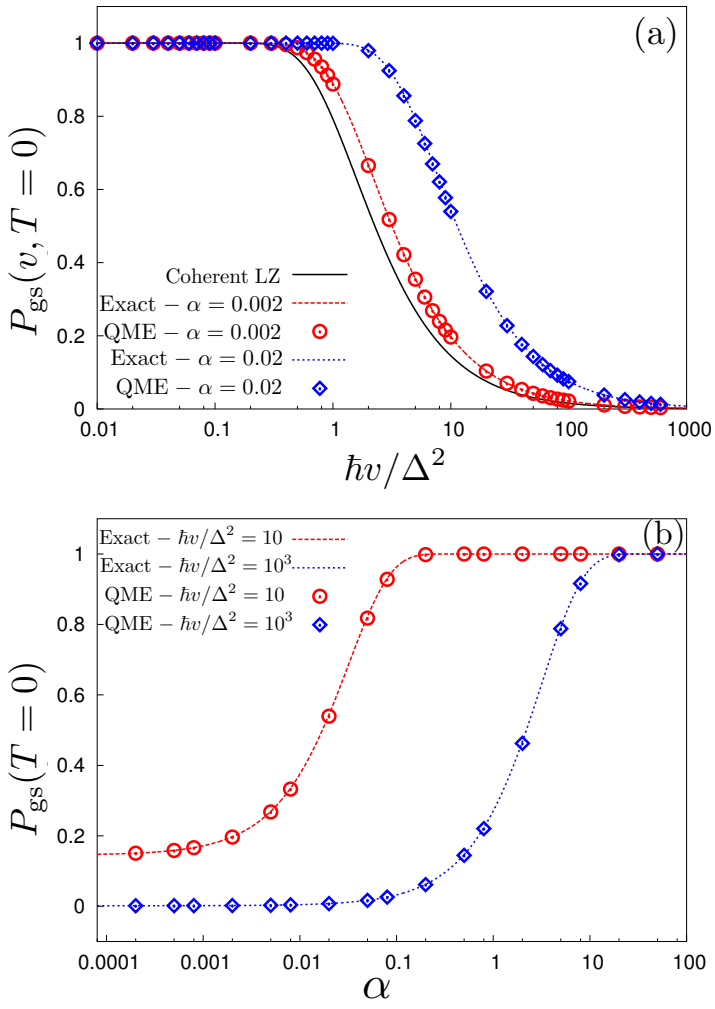

Figure 3.3: Check of the validity of the QME approach at zero temperature for a pure transversal noise, $\theta = \pi/2$. The probability to follow the ground state at zero temperature $P_{\rm gs}(T = 0)$ *v*ersus (a) the driving velocity $\hbar v/\Delta^2$ and (b) the coupling strength α. The lines are the exact predictions obtained using Eq. (3.15), while the points correspond to the solution of our QME without RWA, given in Appendix B.3. Here $\hbar\omega_c = 10\Delta$.

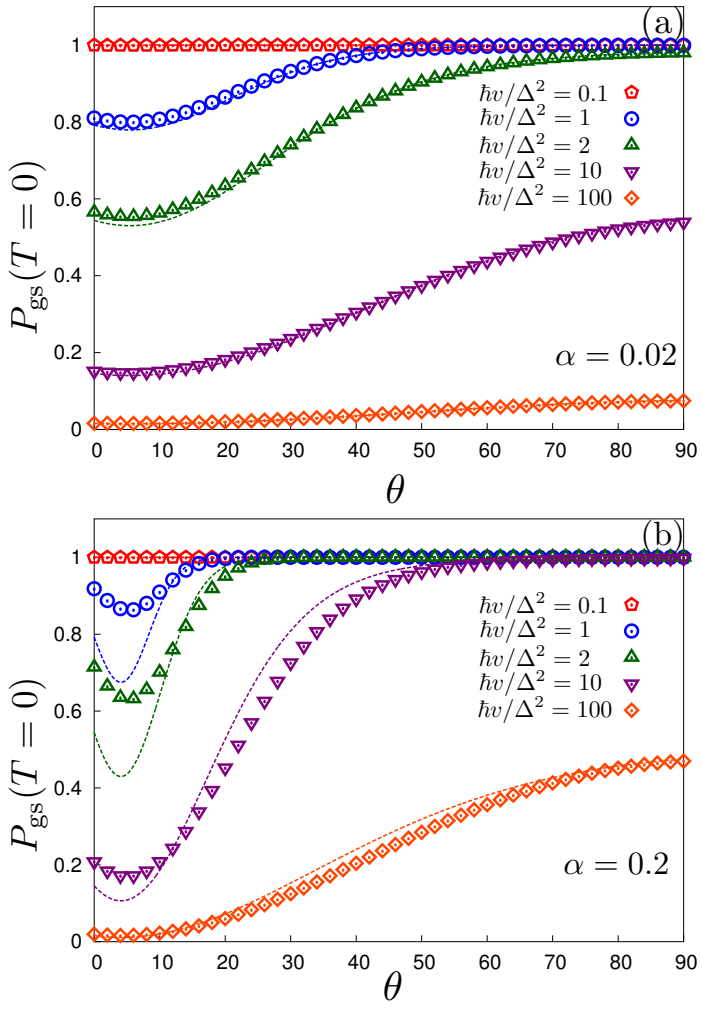

Figure 3.4: Check of the validity of the QME approach at zero temperature. Probability to follow the ground state $P_{\rm gs}(v, T = 0)$ for fixed driving velocities $\hbar v/\Delta^2$ *versus* the noise coupling direction θ for $\alpha = 0.02$ (a), and $\alpha = 0.2$ (b). Lines are the exact results of Ref. [91], points correspond to our QME without RWA, given in Appendix B.3.

3.3.2 Finite temperature

The previous discussion, besides witnessing the reliability of the QME at $T = 0$, has shown that a coupling transverse to the driving direction at $T = 0$ can improve the final ground state probability over the coherent value. The crucial question now is: will a finite-T bath improve or be detrimental to the $T = 0$ dynamics in presence of a transverse noise? The answer is given in Fig. 3.5, where we plot $P_{\rm gs}(v, T)$ versus the adiabatic parameter $\hbar v/\Delta^2$ for both purely longitudinal and transverse couplings, at different temperatures. Data are obtained by our QME without RWA, benchmarked with QUAPI, as we will discuss. Let us first consider the known purely longitudinal $\hat{\sigma}^z$-coupling case, $\theta = 0$, already studied in Ref.s [93, 101]. In Fig. 3.5(a), notice that increasing the bath temperature reduces $P_{\rm gs}(v, T)$ from the coherent evolution and $T = 0$ value $P_{\rm gs}(v, 0) = P_{\rm gs}^{\rm LZ}(v)$, and it does so in a rather non-monotonic fashion, depending on the coupling constant α, as previously reported [93, 101]. Therefore, no thermal improvement is found. But let us now focus on transverse noise. The data in Fig. 3.5(b) show a very intriguing behavior of $P_{\rm gs}(v, T)$ with temperature. Remarkably, for a sufficiently fast driving $\hbar v/\Delta^2 \gg 1$, a higher bath temperature can significantly enhance the performance of the annealing protocol with respect to the $T = 0$ case, hence effectively providing a *"thermally assisted" AQC* [33]. On the contrary, this beneficial effect of a bath-temperature increase disappears, turning into detrimental, in the opposite regime of small driving velocity $\hbar v/\Delta^2 \ll 1$.

At $T > 0$ no analytic results are available, and we therefore use QUAPI to benchmark our QME data. As Fig. 3.6 shows, the agreement between the QME results (lines) and the QUAPI data (points) is quite good in the weak coupling regime and (not shown) for all the temperatures for which a QUAPI simulation is feasible. Unfortunately, the QUAPI does not provide a very good benchmark for the $\theta = \pi/2$ case at finite temperature. The reason for this has to do with the Trotter error, which is proportional to $|\epsilon(t)|(\delta t)^3$, δt being the Trotter step. This implies that the Trotter error is very large at the initial and final stages of the evolution, where $|\epsilon(t)| = v|t| \gg \Delta$ unless the corresponding Trotter time δt is decreased accordingly. In practice, this makes large values of the evolution time-interval $[-t_a, t_a]$ intractable with QUAPI. Nevertheless, we have benchmarked our finite-T QME data by comparing against QUAPI the results of evolutions restricted to smaller time-intervals, with $vt_a \approx 20\Delta$, for which however $\mathrm{P}_{\rm gs}(t_{\rm f})$ deviates quantitatively from $P_{\rm gs}(v, T)$. In this way, as shown in Fig. 3.6(b), we verified a rather good agreement between QUAPI and QME also for transverse noise, for all the temperatures we have studied, at least in the weak-coupling region.

We also explored the strong coupling regime at finite temperature for a purely longitudinal coupling. In this case, the analysis was done only with QUAPI, as the QME would not be reliable at large values of α for $\theta = 0$. We find that $P_{\rm gs}(v, T)$ exhibits a non-monotonic behavior for increasing coupling α, at fixed v, especially relevant in the adiabatic driving regime (small $\hbar v/\Delta^2$). This is shown in Fig. 3.7,

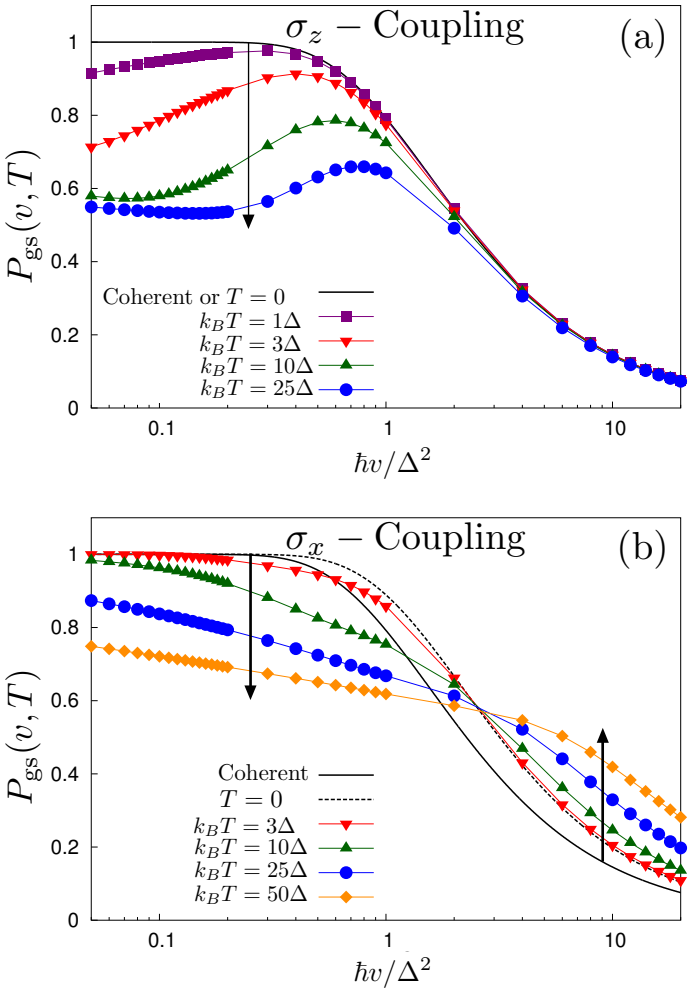

Figure 3.5: The probability $P_{\rm gs}(v,T)$ of remaining in the ground state of the Hamiltonian $\widehat{H}_{\rm S}(t)$ *versus* the driving velocity $\hbar v/\Delta^2$, for a purely longitudinal $\hat{\sigma}^z$-coupling (a) and for a purely transverse $\hat{\sigma}^x$-coupling (b) to the ohmic environment, with cut-off frequency $\omega_c = 10\Delta/\hbar$ and coupling $\alpha = 2\times10^{-3}$. The black solid line is the coherent-evolution result $P^{\rm LZ}_{\rm gs}(v)$, the black dashed line in panel (b) is the exact probability at zero temperature $P_{\rm gs}(v,T=0)$ obtained from Eq. (3.15) [90, 91], while the various points are QME (without RWA) data for different bath temperatures. Black arrows indicate the direction of increasing T. For a transverse coupling, *thermally assisted AQC* happens also at $T>0$, but only in the non-adiabatic region.

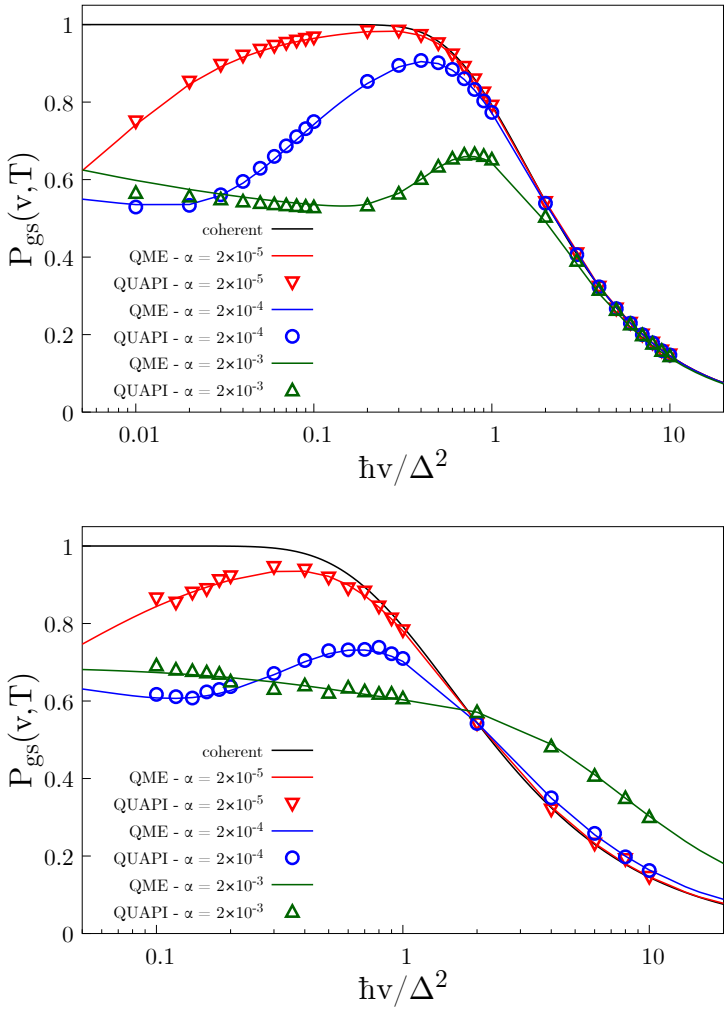

Figure 3.6: $\mathrm{P}_{\mathrm{gs}}(t_f)$ as a function of the driving $\hbar v/\Delta^2$ for pure longitudinal (top) and purely transverse (bottom) noise, at finite temperature $k_B T = 25\Delta$ and different values of the ohmic coupling strength α, with $\hbar\omega_c = 10\Delta$. Lines correspond to QME results, points to QUAPI. The black solid line shows, as a guide to the eye, $P_{\mathrm{gs}}^{\mathrm{LZ}}(v) \equiv P_{\mathrm{gs}}(v, T = 0)$. Notice that $\mathrm{P}_{\mathrm{gs}}(t_f) = P_{\mathrm{gs}}(v, T)$ only for the purely longitudinal noise.

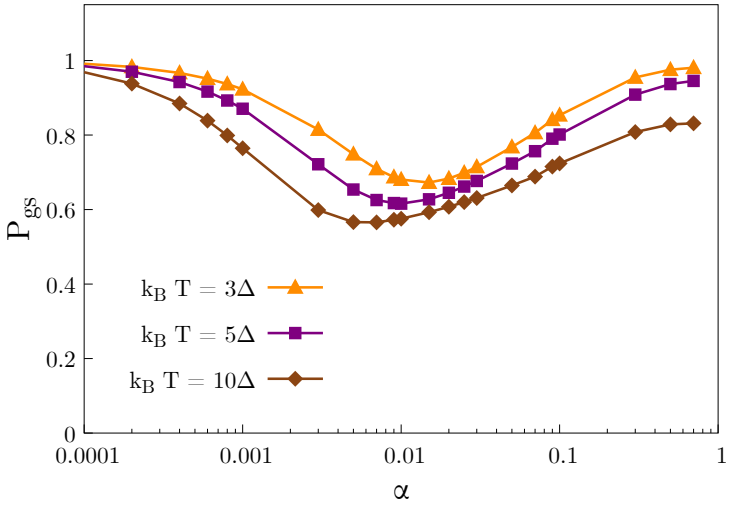

Figure 3.7: P_{gs} *versus* the ohmic coupling strength at a fixed driving velocity $\hbar v = 0.2\Delta^2$ and different bath temperatures. Data obtained using QUAPI, with $\hbar\omega_c = 10\Delta$.

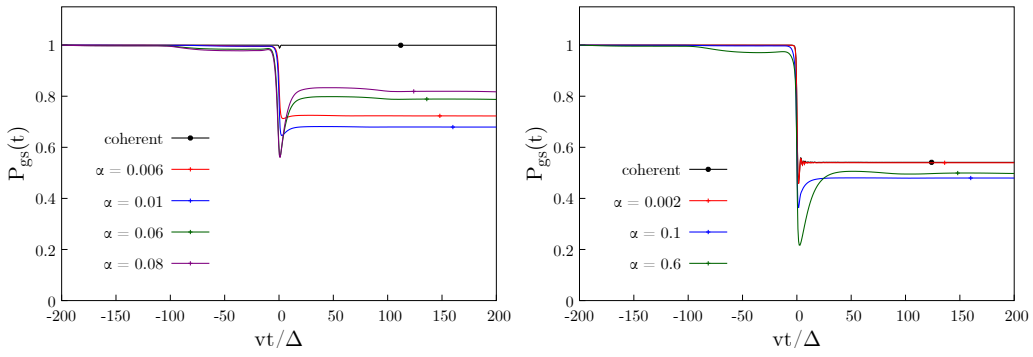

Figure 3.8: Detail of the time-evolving $P_{gs}(t)$ for "slow" (left, $\hbar v/\Delta^2 = 0.2$) and "fast" (right, $\hbar v/\Delta^2 = 2$) drivings, for various couplings α and $k_BT = 3\Delta$ and $\hbar\omega_c = 10\Delta$. Data obtained using QUAPI.

where we plot $P_{\rm gs}(v,T)$ at a fixed value of $\hbar v/\Delta^2 = 0.2$ and for different temperatures, as a function of the coupling constant α. While for weak coupling the probability $P_{\rm gs}(v,T)$ decreases as α increases, the inverse tendency, characterized by a $P_{\rm gs}(v,T)$ increasing back towards $P_{\rm gs}^{\rm LZ}$, is found when α increases beyond a certain T-dependent characteristic $\alpha_{min}(T)$. Although the dynamics tends to become more and more incoherent for large α, the overall form of $P_{\rm gs}(v,T)$ would be very close to the fully coherent value of $P_{\rm gs}^{\rm LZ}$, in agreement with the Fermi-Golden rule results of Ref. [102], obtained from a fully incoherent population-dynamics evolution. Figure 3.8 shows details of the dynamical evolution of $\mathrm{P}_{\rm gs}(t)$ obtained from QUAPI at different values of the parameters. In Fig. 3.8(left) the driving velocity is "small" ($\hbar v/\Delta^2 = 0.2$), the coherent evolution is essentially adiabatic, and we notice the effect of the finite-temperature bath in the form of a rather sharp decrease of $\mathrm{P}_{\rm gs}(t)$ around the transition region, followed by a partial recovery which tends to push $\mathrm{P}_{\rm gs}(t_{\rm f})$ towards values which are closer and closer to $P_{\rm gs}(v,T=0)$ as the coupling α becomes stronger. In Fig. 3.8(right) the driving velocity is rather "large" ($\hbar v/\Delta^2 = 2$): here we observe that while for small couplings $\mathrm{P}_{\rm gs}(t)$ is basically on top of the corresponding coherent evolution dynamics (including almost invisible, on the scale of the figure, coherent dynamics oscillations), at larger couplings the drop of $\mathrm{P}_{\rm gs}(t)$ is rather sharp and non-oscillatory, again with a partial recovery which tends to push $\mathrm{P}_{\rm gs}(t_{\rm f})$ towards $P_{\rm gs}(v,T=0)$ as the coupling α becomes stronger.

3.3.3 Single oscillator bath and the thermal enhancement mechanism

To better understand the physics behind the mechanism of dissipative improvement we just discussed, we consider a drastically simplified model of "environment", which is reduced to a *single harmonic oscillator* [103], with a fixed frequency Ω coupled to the system along a fixed direction in spin-space, parameterized as before with the angle θ. The Hamiltonian is therefore

$$\widehat{H}(t) = \widehat{H}_{\rm S}(t) + \hbar\Omega\hat{b}^\dagger\hat{b} + \lambda(\cos\theta\hat{\sigma}^z + \sin\theta\hat{\sigma}^x)(\hat{b}^\dagger + \hat{b}) \; . \tag{3.17}$$

According to the predictions of Ref. [91], such a zero-temperature "single-oscillator bath" would still lead to a $P_{\rm gs}(v,T=0)$ given by Eq. (3.15), where now

$$W_\theta^2 = \left|\Delta - \frac{2\lambda^2}{\hbar\Omega}\sin 2\theta\right|^2 + 4\lambda^2\sin^2\theta \; . \tag{3.18}$$

Notice that we can tune Ω and λ so as to get the same W_θ^2 we would have for a set of infinitely many harmonic oscillators with Ohmic spectrum (see Eq. (20) in Ref. [91]). Therefore, the behaviour of $P_{\rm gs}(v,T=0)$ for a Ohmic dissipative problem can be perfectly mapped into a specific "single-oscillator environment" coupled to the system. This analogy, which is in principle justified only for $T = 0$ and for

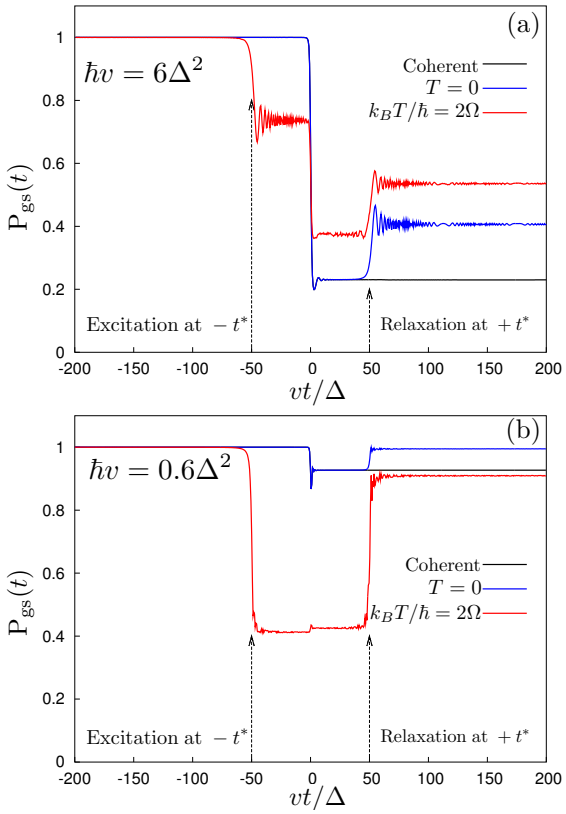

Figure 3.9: Single oscillator approach. Ground state probability $P_{gs}(t)$ versus time for (a) $\hbar v/\Delta^2 = 6$ and (b) $\hbar v/\Delta^2 = 0.6$. Here $\lambda = 0.5\Delta$ and $\theta = \pi/2$. The black line is the coherent evolution $P_{gs}(t)$ in absence of dissipation; the blue and red lines are $P_{gs}(t)$ at $T = 0$ and $k_BT = 2\hbar\Omega$, respectively. In both cases $\hbar\Omega = 50\Delta$. Vertical lines at $\pm t^*$, the resonance times in Eq.(3.19), highlight the excitation/relaxation mechanisms.

the infinite-time Landau-Zener problem, helps to elucidate some of the physics of the problem, which becomes very transparent in the single-oscillator setting. In the following we will take $\hbar\Omega = 50\Delta$ and a coupling $\lambda = 0.5\Delta$. The time evolution of this simple driven qubit can be studied both at zero and finite temperature utilizing an exact diagonalization-based Schrödinger dynamics, provided the oscillator Hilbert space is properly truncated. Fig. 3.9 shows the results of such a study for a purely transverse coupling $\theta = \pi/2$ in the non-adiabatic regime, $\hbar v/\Delta^2 = 6$ (a), and in the "adiabatic" regime $\hbar v/\Delta^2 = 0.6$ (b), compared to the "free" coherent evolution. We observe that a $\hat{\sigma}^x$-coupling "bath" is indeed active when the instantaneous gap of the qubit $E(t) = \sqrt{(vt)^2 + \Delta^2}$ matches exactly the oscillator energy $\hbar\Omega$. This

resonance condition happens at two times $\pm t^*$ with

$$t^* = \frac{1}{v}\sqrt{(\hbar\Omega)^2 - \Delta^2}\,, \tag{3.19}$$

in which excitation/relaxation of the system can take place by absorption/emission of a quantum of vibration. The final result is however very different depending on the driving velocity v. In the fast-driving regime, Fig. 3.9(a), immediately after the avoided crossing ($0 < t < +t^*$), the system ends up in the excited state with a significant probability, both at zero and at finite temperature. Thus, a relaxation mechanism occurring at $t = +t^*$ is quite effective in increasing $\mathrm{P_{gs}}(t)$ (the $\hat{\sigma}^x$-coupling providing the necessary matrix element at this resonant condition) above the coherent-dynamics probability (solid black line). We also observe that, at $T = 0$ (blue solid line), the relaxation associated with a resonant emission of a quantum of vibration at $t = +t^*$ is the only possible process, since the oscillator is unable to excite the system at $t = -t^*$. On the contrary, for $T > 0$ (red solid line), the bath can excite the qubit *before* the avoided crossing, by a resonant absorption of a quantum of vibration at $t = -t^*$. This effect, which reflects itself in a marked decrease of $\mathrm{P_{gs}}(t)$ at $t \sim -t^*$, is actually beneficial to the final ground state probability after the avoided crossing (where the instantaneous ground state is indeed flipped), providing an enhancement of $\mathrm{P_{gs}}(t)$ over the coherent evolution result at times $0 < t < +t^*$ (red solid line). Finally, the subsequent relaxation process at $t = +t^*$, although less effective than at $T = 0$, further improves the final probability $\mathrm{P_{gs}}(t_\mathrm{f})$ up and above the coherent evolution result. This state of matter changes if the driving velocity is small, as shown in Fig. 3.9(b), corresponding to $\hbar v/\Delta^2 = 0.6$. Here, the coherent dynamics is nearly adiabatic. While a zero temperature transverse bath further improves $P_\mathrm{gs}(v, 0)$ above $P_\mathrm{gs}^\mathrm{LZ}$, at finite T the combined effect of the excitation at $t = -t^*$ and the subsequent relaxation at $t = +t^*$ is eventually slightly detrimental.

3.3.4 Rotating-wave approximation

Until now, we have never shown results obtained from the QME with RWA. Indeed, we found that there is no compelling reason to adopt this approximation in the present time-dependent case, apart from a small simplification of the QME equations — see Appendix B.3. First, we have verified that our density matrix remains *positive definite at all times*, even if we do not have the master equation in Lindblad form. Furthermore, we overall find that the difference in the results obtained with and without RWA is rather small if one stays in the weak-coupling region.

Nevertheless, the RWA results tend to produce, as an artifact of the approximation, a certain tendency to increase $P_\mathrm{gs}(v, T)$ in the large v tails, above the coherent evolution result. We show this in Fig. 3.10, where we plot QME results obtained with and without RWA, benchmarked against numerically exact QUAPI data at the moderate coupling $\alpha = 0.02$. The RWA line shows a quite clear over-shooting above

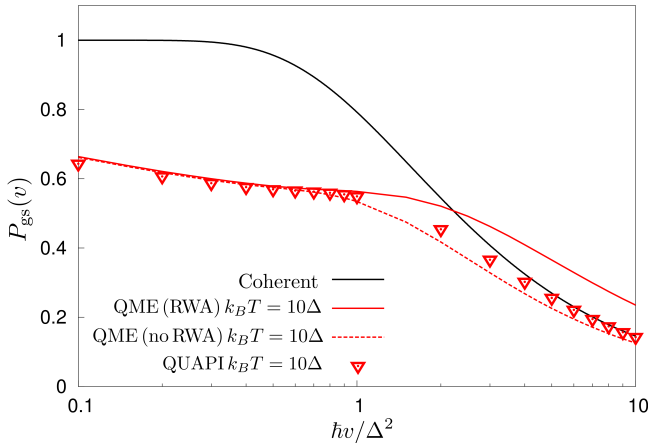

Figure 3.10: Comparison of QME results obtained with and without the RWA for a longitudinal bath coupling with $\alpha = 0.02$ and $k_BT = 10\Delta$. The points denote numerically exact QUAPI data. The RWA line shows a quite clear over-shooting above the coherent evolution result, which is an artifact of the approximation.

the coherent evolution result. This over-shooting was also found in Ref. [101], where the QME with RWA was used, but there no benchmark was used to test whether the results were reliable or not.

3.3.5 Sub/super-ohmic bath spectral functions

We explore here the cases of *sub-ohmic* and *super-ohmic* bath spectral functions (not presented in Ref. [31]). Let us stress that our approach is not strictly valid in the sub-ohmic case. The reason is that the analytic expression of the Fourier transform of the correlation function, $\gamma(\omega)$, is no more well defined in the limit $\omega \to 0$. Indeed, looking at Eq. (A.3) in Appendix A, while for a super-ohmic spectral function we would have $\gamma_{sup}(\omega \to 0) = 0$, for any sub-ohmic case the same quantity would diverge. We try to go on ignoring this issue and setting $\gamma_{sub}(\omega \to 0) = 0$ even for the sub-ohmic case. We will see that this very rude and unjustified act of violence provides anyway good results against our benchmarks.

Let us start from $T = 0$. From the exact results in Ref.s [90, 91], we know that for a purely longitudinal coupling dissipation does not change the coherent Landau-Zener probability. We found exactly the same from our data. For a purely transverse coupling, we obtain again very good agreement, especially in the super-ohmic case, as can be seen from Fig. 3.11. Regarding the sub-ohmic case, if at $\alpha = 0.002$ the discrepancy between exact and numerical results is almost invisible to the eye (not shown), we see that this difference increases as α is raised. Indeed, as the coupling strength becomes bigger, the terms we are neglecting at zero frequency

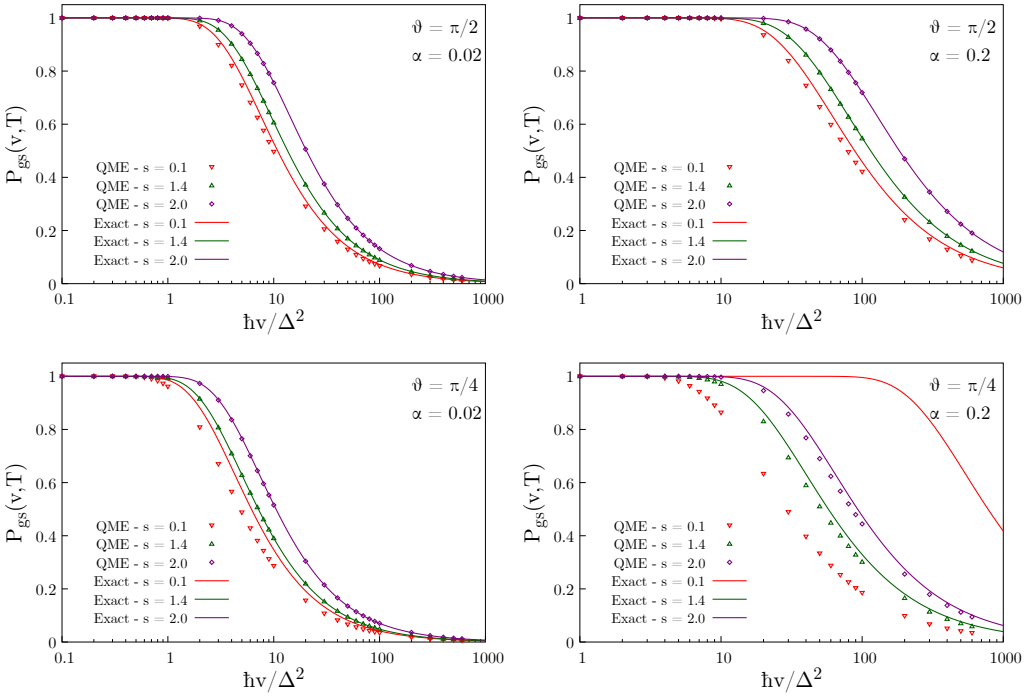

Figure 3.11: QME data tested against the exact results in Ref.s [90, 91], for different sub/super-ohmic coefficients s in the spectral function defined in Eq. (2.7), at $\alpha = 0.02, 0.2$ and $\theta = \pi/2, \pi/4$.

are probably becoming more important. Fig. 3.11 also shows the case of mixed couplings ($\theta = \pi/4$). In this setting the agreement becomes slightly worse, but this is consistent with our previous analysis of the ohmic case. Notice however that the sub-ohmic calculation fails terribly at the intermediate $\alpha = 0.2$.

Finally, let us turn to the finite temperature case and purely longitudinal coupling, where we can safely use QUAPI. Fig. 3.12 benchmarks the QME against QUAPI for different sub/super ohmic coefficients, and compares the data with the coherent Landau-Zener probability. We observe good agreement between the two methods, even for the sub-ohmic cases, despite our crude approximation. Furthermore, we find no thermally assisted AQC even in this case, although Ref. [33] argues that a super-ohmic environment can provide it.

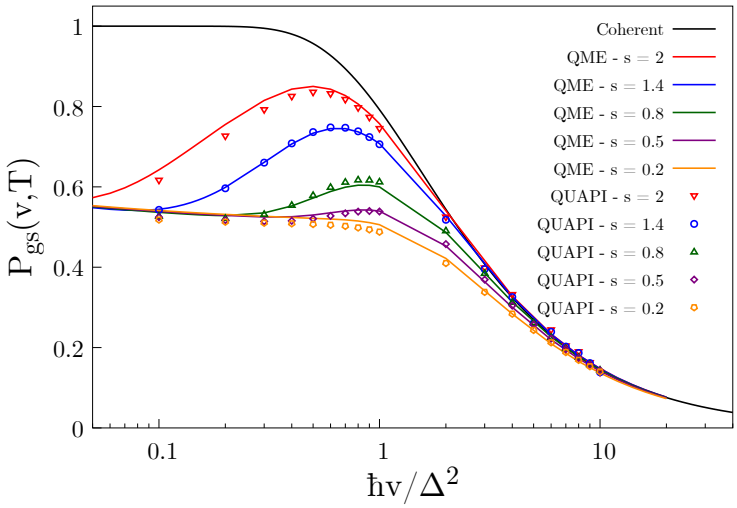

Figure 3.12: Final ground state probability *versus* the adiabatic parameter for $\theta = 0$ and different sub/super-ohmic coefficients s in Eq. (2.7). Lines are obtained from the QME, points from QUAPI. We highlight a very good agreement and find no thermal improvement over the coherent curve (black line).

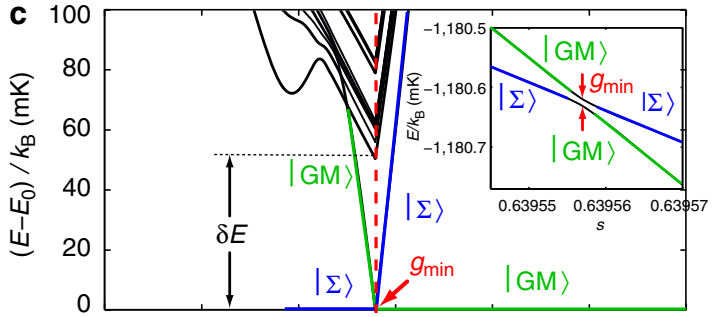

Figure 3.13: Copy of Fig. 2(c) in Ref. [34]. Difference between each energy level and the instantaneous ground state *versus* time. In the inset, a zoom on the avoided crossing region, which is engineered to be extremely narrow.

3.4 Final remarks

In this study, we have investigated the role of the bath temperature and the spin-coupling direction in a simple dissipative LZ model, showing that thermally assisted AQC requires a transverse component of the coupling and is generally effective only in the fast driving regime. In this setting, we have also benchmarked the Bloch-Redfield QME, reporting a very good reliability, especially for a purely transverse system-bath interaction.

We can now try to discuss the results of Ref. [34] in the light of our findings. Ref. [34] deals with an explicit realization of an approximate two-level system LZ dynamics using 16-qubit of the D-Wave® machine. For the reader's convenience, in Fig. 3.13 we have reproduced Fig. 2(c) of Ref. [34], which illustrates the scheme of the energy levels for that model. The gap at the anti-crossing between the two low-lying instantaneous eigenstates is engineered to be rather small, $\Delta = g_{min} = 0.011$ mK/k_B, compared to a rather large energy separation, $\delta E \approx 50.5$ mK/k_B, from all the higher-lying states. In the experiment, several annealing runs are performed at different driving velocities and temperatures, with T ranging from $T_{\rm low} = 19.9$ mK up to 100.8 mK. Particularly interesting are the first four temperature datasets, ranging from $T_{\rm low}$ up to $T_{\rm high} = 34.9$ mK, where the two-level-system approximation is reasonable, since $k_B T < \delta E$. The extrapolation of the lowest experimental annealing data down to $T = 0$ (see Fig. 3 of Ref. [34], reproduced here in Fig. 3.14) allows to extract $P_{\rm gs}(v, T = 0)$, which closely matches a Landau-Zener type of expression. This is, in a sense, not surprising, because of the exact results of Refs. [90, 91]; it is also perfectly in line with the Fermi golden rule findings in the incoherent-tunnelling-dominated regime associated with a significant sub-ohmic flux noise [102], as well as with the seminal analysis by Ao and Rammer [89]. But, as we have discussed, a LZ form is rather generic: it does not tell you if the coupling is predominantly in the longitudinal $\hat{\sigma}^z$-direction, or if there is some component of transverse noise.

The finite-T experimental curves with $T = 19.9 \div 34.9$ mK are in some sense an argument in favour of the fact that *there should be some transverse noise* affecting the annealing dynamics. Indeed, Fig. 4 of Ref. [34] (reproduced here in Fig. 3.14) clearly shows that $P_{gs}(v, T)$ is considerably improved over the $T = 0$ curve in its fast-driving tail, which would be impossible with a purely longitudinal noise. Consistently with our findings, this "thermally assisted" QA turns into a detrimental effect in the slow-driving regime. What is hard to explain from our very rough modelling is the fact that the experimentally extracted $P_{\rm gs}(v, T)$ remains quite different from $1/2$ — the value you would expect at $T = \infty$ — at temperatures which are incredibly large compared to the minimum gap, $k_B T/\Delta = 1809 \div 3172$. A detailed understanding of the experimental findings needs a more refined modelling, possibly including time-dependence of the couplings to the environment, as well as the possible presence of sub-ohmic noise components, very hard to tackle with traditional QME weak-coupling techniques. Actually, more than one year after our publication, the study presented in Ref. [104] reproduced qualitatively the results of the experiment in Ref. [34]. The authors developed a theory that includes both low and high-frequency noise, treating the low-frequency one non-perturbatively. They directly studied the complicated 16-qubits problem, without focusing however on the simpler dissipative Landau-Zener model.

In the future, the role of a $\hat{\sigma}^y$-coupling, which we have not explicitly addressed, might also be worth looking at. Indeed $\hat{\sigma}^y$ is precisely the Hamiltonian term realising the *shortcut to adiabaticity* [105], or *transitionless quantum driving*, in Berry's terminology [106], in our LZ problem: this is clear from the presence of the $\dot{\phi}_t\, \hat{\sigma}^y$ term in the rotated Hamiltonian in Eq. (B.25), see also Ref. [107]. Clearly, the possible time-dependence of the bath-couplings, inherited by projecting the two lowest-lying instantaneous eigenstates into an effective two-level system, might also play a role, especially because the larger transverse field present before the anti-crossing might favour thermal excitations over the thermal relaxations phenomena occurring after the anti-crossing [34]. Further work is necessary to fully elucidate all these aspects.

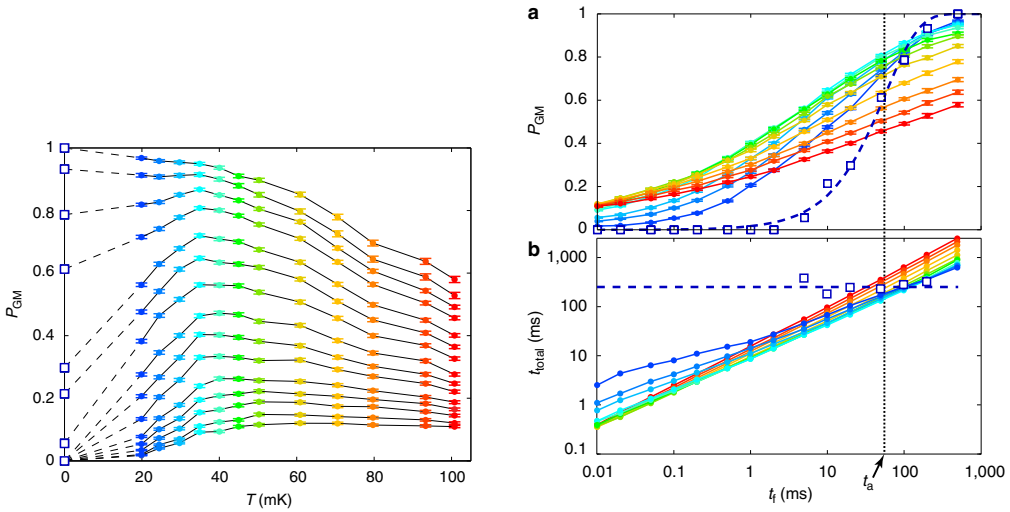

Figure 3.14: Copy of Fig.s 3-4 of Ref [34]. *Left panel:* Final ground state probability $P_{\rm GM}$ *versus* the measured temperature T. Notice the (very rough) extrapolation of the $T = 0$ data by the dashed lines. *Right panel:* (a) Final ground state probability *versus* the annealing time (inversely proportional to our annealing velocity v). The blue dashed line indicates the extrapolated $T = 0$ data, while the others correspond to finite T. Notice how finite T probabilities are above the $T = 0$ ones in the fast driving regime, consistently with our results. (b) Total time needed to achieve $P_{\rm GM} = 0.99$ by running each annealing of length t_f several times, *versus* t_f. From these data, due to dissipation, it seems advantageous to perform very fast annealing runs several times, rather than one very slow and long one.

Chapter 4

Optimal working point in dissipative QA

In this chapter we present our second work, published in Ref. [32], in which we investigate how dissipation from a thermal bath can affect the QA dynamics on a quantum spin-1/2 Ising chain in driven transverse field. It is a simple realization of the general QA Hamiltonian written in Eq. (1.3), where the driven transverse field plays the role of the parameter $s(t)$ connecting target and driving Hamiltonians. Although simple, this model presents a second-order phase transition from order to disorder [108], very useful to study the performance of QA while crossing a critical point, where the gap is closing polynomially in the system size and hence no adiabatic time-scale exist in the thermodynamic limit. To estimate the closeness to the final ground state, one defines the so-called *density of defects*, quantifying the number of anti-aligned spins with respect to the perfectly ferromagnetic final ground state [109]. For a closed system, taking $s(t) = t/\tau$ with τ the annealing time, the density of defects is known to behave as $n_{\rm def}(\tau) \simeq \tau^{-1/2}$, following a Kibble-Zurek (KZ) scaling law [109]. Therefore, the density of defects monotonically decreases as τ becomes larger — that is, the driving is more adiabatic.

The presence of dissipation, however, leads to a different physics. There have been a few studies on the topic: some of them have employed a classical Markovian noise superimposed to the driving field [38, 110, 111] or a Lindblad master equation with suitable dissipators [112, 54]; others have considered the effect of one or several bosonic baths coupled to each spin along the transverse direction [113, 114, 115, 116]. The general common feature that emerges from these studies is that the density of defects stops following the KZ scaling after a certain τ, and starts to increase again. This can be seen in Fig. 4.1, where we report some results presented in Ref.s [110, 54]. This effect has been referred to as *anti-Kibble-Zurek* (AKZ) [1] [110]. This is, in turn,

[1] It is worth mentioning that the term "anti-Kibble-Zurek" appeared for the first time in a completely classical setting, the adiabatic dynamics of multiferroic hexagonal manganites [117], with the crucial difference that the deviation from the expected KZ scenario is there seen as an

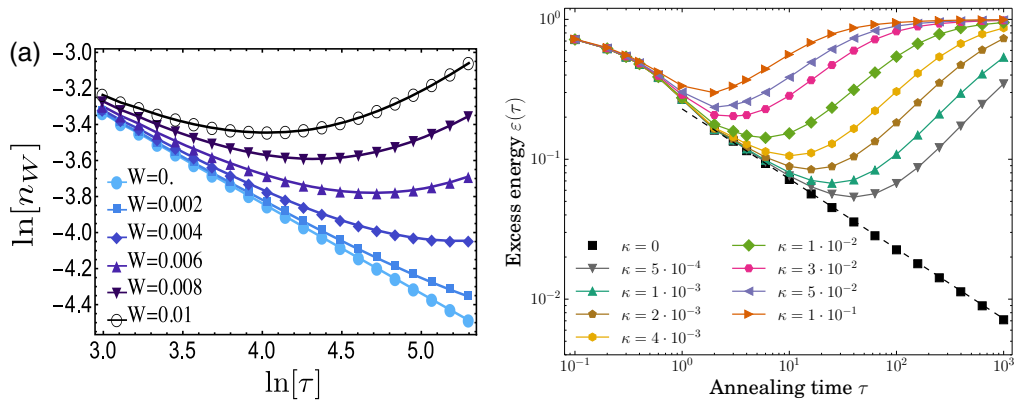

Figure 4.1: Closeness to the final ground state *versus* the annealing time for Ref. [110] (left) and Ref. [54] (right), for different noise strengths. Almost all the data display the AKZ behaviour, with the presence of a global minimum (the OWP), even though in the left panel it is unclear whether this global minimum would appear also at longer annealing times or not.

intrinsically linked to the presence of a *minimum* of $n_{\rm def}(\tau)$ at some intermediate $\tau_{\rm opt}$, known as *Optimal Working Point* (OWP).

In this work, we reconsider these issues in the setting of a thermal bath in interaction with our system. Remarkably, we find that the OWP disappears below a certain temperature, which depends on the system-bath coupling. The possible situations we encounter are summarized in Fig. 4.2, where the density of defects is plotted as a function of the annealing time τ, for various temperatures and fixed system-bath coupling strengths. Notice that three different situations may emerge, in which $n_{\rm def}(\tau)$ either shows a global or local minimum at some $\tau_{\rm opt}$ (*i.e.* the global/local OWP), and situations where $n_{\rm def}(\tau)$ deviates from the simple coherent-dynamics KZ-scaling, but is still monotonically decreasing, hence no OWP is found. Quite remarkably, as we shall discuss later on, the range of temperatures that are relevant for current quantum annealers is such that one would predict the *absence* of an OWP. We will further comment on the validity of the often-used assumption that the density of defects can be computed as a simple sum of two contributions [113, 114, 110, 115, 54]: one given by the purely coherent dynamics, the other coming from a time-evolution governed only by dissipators, *i.e.* neglecting the coherent part. Since we consider also regimes for which relaxation processes after the critical point are important, we will provide evidence that this additivity assumption breaks down for large enough annealing times.

unexplained decrease of $n_{\rm def}(\tau)$ for *fast* annealings, i.e., for $\tau \to 0$. This opposite trend leads to a *maximum* of $n_{\rm def}(\tau)$ for intermediate τ and, as far as we understand, has nothing to do with AKZ which we will address here in our quantum mechanical framework.

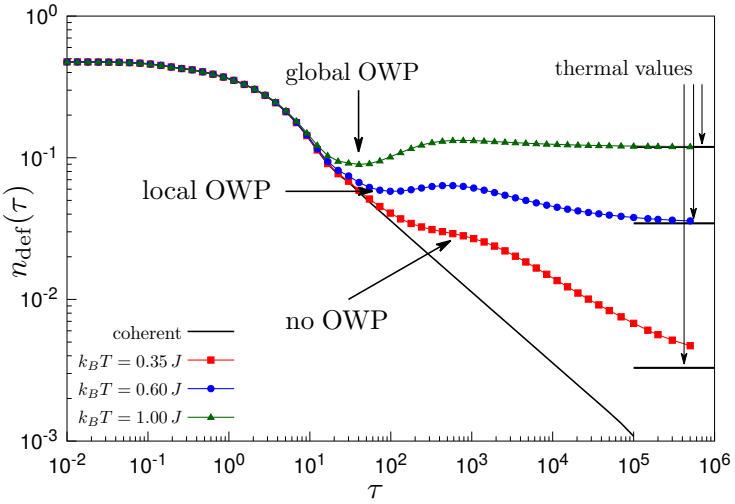

Figure 4.2: Density of defects *versus* annealing time for a quantum Ising chain weakly coupled to an ohmic bath, at different bath temperatures T, compared to the ideal coherent evolution (KZ) behaviour, $n_{\rm def}(\tau) \sim \tau^{-1/2}$. The plot highlights the three distinct behaviours we have found: $n_{\rm def}(\tau)$ can *i*) display a global minimum (green triangles), *ii*) a local minimum (blue circles), *iii*) converge monotonically towards a large-τ thermal plateau (red squares). Here the system-bath coupling constant is kept fixed at $\alpha = 10^{-2}$.

4.1 The dissipative quantum Ising chain in transverse field

The quantum spin-1/2 Ising chain in a driven transverse field is described by the following Hamiltonian [118]:

$$\widehat{H}_{\rm S}(t) = -J \sum_{i=1}^{N} \left[\hat{\sigma}_i^x \hat{\sigma}_{i+1}^x + h(t) \hat{\sigma}_i^z \right], \tag{4.1}$$

where $\hat{\boldsymbol{\sigma}}_i \equiv \left(\hat{\sigma}_i^x, \hat{\sigma}_i^y, \hat{\sigma}_i^z\right)$ are the usual Pauli matrices on the $i^{\rm th}$ site, N the number of sites, $J > 0$ the ferromagnetic coupling strength, and $h(t) \geq 0$ the external (driving) field, which is turned off during the evolution. Periodic boundary conditions (PBC) are assumed, *i.e.* $\hat{\boldsymbol{\sigma}}_{N+1} = \hat{\boldsymbol{\sigma}}_1$. This problem can be analytically tackled by means of a standard Jordan-Wigner transformation, followed by a Fourier transform [119, 120], which allows to rewrite Eq. (4.1) in terms of spinless fermions operators $\hat{c}_k$ in momentum space

$$\widehat{H}_{\rm S}^F = \sum_{k>0} \left[\xi_k(t) (\hat{c}_k^\dagger \hat{c}_k - \hat{c}_{-k} \hat{c}_{-k}^\dagger) + \Delta_k (\hat{c}_k^\dagger \hat{c}_{-k}^\dagger + \text{H.c.}) \right], \tag{4.2}$$

where $\xi_k(t) = 2J\big(h(t) - \cos k\big)$ and $\Delta_k = 2J \sin k$. The k values in the sum depend on the considered fermionic sector, since $\widehat{H}_{\rm S}^F$ commutes with the fermion parity [109]. The initial ground state belongs to the even-parity sector for any value of the transverse field, hence the time-evolving state always belongs to that sector. Due to this fact, one can restrict the choice of the k values to $k = \pi(2n-1)/N$, with $n = 1, \ldots, N/2$, thus fixing the antiperiodic boundary conditions (ABC) for fermions. With this approach, one can very easily compute the dynamics of the full system as the dynamics of $N/2$ two-level systems, overcoming the problem of the exponentially growing Hilbert space.

Let us now introduce dissipation in this setting. As before, we assume a total Hamiltonian in the form of Eq. (2.1), *i.e.* $\widehat{H}_{\rm tot}(t) = \widehat{H}_{\rm S}(t) + \widehat{H}_{\rm B} + \widehat{H}_{\rm SB}$. In analogy with Ref. [115], we write the system-bath interaction Hamiltonian as

$$\widehat{H}_{\rm SB} = -\frac{1}{2}\sum_{i=1}^{N} \hat{\sigma}_i^z \otimes \hat{B}, \tag{4.3a}$$

$$\hat{B} = \sum_l \lambda_l (\hat{b}_l^\dagger + \hat{b}_l), \tag{4.3b}$$

where the $\hat{b}_l$ are bosonic annihilation operators, and λ_l are the system-bath coupling constants. The bath Hamiltonian is taken, as usual, as $\widehat{H}_{\rm B} = \sum_l \hbar\omega_l \hat{b}_l^\dagger \hat{b}_l$, where ω_l are the harmonic oscillator frequencies. The coupling between the system and the environment is captured by the ohmic spectral function already defined in Eq. (2.6), where α quantifies the system-bath coupling strength and ω_c is a cutoff frequency. Notice that here we are considering a *single* (common) bath, which is coupled to all the spins along the z-direction, as done in Ref. [115]. This is, essentially, the quantum version of a noise term acting on the transverse field, whose classical counterpart was treated in Refs. [38, 110].

To solve for the dissipative dynamics induced by a generic form of the interaction, one would in principle take into account the full system density matrix. But, unfortunately, this becomes a very challenging problem as soon as the size of the system grows above few sites. However, the specific choice of system-bath coupling in Eq. (4.3a), which generates infinite-range correlations between all the spins in the chain, allows us to proceed, after further simplifying assumptions, with simple perturbative QMEs for two-level systems. The fact that the single bath operator $\hat{B}$ couples to a translationally invariant term, $\sum_i \hat{\sigma}_i^z = -2\sum_{k>0}(\hat{c}_k^\dagger \hat{c}_k - \hat{c}_{-k}\hat{c}_{-k}^\dagger)$, ensures momentum conservation for the fermions. As argued in Ref. [115], this in turn implies that the self-energy for the one-body fermionic Green's function is k-diagonal, and all fermionic momenta connected to the external lines have momentum k. Different momenta $k' \neq k$ appear only in closed internal loops. At the lowest order level (second-order) and within the usual Markovian approximation, the tadpole diagram, which contains a loop, simply provides a shift of energy levels and

can be neglected, while the only relevant self-energy diagram has momentum k in the fermionic internal line [114]. This suggests that, at least at weak coupling and within a Born-Markov approximation, it is legitimate to assume that each momentum k does not interact with other momenta $k' \neq k$, and that we could write the coupling to the bath as

$$\widehat{H}_{\rm SB} = \sum_{k>0} (\hat{c}_k^\dagger \hat{c}_k - \hat{c}_{-k} \hat{c}_{-k}^\dagger) \otimes \hat{B}_k, \tag{4.4a}$$

$$\hat{B}_k = \sum_l \lambda_l (\hat{b}_{l,k}^\dagger + \hat{b}_{l,k}), \tag{4.4b}$$

and $\widehat{H}_{\rm B} = \sum_{k>0} \sum_l \hbar\omega_l \, \hat{b}_{l,k}^\dagger \hat{b}_{l,k}$, where we have effectively replicated the original unique bath into $N/2$ identical copies, one for each fermionic k-value, all with identical bath spectral function $J(\omega)$. This choice greatly simplifies the problem, since the total Hamiltonian can be written as a sum in k-space:

$$\widehat{H}_{\rm tot}(t) = \sum_{k>0} \widehat{H}_k(t). \tag{4.5}$$

This automatically leads to an ensemble of independent dissipative two-level systems. Indeed, it is convenient to map the even-parity fermionic Hilbert space to a collection of pseudo-spin-1/2 quasiparticles, one for each $k > 0$, with the identification $|\uparrow\rangle_k \equiv \hat{c}_k^\dagger \hat{c}_{-k}^\dagger |0\rangle$, and $|\downarrow\rangle_k \equiv |0\rangle$. Introducing the pseudo-spin Pauli matrices $\hat{\boldsymbol{\tau}}_k \equiv \left(\hat{\tau}_k^x, \hat{\tau}_k^y, \hat{\tau}_k^z\right)$ to represent such two-dimensional space, the Hamiltonian for each k mode reads

$$\widehat{H}_k(t) = \left(\xi_k(t) + \hat{B}_k\right) \hat{\tau}_k^z + \Delta_k \, \hat{\tau}_k^x + \sum_l \hbar\omega_l \, \hat{b}_{l,k}^\dagger \hat{b}_{l,k} \, . \tag{4.6}$$

Hence, as anticipated, each driven two-level system is coupled with its own bath of harmonic oscillators through a $\hat{\tau}_k^z$ term. It is worth to stress that this simplifying assumption of k-decoupled baths does not modify the thermal steady state that the system reaches at long time, as we will explicitly show in a short while.

Summarizing the previous discussion, for our specific choice of the system-bath coupling, the dissipative dynamics of a translationally invariant quantum Ising chain can be computed by studying the time evolution of $N/2$ two-level systems in momentum space, each coupled to an *independent identical* bath, described by a Gibbs density matrix at temperature $T_b = (k_B \beta_b)^{-1}$, where k_B is the Boltzmann's constant:

$$\hat{\rho}_{\rm B} = \frac{{\rm e}^{-\beta_b \widehat{H}_{\rm B}}}{{\rm Tr}\left\{{\rm e}^{-\beta_b \widehat{H}_{\rm B}}\right\}} \, . \tag{4.7}$$

One might wonder how reasonable is our rather special choice of bath in representing the dissipative dynamics of an Ising chain. To answer this question, we have looked at the relaxation towards equilibrium at fixed values of the transverse field,

by solving the corresponding Bloch-Redfield QME — see Appendix (B.3) — through a IV order Runge-Kutta method. Any reasonable weakly coupled bath at temperature T_b should allow the system to reach thermal equilibrium values for the operators one wants to measure. This is indeed what our Bloch-Redfield QME does, but the equilibrium temperature T that the system reaches is actually given by $T = T_b/2$, for a reason which is discussed in detail in Appendix C. In essence, a peculiarity of our bath-coupling is momentum conservation. For each of the $N/2$ sectors at fixed k there would be four different possible states, $\{\hat{c}_k^\dagger|0\rangle, \hat{c}_{-k}^\dagger|0\rangle, \hat{c}_k^\dagger\hat{c}_{-k}^\dagger|0\rangle, |0\rangle\}$, but the dissipative dynamics remains always restricted to just two of them, $\{\hat{c}_k^\dagger\hat{c}_{-k}^\dagger|0\rangle, |0\rangle\}$, *i.e.* those with presence or absence of pairs of fermions with opposite momenta. States with only one fermion of momentum k or $-k$, $\{\hat{c}_k^\dagger|0\rangle, \hat{c}_{-k}^\dagger|0\rangle\}$, cannot be reached. This does no justice to the equilibrium thermodynamics, which takes into account *all states* in the Hilbert space, $2^N = 4^{N/2}$, and not only a dynamically conserved subspace of dimension $2^{N/2}$. It turns out, however, that accounting for such a part of the Hilbert space simply amounts to having a temperature $T = T_b/2$, see Appendix C for details. Hence, in all the plots we always indicate the effective temperature $T = T_b/2$ that the system would reach at thermodynamic equilibrium, rather than the bath-temperature T_b used in our simulations.

4.2 Numerical results

Before presenting our results, it is mandatory to introduce the QA protocol we are going to simulate, and the figure of merit we will use to quantify its performance. We choose to vary the external field $h(t)$ in Eq. (4.1) in the time interval $t \in [0, \tau]$, where τ denotes the total annealing time, and implement a standard linear schedule $h(t) = (1 - t/\tau)\, h_0$, where h_0 is the initial value of the field. In this way, the annealing crosses the zero-temperature critical point of the quantum Ising chain, $h_c = 1$, separating a paramagnetic phase ($h > h_c$) from a ferromagnetically ordered phase ($h < h_c$) in the $\hat{\sigma}^x$ direction. In all the numerical calculations, we fix the number of sites at $N = 1000$. Concerning the bath, we choose $\hbar\omega_c = 10J$ as cutoff frequency in the ohmic spectral function. The initial condition $\hat{\rho}_{\rm S}^{(k)}(0)$ is chosen to be the ground state of $\widehat{H}_{\rm S}^{(k)}(0)$ for $h(0) = h_0 \gg 1$ (we fix $h_0 = 10$). The time evolution of $\hat{\rho}_{\rm S}^{(k)}(t)$ is then calculated by integrating the corresponding equations of motion by means of a standard fourth-order Runge-Kutta method. These equations are provided in Appendix B.3.

To assess the quality of the annealing, we compute the average density of defects [109, 121] over the ferromagnetic classical Ising state. In the original spin language, the operator counting such defects reads

$$\hat{n}_{\rm def} = \frac{1}{2N} \sum_{i=1}^{N} \left(1 - \hat{\sigma}_i^x \hat{\sigma}_{i+1}^x\right) . \tag{4.8}$$

Translating it into fermions and pseudo-spins, we can write the desired average as:

$$n_{\rm def}(t) = \frac{1}{N}\sum_{k>0} \mathrm{Tr}\{\hat{n}_{\rm def}^{(k)}\,\hat{\rho}_{\rm S}^{(k)}(t)\} \tag{4.9}$$

where $\hat{n}_{\rm def}^{(k)} = \mathbb{1} - \hat{\tau}_k^z \cos k + \hat{\tau}_k^x \sin k$.

In the following, we discuss the dependence of the final density of defects $n_{\rm def}(t = \tau)$ on the annealing time τ, for different system-bath coupling strengths α and temperatures $T = T_b/2$. In particular, we characterise the regimes for which an OWP is present or not, and study how the defect density approaches thermal values for long annealing times. We also analyse the conditions under which the processes of coherent and incoherent defect production can be regarded as independent, and highlight regimes in which this assumption fails.

4.2.1 The optimal working point issue

Let us start by looking at the behaviour of the final density of defects $n_{\rm def}(\tau)$ as a function of the annealing time τ. In Fig. 4.3 we consider $\alpha = 10^{-3}$ and 10^{-2}, for which we have seen in the previous chapter that our perturbative approach is reliable [31], and different values of T. For sufficiently high temperatures, we observe a clear AKZ trend: after the initial decrease, $n_{\rm def}(\tau)$ attains an absolute minimum at some value $n_{\rm opt} = n_{\rm def}(\tau_{\rm opt})$ — corresponding to the OWP $\tau_{\rm opt}$ — and then starts to increase again towards a large-τ plateau at $n_\infty = n_{\rm def}(\tau \to \infty)$. By decreasing T, however, the plateau value n_∞ can become smaller than $n_{\rm opt}$, hence $\tau_{\rm opt}$ would correspond to a *local minimum* — surrounded by two inflection points where the second derivative changes sign — and should be called, strictly speaking, a "*local* optimal working point". A further reduction of T leads to the disappearance of the local minimum at $\tau_{\rm opt}$ — by a merging of the two inflection points —, with a monotonic decrease of $n_{\rm def}(\tau)$ as τ grows. By comparing the two plots, it is clear that the presence of an OWP is determined by the interplay between the temperature T and system-bath coupling strength α.

Fig. 4.4 displays the final density of defects for a fixed temperature, $k_B T = J$, while scanning α in the range $[10^{-4}, 10^{-1}]$: we see that very weak couplings favour an AKZ behaviour, while stronger couplings tend to lack an OWP. Moreover, it appears neatly that $n_{\rm def}(\tau)$ exhibits a convergence, for large τ, towards a value $n_\infty(T)$ which depends *only* on the temperature T. We have verified that such limiting value coincides with the final ($h = 0$) thermal value $n_{\rm therm}(T) \equiv n_{\rm def}^T(h = 0)$, indicated by a horizontal dashed line in Fig. 4.4 and calculated from the equilibrium average

$$n_{\rm def}^T(h) = \frac{1}{N}\sum_{k>0} \mathrm{Tr}\{\hat{n}_{\rm def}^{(k)}\,\hat{\rho}_{\rm S}^T(h)\}\ , \tag{4.10}$$

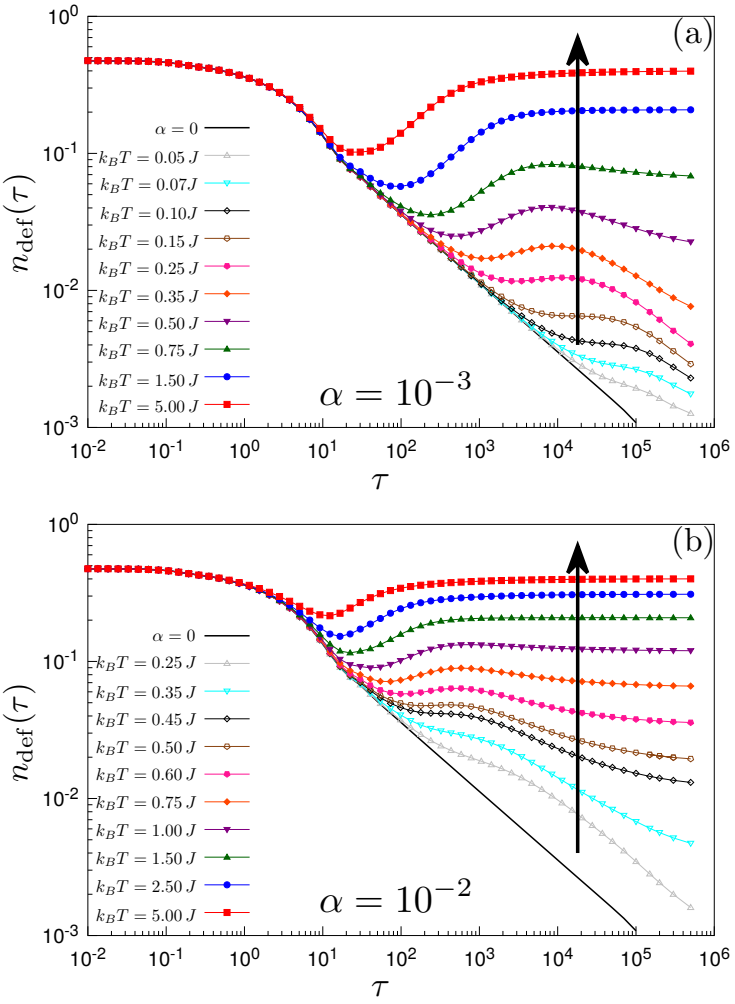

Figure 4.3: Density of defects *versus* annealing time τ for (a) $\alpha = 10^{-3}$, (b) $\alpha = 10^{-2}$, for different effective temperatures T, as indicated in the legend. The arrows indicate the direction of increasing temperatures. The trend for high T is of AKZ type, with an emergent OWP. At lower T and/or higher α values a monotonic trend smoothly appears, with the absence of OWP.

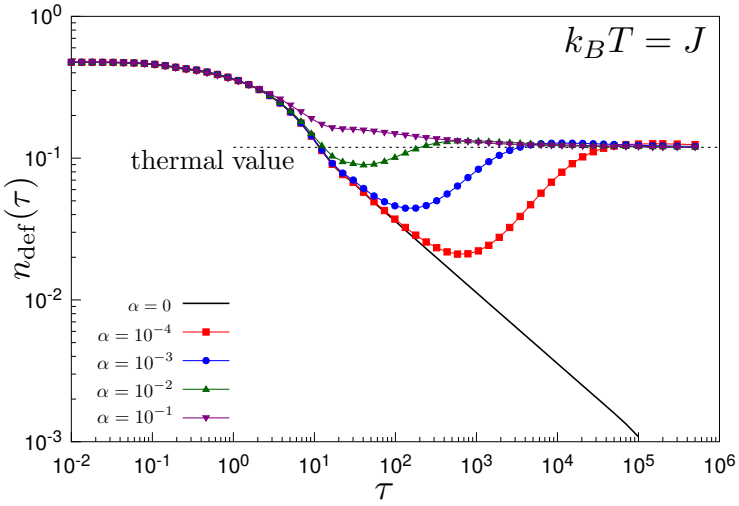

Figure 4.4: Density of defects *versus* annealing time τ for $k_BT = J$, at different coupling strengths α. Note that, for large enough annealing times, $n_{\rm def}(\tau)$ converges towards the thermal value.

where $\hat{\rho}_{\rm S}^{T}(h)$ is the system thermal state at bath temperature $T_b = 2T$, when the transverse field is h. The explicit calculation of $n_{\rm therm}(T)$, following Appendix C, leads to

$$n_\infty(T) \equiv n_{\rm therm}(T) = \frac{1}{2}\big(1 - \tanh(\beta J)\big) \,. \tag{4.11}$$

Notice that, for each two-level system, the final gap at $t = \tau$ is $4J < \hbar\omega_c$. Hence, the bath influences the dynamics until the end. This is at variance with the dissipative Landau-Zener model, where the final gap is usually much bigger than the bath cutoff frequency and the final ground state probability does not fully reflect thermal equilibrium with the bath [124, 94]. Figure 4.5(a) summarizes the values obtained for $n_{\rm opt}(T)$ versus T, for various α. The stars mark the temperatures $T_{\rm up}(\alpha)$ where $n_{\rm opt}(T)$ crosses the (infinite-time limit) thermal value $n_{\rm therm}(T)$: given α, only for $T > T_{\rm up}$ the minimum at $\tau_{\rm opt}$ is an absolute minimum of $n_{\rm def}(\tau)$. For $T < T_{\rm low}(\alpha)$ the minimum disappears completely — $n_{\rm def}(\tau)$ is a monotonically decreasing function of τ. For $T_{\rm low}(\alpha) < T < T_{\rm up}(\alpha)$, $n_{\rm opt}$ survives only as a local minimum. Summarizing, for the range of α we have investigated (the weak-coupling region $\alpha < 10^{-1}$) one can construct two characteristic temperature curves, $T_{\rm low}(\alpha) < T_{\rm up}(\alpha)$ and a phase diagram, sketched in Fig. 4.5(b). Notice that the two curves are difficult to extrapolate from the data for $\alpha \to 0$ because the simulations would require a too large time-scale to observe the presence or absence of the local minimum in $n_{\rm opt}$. We can however argue, on rather simple grounds, that $T_{\rm up}(\alpha \to 0)$ should drop to zero as $\sim 1/\log(1/\alpha)$. Indeed, as seen from Fig. 4.5(a), $n_{\rm opt}(T, \alpha)$ appears to be roughly linear in T in the region where it crosses the thermal curve, $n_{\rm opt}(T, \alpha) \simeq A_\alpha T$, with

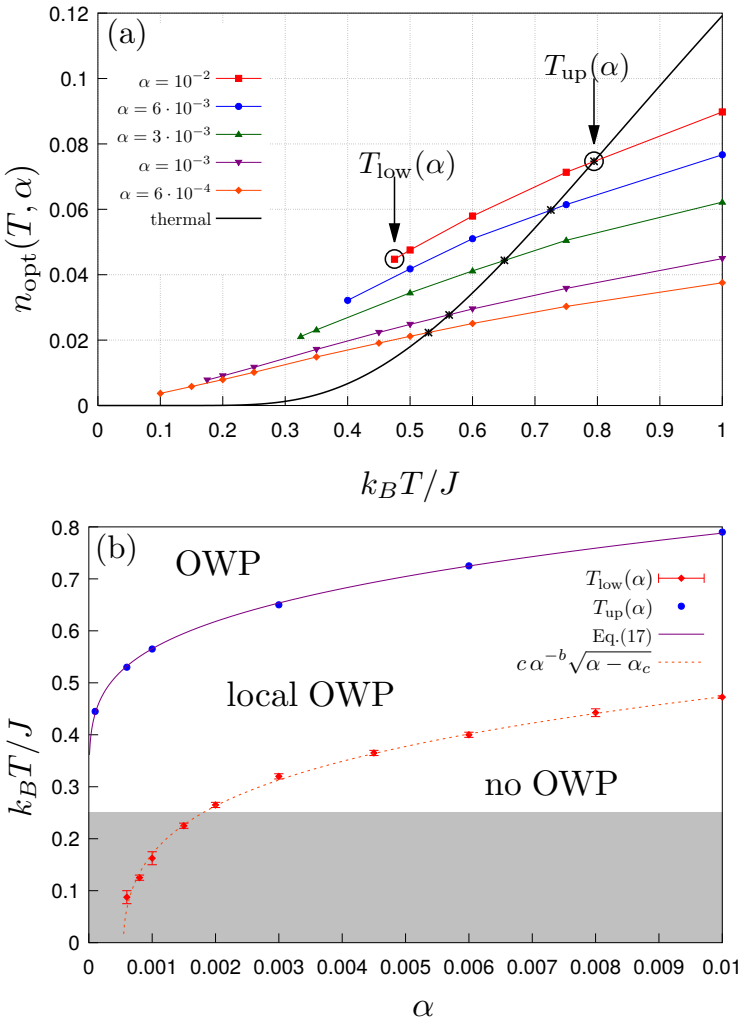

Figure 4.5: (a) Dependence of $n_{\rm opt}$ on T, for various values of α. Each curve defines an upper value $T_{\rm up}(\alpha)$ at which $n_{\rm opt}(T_{\rm up}) = n_\infty(T_{\rm up})$ (marked by stars), and a lower $T_{\rm low}(\alpha)$ at which the local minimum defining $n_{\rm opt}$ disappears. (b) Phase diagram in the $T - \alpha$ plane with $T_{\rm up}(\alpha)$ and $T_{\rm low}(\alpha)$. A proper OWP only exists for $T > T_{\rm up}(\alpha)$. The black solid line is a fit of $T_{\rm up}(\alpha)$ using Eq. (4.13), with $C = 2.08$ and $D = 12.3$. The red dashed line is a fit with $T_{\rm low}(\alpha) = c\alpha^{-b}\sqrt{\alpha - \alpha_c}$, where we find $\alpha_c = 5.5 \cdot 10^{-4}$, $c = 3.58$, and $b = 0.22$. The shaded area alludes to the typical range of temperatures of interest for the D-Wave® hardware [122, 123], with $k_B T \simeq 12$ mK and $J \gtrsim 80$ mK.

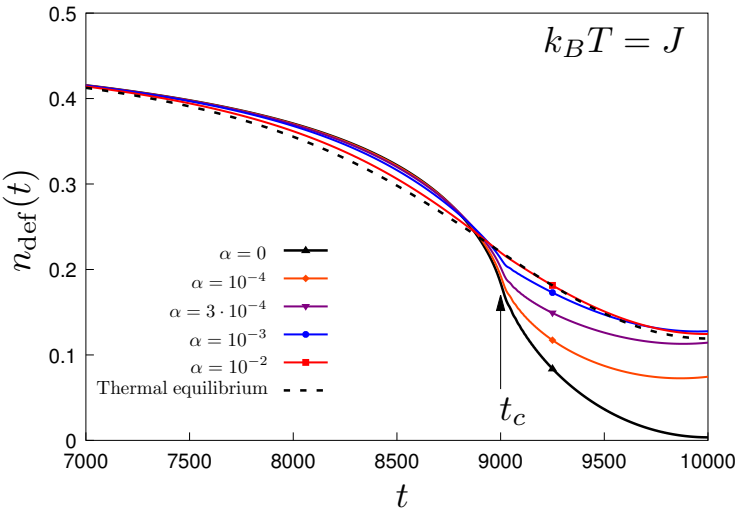

Figure 4.6: Density of defects *versus* time for $\tau = 10^5$, $k_BT = J$ and different system-bath coupling strengths. The arrow at t_c marks the value of t at which the transverse field crosses the critical value, $h(t_c) = h_c$. For $\alpha = 10^{-2}$, where the defects density has fully converged (see Fig. 4.4), $n_{\rm def}(t)$ is almost superimposed to the exact instantaneous thermal one computed from Eq. (C.4).

a slope A_α which, as we have verified, depends on α in a power-law fashion. Since $n_{\rm therm}(T) \sim \mathrm{e}^{-2J/k_BT}$ for small T, we can write the implicit relationship:

$$n_{\rm opt}(T_{\rm up}, \alpha) \simeq A_\alpha T_{\rm up} \simeq \mathrm{e}^{-2J/k_B T_{\rm up}} \ . \tag{4.12}$$

Assuming a power-law for A_α we get, up to sub-leading corrections,

$$T_{\rm up}(\alpha) \sim \frac{C}{\log \frac{1}{\alpha} + D \left(\log \log \frac{1}{\alpha} \right)} \ . \tag{4.13}$$

where C, D are constants. This functional form fits our numerical data in a remarkably good way. The behaviour of the $T_{\rm low}(\alpha)$ curve is considerably less trivial. On the practical side, it is computationally harder to obtain information on the temperature below which a local OWP ceases to exists. Our data suggest that there might be a critical value $\alpha_c \approx 5.5 \cdot 10^{-4}$ below which a local OWP exists even at the smallest temperatures, but this might be an artifact of some of the approximations involved in our weak-coupling QME. All in all, the phase diagram is quite clear — at least for weak-moderate values of α — in predicting the presence of a true OWP only for relatively large temperatures T. We will discuss this in the concluding section.

The fact that the system converges to a thermal state for long annealing times is quite reasonable, and perhaps expected. Indeed, if the thermalization time-scale becomes smaller than the annealing time-scale, one would expect that the system's

state remains close to the instantaneous thermal equilibrium state at every time during the whole dynamics. Figure 4.6, where we plot $n_{\rm def}(t)$ *vs* time at fixed $k_BT = J$ and fixed annealing time $\tau = 10^5$, confirms this expectation. In Fig. 4.6 the dashed line indicates, as a guide, the "instantaneous" exact thermal value $n^T_{\rm def}(h(t))$ computed according to Eq. (4.10) (see App. C for details), while the arrow at t_c marks the value of t where the transverse field $h(t)$ crosses the critical point, $h(t_c) = h_c = 1$. We observe that, for increasing couplings α, the curves tend to be closer and closer to the instantaneous thermal one, since the thermalization time-scale decreases.

4.2.2 Interplay between coherent and incoherent defects production

As mentioned above, in absence of dissipation, the defects produced are due to violations of adiabaticity in the coherent dynamics,

$$\frac{d}{dt}\hat{\rho}^{(k)}_{\rm coh}(t) = -\frac{i}{\hbar}\Big[\widehat{H}^{(k)}_{\rm S}(t), \hat{\rho}^{(k)}_{\rm coh}(t)\Big] \,, \tag{4.14}$$

and would be given by

$$n^{\rm coh}_{\rm def}(t) = \frac{1}{N}\sum_{k>0} {\rm Tr}\big\{\hat{n}^{(k)}_{\rm def}\,\hat{\rho}^{(k)}_{\rm coh}(t)\big\} \,. \tag{4.15}$$

As well known, $n^{\rm coh}_{\rm def}(t=\tau)$ obeys the usual KZ scaling [125]. In the present case, for the Ising chain, $n^{\rm coh}_{\rm def}(\tau) \sim \tau^{-1/2}$.

In the literature related to dissipative QA, it is often found that the density of defects can be regarded as the sum of two independent contributions:

$$n_{\rm def}(t) \approx n^{\rm coh}_{\rm def}(t) + n^{\rm diss}_{\rm def}(t) \,. \tag{4.16}$$

The second contribution, $n^{\rm diss}_{\rm def}(t)$, should be due to a *purely dissipative* time-evolution of the system state,

$$\frac{d}{dt}\hat{\rho}^{(k)}_{\rm diss} = -\Big(\big[\hat{\tau}^z_k, \hat{S}_k(t)\,\hat{\rho}^{(k)}_{\rm diss}\big] + {\rm H.c.}\Big), \tag{4.17a}$$

$$n^{\rm diss}_{\rm def}(t) = \frac{1}{N}\sum_{k>0} {\rm Tr}\big\{\hat{n}^{(k)}_{\rm def}\,\hat{\rho}^{(k)}_{\rm diss}(t)\big\} \,, \tag{4.17b}$$

where in Eq. (4.17a) we employed the Bloch-Redfield QME *without* coherent evolution, with $\hat{S}_k(t)$ being the bath-convoluted system operator defined in Eq. (2.28). In particular, based on this "additivity" assumption, Refs. [113, 114] computed scaling laws for the defects density in presence of dissipation due to several thermal bosonic baths independently coupled to the system. In Ref. [115], an "additive" scaling law

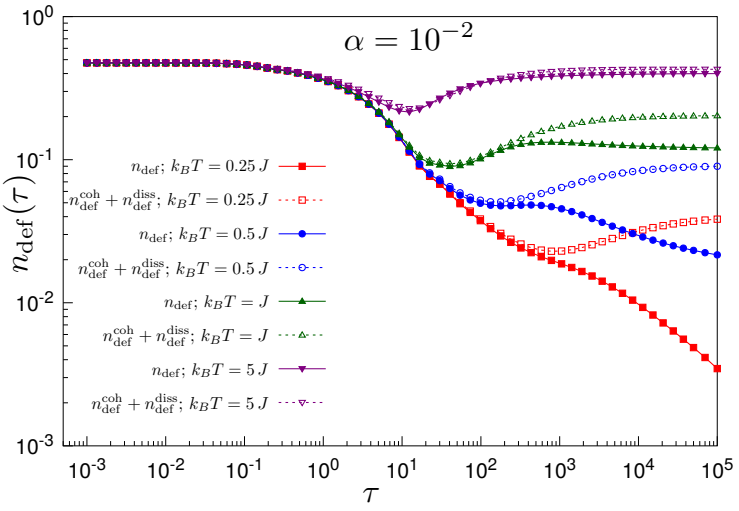

Figure 4.7: Test for the additivity assumption Eq. (4.16) for the formation of defects. We compare $n_{\rm def}(t = \tau)$, calculated with the full Bloch-Redfield evolution (continuous curves, filled symbols), to the sum of $n_{\rm def}^{\rm coh}(\tau)$ plus the purely-dissipative evolution contribution $n_{\rm def}^{\rm diss}(\tau)$ (dashed curve, empty symbols).

for the same model, derived for the case of a single bath coupled to the system, is shown to be in excellent agreement with the density of defects obtained from a dissipative QME time evolution. However, a crucial requirement for these scaling laws to hold is that thermalization effects after the critical point has been crossed must be negligible: indeed, in Refs. [113, 114], the adiabatic sweep is stopped *at the critical point* or immediately below it, so giving no time to the system to "feel" the thermal environment; in Ref. [115], the analysis is carried out for a very small system-bath coupling α, so that the thermalization time is extremely long, much longer than the characteristic annealing time scale. As a consequence, after the critical point crossing, the system is very weakly affected by the bath and the additivity assumption still holds.

Here we are considering an annealing protocol that can leave enough time to the system to thermalize after the critical point crossing: indeed, the quantum critical point is crossed when $h(t_c) = (1 - t_c/\tau)h_0 = 1$, in our units, hence $t_c = (1 - 1/h_0)\tau = 0.9\tau$, for $h_0 = 10$. This means that, after the critical point, the system has $t_{\rm avail} = 0.1\tau$ time to relax to the thermal state, *i.e.* a time proportional to the annealing time τ. Therefore, for all the τ values for which $t_{\rm avail}$ is comparable or larger than the bath thermalization time, the effect of the bath after the quantum critical point will be not negligible.

Figure 4.7 shows a test of the additivity assumption for four different bath temperatures at fixed coupling $\alpha = 10^{-2}$; for each temperature, we compare the defects density obtained via the usual Bloch-Redfield QME with that obtained by the sum

of $n_{\rm def}^{\rm coh}$ and $n_{\rm def}^{\rm diss}$. For τ small enough, the additivity assumption always holds, since $t_{\rm avail}$ is too short, *i.e.* there is not enough time to feel the effect of the bath after the critical point is crossed. However, for longer annealing times the additivity starts to fail: the lower the temperature, the worse it is. In particular, we see that additivity would *always* predict the presence of an OWP, but in some regimes the interplay between coherent and dissipative effects is non-trivial and the two contributions cannot be considered separately. Note also that for $k_BT = 5J$ the additivity assumption seems to hold for every annealing time, even after converging to its thermal value. However, this is probably because both values tend to converge to the maximum for the density of defects, and therefore additivity holds better.

4.3 Final remarks

In the work presented in this chapter, we have revisited some of the issues related to QA in the presence of dissipation. In particular, we have investigated under which conditions it is possible to find an "optimal" annealing time, the optimal working point (OWP), that minimizes the number of defects, and therefore maximizes the annealing performance.

Interestingly, a proper OWP can be seen essentially only in a high-temperature regime, $k_BT \gtrsim 0.5J$. For temperatures which might be relevant for current [122, 123], and presumably future quantum annealers, $k_BT \ll J$, schematically sketched by a shaded area in the phase-diagram of Fig. 4.5(b), we found that $n_{\rm def}(\tau)$ would be monotonically decreasing (hence without OWP), except for very weak bath couplings, $\alpha \lesssim 10^{-3}$. In the intermediate temperature regime, $n_{\rm def}(\tau)$ displays a *local minimum* at finite τ, but the actual global minimum is attained as a $\tau \to \infty$ thermal plateau. The previous considerations would apply to experimental realizations where the coupling to the environment can be considered to be weak and ohmic, which apparently is not the case for the D-Wave® hardware [122, 123], where $1/f$ noise seems to play an important role [126]. The extension of our study to cases where the bath spectral density has different low-frequency behaviours, such as sub-ohmic or with $1/f$ components, is a very interesting open issue which we leave to future work.

Previously related studies [113, 114, 115] on the same model did not detect all these different behaviours, because they either stopped the annealing close to the critical point [113, 114] — to highlight some universal aspects which survive in the presence of the environment — or considered an extremely small, $\alpha \sim 10^{-6}$, system-bath coupling [115]: this amounts, in some sense, to effectively disregarding thermalization/relaxation processes occurring after the critical point has been crossed. Furthermore, we found that additivity *Ansatz* on the density of defects, Eq. (4.16), breaks down as soon as the bath thermalization time is effectively shorter than the characteristic time-scale for the system dynamics.

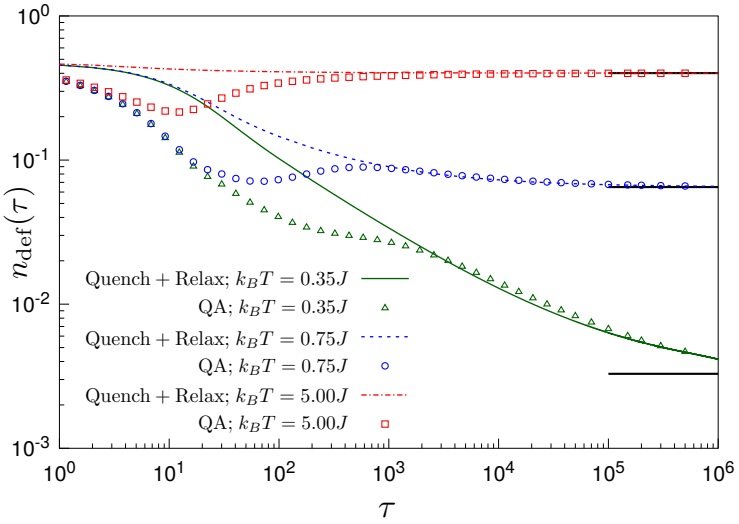

Figure 4.8: Comparison between our dissipative QA results (points) and sudden quenches from $h_0 = 10$ to $h_0 = 0$ followed by thermal relaxation (lines), for $\alpha = 0.01$ and different temperatures. Horizontal black lines identify the expected thermal values for each temperature.

Another interesting outcome of our calculation is the answer to the following question: if the long-time limit of a dissipative QA dynamics is thermalization, is it useful to do QA at all? Wouldn't it be better to *suddenly quench* the system to zero transverse field and wait for thermal relaxation to occur? To answer this question, we compare in Fig. 4.8 the data obtained by our dissipative QA dynamics, with those obtained, using the same QME, from a "sudden quench" protocol — from $h_0 = 10$ to $h_0 = 0$ — followed by thermal relaxation with the environment at given T, for three values of temperature, $k_BT/J = 0.35, 0.75, 5$, and $\alpha = 0.01$. The results illustrate that a dissipative QA is in general a better strategy, especially for short-intermediate times, and/or in presence of an OWP.

A final comment deserves the issue of how general might be the picture emerging from our specific model. It is hard to put forward general arguments on this issue, but the results we obtained suggest that the picture might apply to more complicated models. Consider, for simplicity, a disordered quantum Ising chain $\widehat{H}_{\rm S}(t) = -\sum_i \left[J_i\hat{\sigma}_i^x\hat{\sigma}_{i+1}^x + h(t)\hat{\sigma}_i^z\right]$, with $J_i \in [0,1]$, in the presence of a thermal environment. The classical thermal expectation value for the density of defects at temperature T (for $h = 0$) will no longer be exponentially small — $n_{\rm therm}(T) \sim {\rm e}^{-\Delta/k_BT}$ with $\Delta = 2J$ the excitation gap —, since the classical problem is now gapless: on general grounds, for a power-law density-of-states of excitations $\rho(\Delta) \sim \Delta^\omega$ one expects a power-law for the thermal density of defects $n_{\rm therm}(T) \sim T^{\omega+1}$. Hence, $n_{\rm therm}(T)$ can be made quite small by a sufficiently small T. On the contrary, the quantum coherent dynamics is made very slow — indeed, logarithmically slow,

$n_{\rm def}^{\rm coh}(\tau) \sim 1/\log^2(\gamma\tau)$ — by the infinite-randomness quantum critical point with exponentially small gaps [127, 121]. Dissipation typically tends to *increase* the density of defects, $n_{\rm def}(\tau) > n_{\rm def}^{\rm coh}(\tau) \sim 1/\log^2(\gamma\tau)$, hence we generically expect an *extremely slow* approach to thermalization for $\tau \to \infty$: it is not unreasonable to think that such a slow approach to a small thermal value $n_{\rm therm}(T)$ occurs *monotonically* from above, rather than from below, through an intermediate OWP. Clearly, a full proof of this conjecture would require more work on the dissipative disordered quantum Ising chain.

In conclusion, we believe that QA protocols realized with quantum annealers for which thermal effects are sufficiently weak, at sufficiently low temperatures, should not show any OWP, but rather a monotonic decrease of the error towards a large running time thermal plateau. Furthermore, it would be tempting to move away from the reference quantum Ising chain toy-model, and explore the effects of dissipation in more sophisticated models. The use of quantum trajectories [76] or of tensor-network approaches, recently extended to deal with open quantum systems [128, 129], could help in addressing generic one-dimensional (or quasi-one-dimensional) systems, which would be hard to study analytically.

Chapter 5

Dissipation effects in topological pumping

This chapter deals with dissipative effects in the periodically-driven Rice-Mele model, which is a simple model to describe topological adiabatic quantum pumping. Through our study, presented in our third work [47], we reveal a mechanism by which an environment at low enough temperature can help the pumping performance against undesired non-adiabatic effects.

The scientific literature on the topic is very limited. Ref.s [130, 48] have taken into account thermal effects by using a thermal initial state, instead of the Hamiltonian ground state, followed by a unitary dynamics. Within such a framework, Ref. [130] found that charge quantization is robust against non-zero temperatures in the initial state when a single pumping cycle is considered. On the other hand, in the limit of an infinite number of pumping cycles, Ref. [48] found that thermal corrections are exponentially small for low enough temperatures, but they become increasingly relevant when the temperature approaches the insulating gap. Concerning papers where a genuine dissipative dynamics is considered, Ref. [131] studied the Qi-Wu-Zhang model through a Lindblad Markovian quantum master equation, where they found that the pumped charge, starting from the quantized value, decreases monotonically to zero with increasing noise. However, the effect of a physical thermal reservoir on the system's dynamics has never been considered in topological pumping, to our knowledge.

A former study on the periodically-driven (non-dissipative) Rice-Mele model [48] showed that, for slightly non-adiabatic pumping, the pumped charge deviates from the quantized value quadratically in the driving frequency. Here we remarkably find that a bath at low enough temperature can fight such deviation, leading to a pumped charge which can be much closer to perfect quantization. This is what in our work we call *"thermally assisted Thouless pumping"* [47]. Since a bath at zero temperature can only absorb energy from the system, we intuitively explain

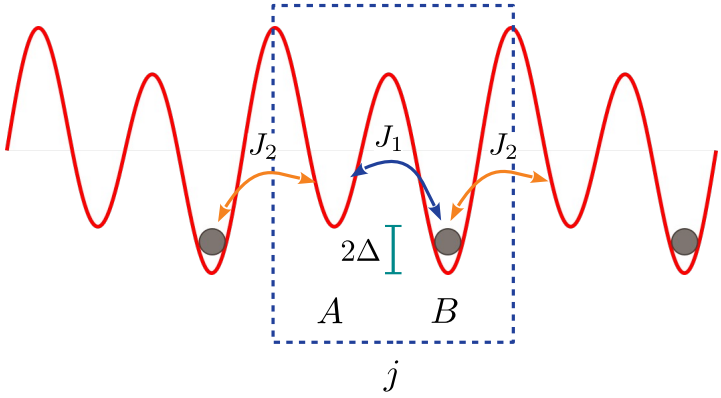

Figure 5.1: Pictorial representation of the Rice-Mele model Hamiltonian.

this effect as the system being cooled down to its instantaneous ground state every time it gets excited by the non-adiabatic driving. This argument, however, does not consider the Berry phase accumulated during the path (which might be destroyed by dephasing), so it cannot be exhaustive. We therefore seek further insight in terms of Floquet bands. It is known that perfect quantization can be obtained whenever the lowest-energy Floquet band is completely populated, while the other Floquet bands are empty. We thus compare the lowest-energy Floquet population for the cases of coherent and dissipative evolutions, confirming that, whenever a dissipative improvement is found, the latter is always higher than the former.

5.1 The Rice-Mele model

The Rice-Mele model [46] is one of the prototypical models for realizing topological adiabatic pumping. It consists of a *bipartite* lattice on which *spinless* fermions hop on nearest-neighboring sites. There is no interaction between the particles, but the hopping terms and the on-site potentials are *periodically driven* in time. The dynamics is governed by the Hamiltonian

$$\begin{aligned}\widehat{H}_{\mathrm{S}}(t) = -\sum_{j=1}^{N}\Big[J_1(t)\,\hat{c}^{\dagger}_{j,B}\hat{c}_{j,A} + J_2(t)\,\hat{c}^{\dagger}_{j+1,A}\hat{c}_{j,B} + \text{H.c.}\Big] + \\ + \Delta(t)\sum_{j=1}^{N}\Big[\hat{c}^{\dagger}_{j,A}\hat{c}_{j,A} - \hat{c}^{\dagger}_{j,B}\hat{c}_{j,B}\Big]\,,\end{aligned} \tag{5.1}$$

where N is the number of diatomic cells, $\hat{c}^{\dagger}_{j,A(B)}$ creates a fermion on site $A(B)$ of the j^{th} cell, $J_1(t)$ and $J_2(t)$ are respectively intra-cell and inter-cell hopping terms and $\Delta(t)$ modulates the staggered on-site energies. A visual representation of the Rice-

Mele model Hamiltonian is given in Fig. 5.1. Notice that periodic driving requires that $\widehat{H}_{\rm S}(t+\tau) = \widehat{H}_{\rm S}(t)$, where τ is the driving period. We assume periodic boundary conditions (PBC), which preserve translational invariance every two sites. We take advantage of this and Fourier transform the fermionic operators for the A and B sites

$$\hat{c}_{j,A(B)} = \frac{1}{\sqrt{N}} \sum_{k}^{\rm BZ} \mathrm{e}^{ikja} \hat{c}_{k,A(B)} \,, \tag{5.2}$$

where the sum over the discrete wave-vectors $k = 2\pi n/(Na)$, with $n = 0, 1, \ldots, N-1$ and a the diatomic cell length, runs inside the first Brillouin Zone (BZ). By applying this transformation to Eq. (5.1), we block-diagonalize the Hamiltonian in sectors of different momentum k,

$$\widehat{H}_{\rm S}(t) = \sum_{k}^{\rm BZ} \widehat{H}_{\rm S}(k,t) = \tag{5.3a}$$

$$= \sum_{k}^{\rm BZ} \begin{bmatrix} \hat{c}^\dagger_{k,A} & \hat{c}^\dagger_{k,B} \end{bmatrix} \widehat{\mathcal{H}}^k_{\rm S}(t) \begin{bmatrix} \hat{c}_{k,A} \\ \hat{c}_{k,B} \end{bmatrix} \,, \tag{5.3b}$$

where $\widehat{\mathcal{H}}^k_{\rm S}(t) = \mathbf{R}(k,t) \cdot \hat{\boldsymbol{\sigma}}$ is a 2×2 operator, expressed in terms of $\hat{\boldsymbol{\sigma}} = (\hat{\sigma}^x, \hat{\sigma}^y, \hat{\sigma}^z)$ three Pauli matrices and $\mathbf{R}(k,t)$ a 3-dimensional vector with real components

$$\begin{aligned} R_x(k,t) &= -J_1(t) - J_2(t)\cos(ka) \,, \\ R_y(k,t) &= -J_2(t)\sin(ka) \,, \\ R_z(k,t) &= \Delta(t) \,. \end{aligned} \tag{5.4}$$

The time-evolution of the system's state $\hat{\rho}_{\rm S}(t)$ is then fully characterized by the independent dynamics of N two-level systems labelled by their momentum k — call them $\hat{\rho}^k_{\rm S}(t)$ — governed by their corresponding k-fixed Hamiltonian $\widehat{\mathcal{H}}^k_{\rm S}(t)$.

Let us analyse the spectral properties of each 2-dimensional k-fixed subspace in Eq. (5.3b). By diagonalizing $\widehat{\mathcal{H}}^k_{\rm S}(t)$, one immediately realizes that the two energy bands are

$$E_\pm(k,t) = \pm|\mathbf{R}(k,t)| = \pm\sqrt{J_1^2(t) + J_2^2(t) + 2J_1(t)J_2(t)\cos(ka) + \Delta^2(t)} \,. \tag{5.5}$$

The energy gap $E_{\rm gap}(k,t) = 2|\mathbf{R}(k,t)|$ never vanishes except for one point (k^*, t^*), defined by

$$\begin{aligned} k^* &= \pi/a \\ J_1(t^*) &= J_2(t^*) \\ \Delta(t^*) &= 0 \,, \end{aligned}$$

for which $E_{\text{gap}}(k^*, t^*) = 0$. This is a crucial property for Thouless pumping in this model, as will be explained in Sec. 5.1.2.

5.1.1 The pumped charge and the current operator

In the periodically-driven Rice-Mele model, the three parameters $J_1(t)$, $J_2(t)$ and $\Delta(t)$ are changed in time in a periodic fashion, so that $\widehat{H}_{\text{S}}(t + m\tau) = \widehat{H}_{\text{S}}(t)$, where τ is the period and m is the number of cycles. A relevant problem in this setting is to quantify how much charge we were able to move during the m^{th} period, the so-called *pumped charge*, which is defined, in the thermodynamic limit, as

$$Q_m = \lim_{L\to\infty} \frac{1}{L} \int_{(m-1)\tau}^{m\tau} dt\ \text{Tr}\Big\{ \hat{\text{J}}(t)\hat{\rho}_{\text{S}}(t) \Big\} , \tag{5.6}$$

where $L = Na$ is the chain length, $\hat{\rho}_{\text{S}}(t)$ is the time-evolved system's state and $\hat{\text{J}}(t)$ is the total current operator. As discussed in Appendix D, this quantity must be *exactly an integer*, provided the evolution is unitary, the driving is adiabatic and the system has a band insulator ground state throughout the whole dynamics [43, 42].

To compute Eq. (5.6), we need to express the current operator $\hat{\text{J}}(t)$ for this model. In real space, we can compute it either by enforcing the continuity equation [132] or by taking the derivative of the Hamiltonian with respect to a Laughlin flux piercing the ring [133]:

$$\hat{\text{J}}(t) = i\frac{a}{2\hbar} \sum_{j=1}^{N} \Big[J_1(t)\ \hat{c}^\dagger_{j,B}\hat{c}_{j,A}\ + J_2(t)\ \hat{c}^\dagger_{j+1,A}\hat{c}_{j,B}\ -\ \text{H.c.} \Big] . \tag{5.7}$$

It is convenient to express Eq. (5.7) by moving to momentum space through Eq. (5.2): the current operator then splits into a set of operators acting separately on each k-Hilbert space. Analogously to Eq. (5.3b), we can thus write the *current operator* as

$$\hat{\text{J}}(t) = \sum_{k\in \text{BZ}} \begin{bmatrix} \hat{c}^\dagger_{k,A} & \hat{c}^\dagger_{k,B} \end{bmatrix} \widehat{\mathcal{J}}^k(t) \begin{bmatrix} \hat{c}_{k,A} \\ \hat{c}_{k,B} \end{bmatrix} \tag{5.8}$$

where

$$\widehat{\mathcal{J}}^k(t) = \frac{a}{2\hbar} \Big[J_2(t)\sin(ka)\ \hat{\sigma}_x + \Big(J_1(t) - J_2(t)\cos(ka) \Big)\ \hat{\sigma}_y \Big] . \tag{5.9}$$

Using Eq. (5.9), we can write the pumped charge in Eq. (5.6) as[1]

$$Q_m = \int_{-\frac{\pi}{a}}^{\frac{\pi}{a}} \frac{dk}{2\pi} \int_{(m-1)\tau}^{m\tau} dt \, \mathrm{Tr}\Big\{ \widehat{\mathcal{J}}^k(t) \hat{\rho}^k_{\mathrm{S}}(t) \Big\} \,, \tag{5.10}$$

where $\hat{\rho}^k_{\mathrm{S}}(t)$ is the time-evolved state relative to the two-level Hamiltonian $\widehat{\mathcal{H}}^k_{\mathrm{S}}(t)$ in Eq. (5.3b). Notice that the currents defined above have the physical dimension of a velocity, $[l]/[t]$. Therefore, the pumped charge is dimensionless, since k has the dimension $1/[l]$. In general, a very interesting regime in periodically-driven systems is the steady-state long-time limit, after the initial transient. To address such steady-state behaviour, we take the limit of infinite pumping cycles and average over all of them, getting the *stationary pumped charge*

$$\overline{Q} = \lim_{M\to\infty} \frac{1}{M} \sum_{m=1}^{M} Q_m \,, \tag{5.11}$$

where M is the number of driving periods.

5.1.2 Driving protocols for topological pumping

To achieve quantization of the pumped charge, see also Appendix D, we have to require that [43]:

1. the system must be a band insulator over the whole time-evolution. We therefore require the *half-filling* condition (*i.e.* N particles in the lattice), so that we fill precisely and only the lowest energy band.

2. the driving must be *adiabatic* ($\tau \to \infty$).

If these two conditions are fulfilled, the pumped charge is a Chern number and must be therefore quantized, as discussed in Appendix D.

From a practical point of view, in this model the Chern number is equal to the number of gapless points that are enclosed in each driving cycle. Therefore, if we perform one pumping cycle, there are *two distinct topological phases* depending on whether or not we encircled the gapless point during the driving. Fig. 5.2 illustrates two topologically inequivalent paths in the parameter space described by $(J_1(t) - J_2(t), \Delta(t))$. Notice that, for $k = \pi/a$, the gapless point is at the origin. Path A encloses the gapless point and hence such a driving pumps a quantum of charge at the end of one loop. Path B, on the other hand, leaves the gapless point outside

[1] We switched from a sum to an integral over k in the standard way:

$$\lim_{L\to\infty} \frac{1}{L} \sum_{k}^{\mathrm{BZ}} f(k) = \int_{\mathrm{BZ}} \frac{dk}{2\pi} f(k) \,.$$

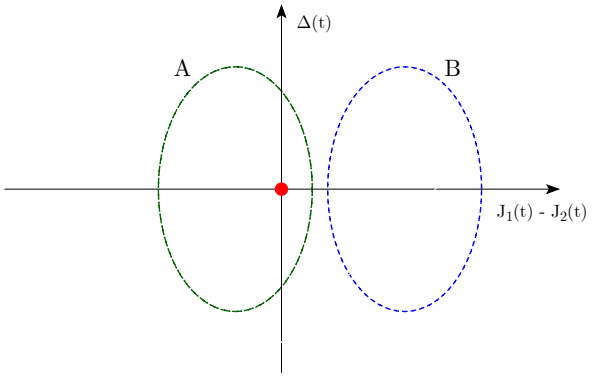

Figure 5.2: Examples of possible paths in the Hamiltonian parameter space under periodic driving. Notice that, with this choice of axes, the gapless point is at the origin, marked by a red circle. Path A encloses the gapless point, therefore adiabatic evolution would lead to $Q = \pm 1$. Path B, on the other hand, would bring $Q = 0$, since it leaves the origin outside.

and therefore moves no charge at the end of the evolution. The intuition behind this is the following: topological properties are independent of smooth variations of the specific driving protocol chosen, as soon as adiabaticity is perfectly fulfilled throughout the whole evolution. Therefore, we should be able to smoothly modify the driving scheme and remain in the same topological phase. However, if we pass by the gapless point, there is an inevitable breakdown of adiabaticity, since the adiabatic time-scale goes as $1/E_{\text{gap}}^2$. Therefore, a path that encircles the gapless point cannot be *adiabatically connected* to a path that leaves the gapless point outside. This justifies the presence of the two topological phases.

In the following, we will be interested in the topological phase where we can pump one quantum of charge per cycle. We therefore parametrize our *driving parameters* so to enclose the gapless point in parameter space,

$$\begin{aligned} J_1(t) &= J_0 + \delta_0 \cos \omega t \\ J_2(t) &= J_0 - \delta_0 \cos \omega t \\ \Delta(t) &= \Delta_0 \sin \omega t \ , \end{aligned} \tag{5.12}$$

where $\omega = 2\pi/\tau$ is the driving frequency and controls the degree of adiabaticity of the driving. With reference to the parameter space illustrated in Fig. 5.2, within the driving scheme in Eq. (5.12) we are drawing ellipses centered at the gapless point, with amplitudes δ_0 along the x-axis and Δ_0 along the y-axis. In most of the results shown below, for a direct comparison with Ref. [48], we fixed $\delta_0 = J_0$ and $\Delta_0 = 3J_0$. We verified that our findings persist qualitatively also at different δ_0 and Δ_0.

5.2 Dissipation in the driven Rice-Mele model

To account for the dissipative dynamics of a quantum many-body system, one would need to keep all the density matrix components, whose number grows exponentially with the size of the chain. This task is incredibly hard, especially if one wants to reach the thermodynamic limit, necessary to see topological charge quantization.

To tackle this issue, we propose here a version of the Rice-Mele model in which *dissipation acts solely within each k-fixed subspace* — where $\widehat{\mathcal{H}}^k_{\mathrm{S}}(t)$ lives, see Eq. (5.3b) — so that we can still factorize the full dynamics as coming from the independent time-evolutions of N dissipative two-level systems, in close analogy with the dissipative Ising chain we dealt with in Chapter 4. To be more specific, we choose to include identical independent harmonic baths for each two-level system Hamiltonian $\widehat{\mathcal{H}}^k_{\mathrm{S}}(t)$, coupled in the usual Caldeira-Leggett spin-boson fashion,

$$\widehat{\mathcal{H}}^k_{tot}(t) = \widehat{\mathcal{H}}^k_{\mathrm{S}}(t) \otimes \mathbb{1} + (\boldsymbol{\lambda} \cdot \hat{\boldsymbol{\sigma}}) \otimes \hat{B}_k + \mathbb{1} \otimes \sum_l \hbar\omega_l \hat{b}^\dagger_{k,l} \hat{b}_{k,l} \,, \tag{5.13}$$

where $\boldsymbol{\lambda}$ specifies a unit vector for the bath coupling, $\hat{B}_k = \sum_l \lambda_l (\hat{b}^\dagger_{k,l} + \hat{b}_{k,l})$ and λ_l are coupling constants. In terms of the original fermions, a $\hat{\sigma}^z$-bath coupling — given by $\boldsymbol{\lambda} = (001)$ — would correspond to a term $(\hat{c}^\dagger_{k,A}\hat{c}_{k,A} - \hat{c}^\dagger_{k,B}\hat{c}_{k,B}) \otimes \hat{B}_k$. This will be our standard choice unless otherwise specified. The interaction between system and environment is encoded in the bath spectral function $J(\omega) = \sum_l \lambda_l^2 \delta(\omega - \omega_l)$. We will consider a standard Ohmic dissipation, modelled in the frequency continuum limit as $J(\omega) = 2\alpha\hbar^2\omega \exp(-\omega/\omega_c)$, where α is the coupling strength and ω_c is the cutoff frequency.

5.3 Dissipative pumping results

We discuss here how a weakly coupled bath affects the pumped charge at different driving frequencies and different bath parameters. The dynamics of the system state $\hat{\rho}_{\mathrm{S}}(t)$ is obtained by computing the independent time-evolutions of $\hat{\rho}^k_{\mathrm{S}}(t)$ for each momentum k, by solving the Bloch-Redfield QME with RWA according to the system energies, see Eq. (2.50), corresponding to the total Hamiltonian in Eq. (5.13). To compute the pumped charge, we approximate the integral over k in Eq. (5.6) with a discrete sum in the first Brillouin zone. All the calculations are performed with sizes N which we have verified to be large enough to be representative of the thermodynamic limit: in practice, $N \sim 100$ is enough in presence of dissipation. The bath coupling strength is taken to be $\alpha = 0.001$, while the cutoff frequency ω_c in the spectral function is chosen to be much bigger than the widest spectral gap: $\omega_c = 1000 J_0/\hbar$. We comment upon different choices of ω_c and α in Appendix E. We observe that the stationary pumped charge $\overline{Q}$ converges, as $\alpha \to 0$, towards a well-defined limiting value, see Appendix E. Our choice of interaction strength

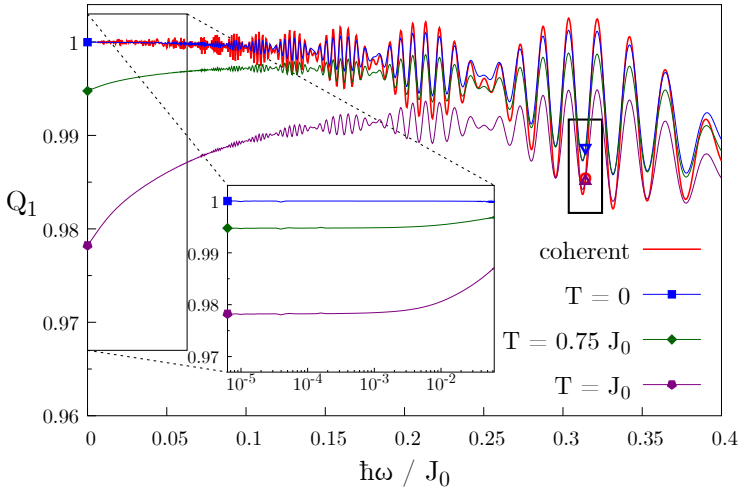

Figure 5.3: Pumped charge over the 1st period Q_1 versus driving frequency $\hbar\omega/J_0$, at bath temperatures T ranging from 0 to J_0, compared to the coherent evolution results of Ref. [48]. *Inset*: zoom of the $\omega \to 0$ region, showing the convergence to finite values depending on T.

aims at capturing this limit, coherently with the weak-coupling regime in which our approach is valid.

Let us start considering the behaviour of the pumped charge after a single cycle. In Fig. 5.3 we plot Q_1 versus the driving frequency ω in Eq. (5.12). On the one hand, at larger values of ω, the bath has almost no effect, and the behaviour at all temperatures remains almost identical to the coherent one, which coincides with that reported in Ref. [48]. On the other hand, at smaller values of ω, the system has enough time to "feel" thermal effects and in general moves away from the ideal quantized pumping, corresponding to $Q_1 = 1$. The charge converges to a finite value which depends on the bath temperature T, see the inset of Fig. 5.3. We will return to this later, while discussing the steady pumped charge.

These results change remarkably when pumping over a larger number of cycles. We find that the charge pumped over the m^{th} cycle, Q_m, can overcome the corresponding coherent result in presence of a thermal bath of sufficiently low temperature. This is shown in Fig. 5.4. Observe that dissipation makes the convergence to the infinite-time average much faster than the coherent case. Notice also that the infinite-time average results are precisely described by the Floquet diagonal ensemble formulas, Eqs. (5.20) and (5.21), shown by horizontal dashed lines. They will be discussed later in Sec. 5.4.1.

Figure 5.5 shows the infinite-time pumped charge $\overline{Q}$ versus the driving frequency ω, for both coherent and dissipative evolutions at different T. The dissipative results come from Eq. (5.11) (with $M = 100$), while the coherent ones are obtained from

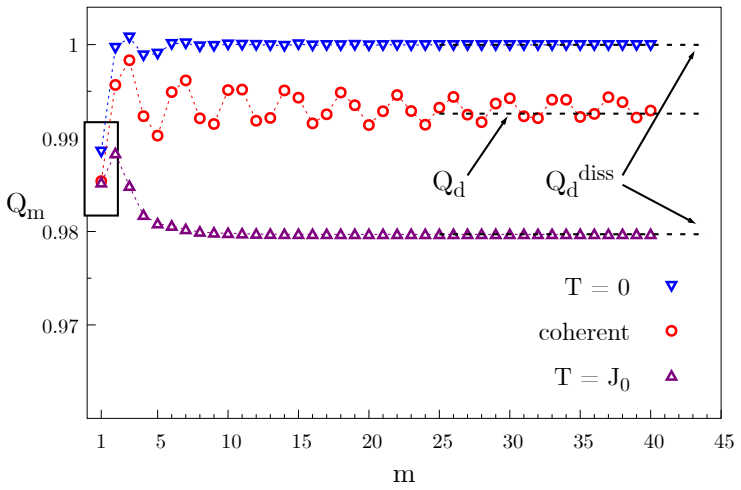

Figure 5.4: Charge pumped in the m^{th} period Q_m versus the cycle number m for the coherent case (circles) compared to two dissipative evolutions (triangles) at different bath temperatures T. Here $\tau = 20\hbar/J_0$, as for the $m = 1$ results in the rectangle shown in Fig.5.3. The three horizontal dashed lines are the corresponding values from the Floquet diagonal ensemble, Eq. (5.20) or Eq. (5.21), discussed in Sec. 5.4.1. Notice that oscillations in the dissipative evolutions are damped much more rapidly.

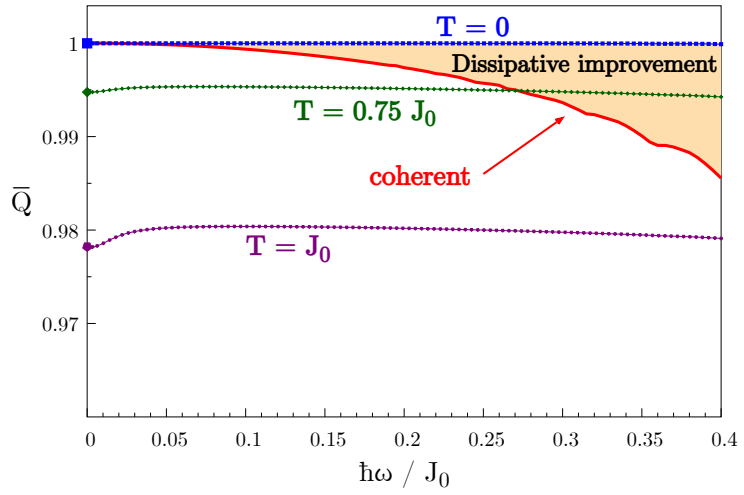

Figure 5.5: Average pumped charge in the infinite-time limit $\overline{Q}$ versus driving frequency $\hbar\omega/J_0$, at bath temperatures T ranging from 0 to J_0, compared to the corresponding data for a coherent evolution (or, equivalently, compared to the Floquet diagonal ensemble values $Q_{\rm d}^{\rm coh}$ in Eq. (5.20)). The region of thermally-assisted improvement over the closed-system pumping is highlighted by a yellow background.

Eq. (5.20), derived in Sec. 5.4 using Floquet theory [2]. Observe that at $T = 0$ *the dissipative results are always well above the coherent ones.* We remark that dissipation at $T = 0$ restores a nearly quantized pumped charge $\overline{Q} = 1$ *away* from the strict adiabatic limit $\omega \to 0$. This dissipative improvement of the pumped charge persists also at finite T, for large enough ω. We dub this phenomenon **thermally assisted Thouless pumping**. This finding is independent of the specific approximation used for the QME. We show evidence for this in Sec. 5.5, where we compare different forms of RWA and the case without RWA, seeing results in good qualitative agreement (although not quantitative). Interestingly, in the small frequency regime we observe that $\overline{Q}(\omega \to 0) \equiv Q_m(\omega \to 0)$ for any $m \geq 1$, *i.e.* the $\omega \to 0$ limit is independent of the number of driving periods. This is because in the $\omega \to 0$ limit the dissipative transient induced by the bath occurs within a single driving period.

Notice that in the literature [130, 48, 134] there have been discussions of thermal effects in the driven Rice-Mele model by studying the *coherent evolution* starting *from an initial thermal state.* We compared the results obtained from this approach with the ones coming from the dissipative evolution described in the present paper: In general, we observed completely different results, both in the short and in the intermediate frequency ranges of study, as illustrated in Fig. 5.6. This is not surprising, but worth mentioning. Fig. 5.6 is important also in another respect: we see that in the dissipative case, if we take very different initial conditions, we get the same asymptotic regime. This is not at all surprising in a dissipative system and marks the difference with the asymptotic regime of the coherent case [135].

Observe how flat is the ω-behaviour of $\overline{Q}$ for the dissipative evolution at $T = 0$: it would be interesting to pin-down if the corrections to the strict adiabatic limit $\overline{Q}(\omega \to 0) = 1$ change from power-law [48] to exponentially small in the presence of zero-temperature dissipation. Unfortunately, this question is extremely difficult to answer from our numerical data. Moreover, this aspect of the story is highly sensitive to the type of weak-coupling approximation performed. Indeed, although the results obtained with other approximations are in good qualitative agreement, they are quantitatively different in that respect (see the discussion in Sec. 5.5). A similar question might be posed concerning the behaviour of $\overline{Q}(\omega \to 0, T)$ as a function of the bath coupling temperature T, a question that is once again numerically elusive and rather sensitive to the details of the QME used.

5.4 Floquet analysis

To get a deeper insight into the dissipative improvement discussed in Sec. 5.3, we look at the density matrix in the basis of the Floquet states related to a unitary evolution. In particular, one can identify a band of states, the so-called lowest-

[2] This is because the coherent results converge to the thermodynamic limit only at very large N and M, so the approach using Eq. 5.11 is computationally longer and less precise.

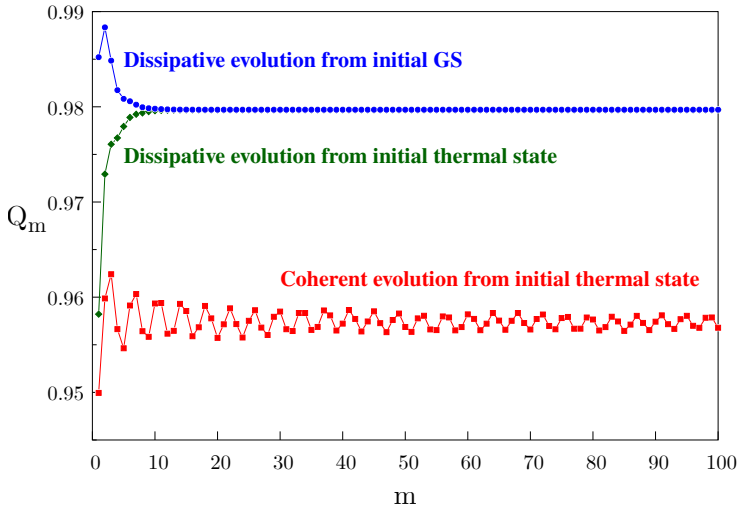

Figure 5.6: Comparison between results from the coherent evolution starting from an initial thermal state at $T = J_0$ (red squares) and the dissipative dynamics induced by a bath at $T = J_0$, both starting from an initial ground state (blue circles) and from the thermal state at the same bath temperature (green diamonds). Here we have a driving period $\tau = 20\hbar/J_0$. The dissipative and coherent results are completely different. Notice that the two dissipative evolutions converge to the same stationary state.

energetic Floquet band [48, 47], with the property that it must be completely filled in the case of perfectly quantized pumping, while the higher-energetic levels must be all empty. Whenever one starts from the ground state and performs a non-adiabatic driving, deviations from perfect quantization of the pumped charge imply non-zero population of these higher-energetic Floquet bands. We prove here that, whenever there is a dissipative improvement like in Fig.s 5.4 and 5.5, the population of the lowest-energetic Floquet band for a dissipatively-evolved state is higher than the one corresponding to unitary dynamics.

To start the discussion, let us introduce some important notions of Floquet theory applied to charge pumping [48, 47]. Since the driving is periodic, *i.e.* $\widehat{H}_{\rm S}(t) = \widehat{H}_{\rm S}(t+\tau)$, from Floquet theory [136, 78, 137] we know that the solutions to the time-dependent Schrödinger equation for the closed system have the following form

$$|\psi_\alpha(t)\rangle = e^{-i\frac{\epsilon_\alpha}{\hbar}t}|u_\alpha(t)\rangle \ , \tag{5.14}$$

where α labels the possible solutions, $|\psi_\alpha(t)\rangle$ are called *Floquet states*, $|u_\alpha(t)\rangle$ are called *Floquet modes* and are $\tau-$periodic, and ϵ_α are the *quasi-energies*. In the present case, using k as a quantum number and $\alpha = \pm$ for two Floquet states $|\psi^k_\alpha(t)\rangle$ at each k, we can always rewrite the density matrix $\hat{\rho}^k_{\rm S}(t)$ in the coherent

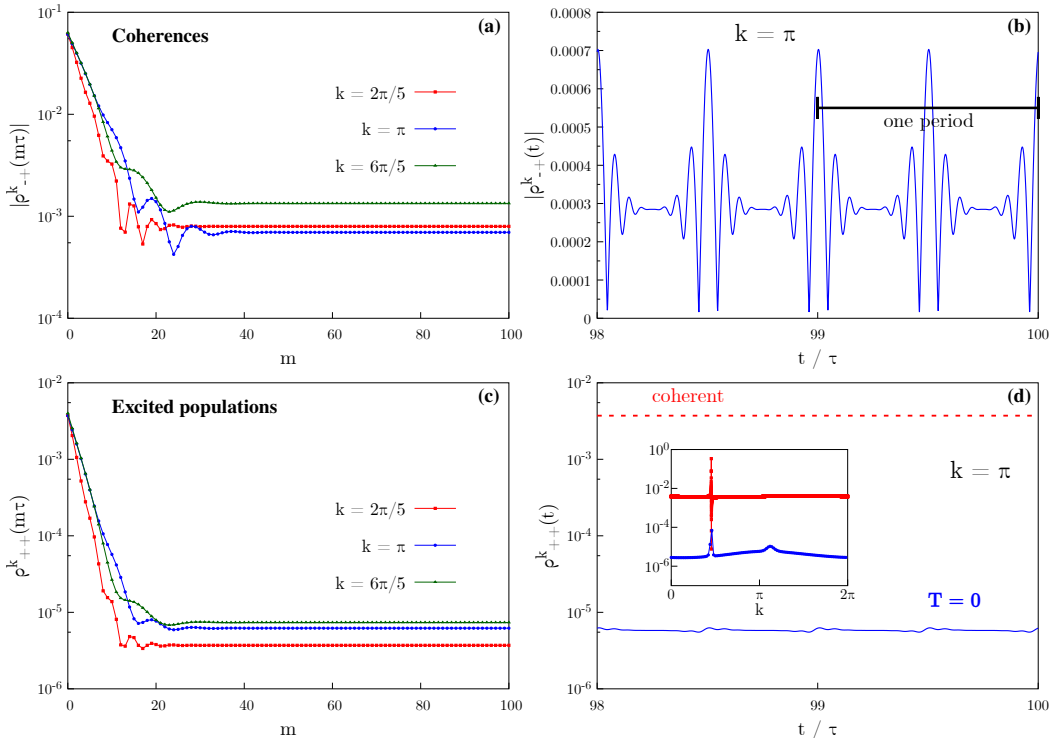

Figure 5.7: **Left panels**: Stroboscopic dynamics of: **(a)** the coherences $|\rho^k_{-+}(m\tau)|$ and **(b)** the excited-Floquet band population $\rho^k_{++}(m\tau)$, for $k = \{2/5, 1, 6/5\}\pi$. Here $T = 0$ and $\tau = 20\hbar/J_0$. **Right panels**: Intra-period dynamics of: **(c)** $|\rho^k_{-+}(t)|$ and **(d)** $\rho^k_{++}(t)$ after stationarity is reached, for $k = \pi$. All the other parameters are fixed as in panels (a)-(b). Observe the $\tau/2$-periodicity. In (d), the red horizontal dashed line shows ρ^k_{++} for the corresponding coherent evolution, much higher than the dissipative result at $T = 0$. **Inset** in (d): Comparison between ρ^k_{++} for the coherent case (red squares) and the time-average $\overline{\rho}^k_{++} = \int_0^\tau dt \rho^k_{++}(t)/\tau$ for the dissipative case (blue circles) versus k.

Floquet basis,

$$\hat{\rho}^k_{\rm S}(t) = \sum_{\alpha,\beta} \rho^k_{\alpha\beta}(t)\, |\psi^k_\alpha(t)\rangle\langle\psi^k_\beta(t)| \,, \tag{5.15}$$

with $\rho^k_{\alpha\beta}(t) = \langle\psi^k_\alpha(t)|\hat{\rho}^k_{\rm S}(t)|\psi^k_\beta(t)\rangle$.

Let us reconsider the dissipative improvement shown in Fig. 5.5 within a Floquet framework. Fig. 5.7 shows that the stroboscopic dynamics of the coherences $|\rho^k_{-+}(m\tau)|$ (panel (a)) and of the excited-band populations $\rho^k_{++}(m\tau)$ (panel (c)) converge to stationary values for $m \to \infty$. The phases of the coherences (not shown) also converge to fixed values. After stroboscopic stationarity is reached, the intra-period behaviour of these quantities is illustrated in panels (b) and (d), respectively: observe a $\tau/2$-periodicity in both cases.

We construct the *lowest-energy Floquet bands* by choosing, for each k, the Floquet mode with (period-averaged) lowest-energy expectation. The results shown in Fig. 5.7(d) allow a direct comparison between the populations of the highest-energy Floquet bands in the coherent and dissipative cases, showing that ρ^k_{++} is generally reduced by several orders of magnitude in presence of dissipation at $T = 0$, hence improving the topological pumping at finite frequencies. In the main figure, we fix k and look at the dependence on time, while in the inset we plot the period-averaged k^{th}-population $\overline{\rho}^k_{++}$ vs the momentum k. In the inset, we note, incidentally, the presence of a value of k where the coherent value shows an irregularity and the dissipative value shows a peak. That peak corresponds to a Floquet quasi-resonance which gives rise to a non-adiabaticity and increases the asymptotic dissipative population of the highest-energy Floquet state [138].

We conclude that dissipation moves the system towards the lowest-energy Floquet state. This state is the one closest to the adiabatic ground state and is the one which pumps a charge equal to the topological value, up to corrections exponentially small in the driving frequency [48, 139].

5.4.1 The dissipative Floquet diagonal ensemble

Floquet theory is very useful to express the steady pumped charge $\overline{Q}$. Consider the Floquet states corresponding to a coherent evolution and write the density matrix in this basis as in Eq. (5.15). Then, employing Eq.s (5.10) and (5.11), we can express the pumped charge at stationarity as

$$\overline{Q} = \lim_{M\to\infty} \frac{1}{M} \sum_{\alpha,\beta} \int_{-\frac{\pi}{a}}^{\frac{\pi}{a}} \frac{\mathrm{d}k}{2\pi} \int_0^{M\tau} \mathrm{d}t \; e^{-\frac{i}{\hbar}(\epsilon^k_\alpha - \epsilon^k_\beta)t} F^k_{\alpha\beta}(t) \; , \tag{5.16}$$

where

$$F^k_{\alpha\beta}(t) = \rho^k_{\alpha\beta}(t)\, \mathbb{J}^k_{\beta\alpha}(t) \; , \tag{5.17}$$

with

$$\mathbb{J}^k_{\beta\alpha}(t) = \langle u^k_\beta(t)|\hat{\mathcal{J}}^k(t)|u^k_\alpha(t)\rangle \tag{5.18}$$

being the matrix element of the current operator between Floquet modes, hence an explicitly periodic quantity. In the coherent evolution case [48], the density matrix $\rho^k_{\alpha\beta}(t)$ turns out to be *time-independent* and related to the initial state $|\psi_k(0)\rangle$ as

$$\rho^{k,\mathrm{coh}}_{\alpha\beta} = \langle u^k_\alpha(0)|\psi_k(0)\rangle\langle\psi_k(0)|u^k_\beta(0)\rangle \; . \tag{5.19}$$

In turn, if the quasi-energies are non degenerate, when $\alpha \neq \beta$, the k-integral will vanish in the limit $t \to \infty$, since the oscillating phase factors $\mathrm{e}^{-i(\epsilon^k_\alpha - \epsilon^k_\beta)t}$ will lead to destructive interference cancellations. More formally, this is a consequence of the Riemann-Lebesgue lemma applied to the k-integration [135, 140]. Using this result

in Eq. (5.16), and exploiting the infinite-time integration, it follows that only the populations $\rho^{k,\mathrm{coh}}_{\alpha\alpha} = |\langle u^k_\alpha(0)|\psi_k(0)\rangle|^2$ of the Floquet bands come into play, and one arrives at the so-called *Floquet diagonal ensemble* [135]

$$\overline{Q} = Q_{\mathrm{d}}^{\mathrm{coh}} = \int_{-\frac{\pi}{a}}^{\frac{\pi}{a}} \frac{\mathrm{d}k}{2\pi} \sum_\alpha \rho^{k,\mathrm{coh}}_{\alpha\alpha} \int_0^\tau \mathrm{d}t\, \mathbb{J}^k_{\alpha\alpha}(t)\,. \tag{5.20}$$

In the dissipative case, $\rho^k_{\alpha\beta}(t)$ is generally time dependent. However, if we look at the data in Fig. 5.7(b,d), we observe that the density matrix components $\rho^k_{\alpha\beta}(t)$ become τ-periodic at stationarity. Hence, we can again apply the Riemann-Lebesgue lemma as done in Ref. [140] and show that only the diagonal terms contribute, arriving at the *dissipative* version of the *Floquet diagonal ensemble* formula for the average pumped charge:

$$\overline{Q} = Q_{\mathrm{d}}^{diss} = \int_{-\frac{\pi}{a}}^{\frac{\pi}{a}} \frac{\mathrm{d}k}{2\pi} \sum_\alpha \int_0^\tau \mathrm{d}t\, \rho^k_{\alpha\alpha}(t)\, \mathbb{J}^k_{\alpha\alpha}(t)\,. \tag{5.21}$$

Fig. 5.4 compares this formula with the actual data obtained by evolving a state for M cycles, with M large enough to reach stationarity. The horizontal dashed lines show the predictions from Eq.s (5.20) and (5.21), highlighting that the dissipative Floquet diagonal ensemble of Eq. (5.21) characterizes the stationary pumped charge extremely well.

As in Ref. [48], the asymptotic pumped charge can be related to the properties of the Floquet quasienergies. To do that, a result coming from our numerics is crucial: if we approximate $\rho^k_{\alpha\alpha}(t)$ at stationarity with its average value on one period $\overline{\rho}^k_{\alpha\alpha}$, we get corrections to the pumped charge of the order $\sim 10^{-6}$. So, to a very good approximation we can replace $\rho^k_{\alpha\alpha}(t)$ with $\overline{\rho}^k_{\alpha\alpha}$. With this approximation, using arguments strictly similar to those of Ref. [48], we find that the asymptotic pumped charge can be written in the form

$$Q_{\mathrm{d}}^{diss} = \frac{1}{\hbar\omega} \int_{-\frac{\pi}{a}}^{\frac{\pi}{a}} \mathrm{d}k \sum_\alpha \overline{\rho}^k_{\alpha\alpha}\, \partial_k \epsilon^k_\alpha\,, \tag{5.22}$$

which looks very similar to Eq. (4) in Ref. [48], obtained for a coherent dynamics. Because the derivative with respect to k can be recast as the derivative with respect to an external flux [48], this equation is also strictly analogous to Eq. (19) of Ref. [79], where pumping in a dissipative superconducting nanocircuit was considered.

5.5 Test of the generality of the results

All the dissipative results shown in Sec. 5.3 were obtained using the Bloch-Redfield QME with RWA in the energy basis, see Eq.s (2.50) and (B.7), and by fixing the

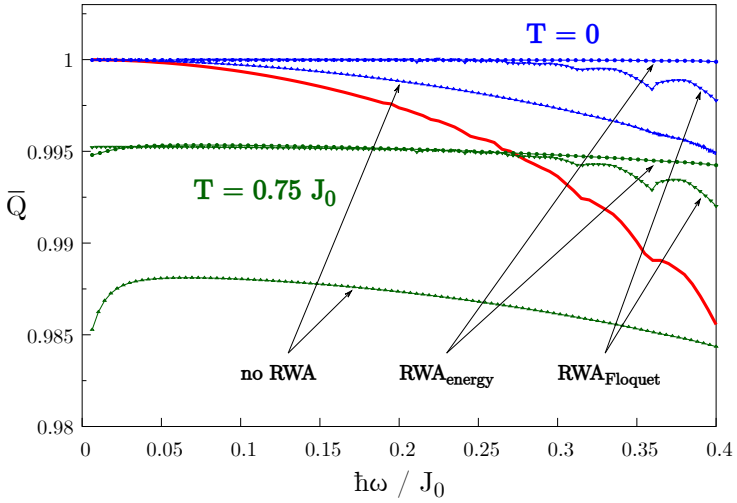

Figure 5.8: $\overline{Q}$ vs driving frequency ω for the dynamics induced by the Bloch-Redfield equation under different approximations. For all the cases, we still find a remarkable improvement over the coherent results if T is low enough. Notice, in particular, the good agreement between the two different RWA schemes.

system coupling operator along $\hat{\sigma}_z$, *i.e.* $\boldsymbol{\lambda} = (0, 0, 1)$. Here we aim at generalizing our results to other QMEs and other coupling directions, showing that these cases are in good *qualitative* agreement with the ones shown in Sec.5.3.

We therefore repeated the calculations shown in Sec. 5.3, but this time with the dissipative evolution computed by means of the Bloch-Redfield QME *without RWA*, see Eq.s (2.25) and (B.17), and *with RWA* in the *Floquet basis*, see Eq. (2.62) and (B.35). In Fig. 5.8, we plot $\overline{Q}$ versus the driving frequency for the three different QMEs employed, analogously to Fig. 5.5 in Sec. 5.3. There, "no RWA" stands for the QME without RWA; "$\text{RWA}_{\text{energy}}$" corresponds to the QME with RWA in the energy basis — the one used for the results in the main text —; finally, "$\text{RWA}_{\text{Floquet}}$" points at the results obtained from the QME with RWA in the coherent Floquet basis. We observe that the improvement over the coherent curve is obtained in all the three cases, suggesting some generality for this behaviour. Furthermore, the results obtained from the two versions of the RWA seem to match quite well, especially at smaller frequencies. Nevertheless, the data are quantitatively different, especially the ones obtained without RWA. For example, at $T = 0.75 J_0$ and in the frequency range studied, one might get or not an improvement over the coherent case depending on the approach used.

Let us now move to the study of system-bath coupling operators different from $\hat{\sigma}_z$. We focus here on the case in which each two-level system is coupled to the reservoir via the $\hat{\sigma}_x$ operator, which would correspond to choosing $\boldsymbol{\lambda} = (100)$ in Eq. (5.13). Fig. 5.9 shows the result for $\overline{Q}$ vs the driving frequency. We see that

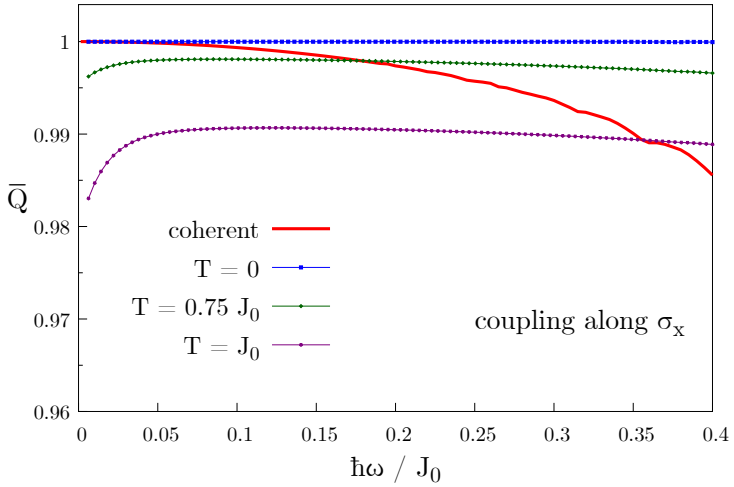

Figure 5.9: $\overline{Q}$ vs driving frequency ω for a bath coupled to the system via the $\hat{\sigma}_x$ operator ($\boldsymbol{\lambda} = (100)$). We observe a qualitative agreement with the results in Fig. 5.5, corresponding to a coupling along $\hat{\sigma}_z$ ($\boldsymbol{\lambda} = (001)$).

there is no qualitative difference with the result shown in Fig. 5.5, corresponding to a coupling via $\hat{\sigma}_z$. We tried also other coupling operators (for generic $\boldsymbol{\lambda}$) and we obtained qualitatively similar results.

5.6 Final remarks

In the present chapter [47], we analysed the role of dissipation from a somewhat idealized thermal environment — coupling independent baths to each fermionic k-mode — on topological adiabatic pumping in the Rice-Mele model. We found that a low-temperature bath can assist against undesired (inevitable) non-adiabatic effects. Dissipation induces this improvement because it increases the population of the lowest-energy Floquet band. Indeed, the pumped charge would be essentially quantized — up to exponentially small terms — when this band is completely filled. Our findings are qualitatively independent of the system-bath coupling chosen as long as we stay in a weak coupling regime. We also remark that the phenomena we see are qualitatively robust if we change the specific approximations behind the quantum master equation we use (although the quantitative details are different).

The fact that thermal effects can be beneficial is remarkable and interesting for future experimental realizations. We stress that the effect is not related to a *bath engineering*, exploited in the literature for other topological models [20].

A further step towards a deeper understanding would be to study more realistic couplings to the environment, *e.g.* via operators acting on sites in real space, which

break the entanglement in physical space. However, this analysis requires more sophisticated approaches [76, 141, 61], and is left to future studies.

Another interesting direction would be to study topological measures, such as the Uhlmann phase [142] and the Ensemble Geometric Phase (EGP) [134]. In particular, it would be interesting to inquire if the Uhlmann phase of the asymptotic time-periodic effective density matrix has a relation with the pumped charge, in analogy with the Berry or the Aharonov-Anandan geometric phase in the coherent cyclic case [79, 43].

Final discussion and outlook

This PhD thesis described research activity in the field of driven-dissipative quantum systems, with special focus on quantum annealing and topological adiabatic quantum pumping. Dissipation was induced by interaction with a thermal bosonic reservoir, modelled as a Caldeira-Leggett bath. Almost all the studies have been carried out assuming weak system-bath couplings and the Born-Markov approximation, so to justify the use of the Bloch-Redfield QME to compute the dissipative dynamics.

We first tackled the dissipative Landau-Zener problem. On the one hand, we benchmarked the QME to understand its regimes of reliability: despite the approximations involved in its derivation, we found it works surprisingly well, beyond our expectations. On the other hand, we shed light upon the mechanism of thermally-assisted quantum annealing, which we found to happen only whenever the system and the bath couple (at least partially) along the direction of the tunnelling amplitude. We never observed such an effect for couplings longitudinal to the driving field, neither for ohmic nor for sub/super-ohmic bath spectral functions.

We then studied dissipation in quantum annealing while crossing a second-order phase transition in the quantum spin-1/2 Ising chain in transverse field. We characterized the regimes of bath temperatures and system-bath interaction strengths for which one can observe an optimal annealing time or not, concluding that the current quantum annealing hardware should show no optimal annealing time. Therefore, slower annealings should lead to better results, as for unitary evolutions. Moreover, we found that the additivity *Ansatz* for the density of defects only holds when the annealing time is shorter than the relaxation time. We also studied whether exploiting relaxation without driving could be favourable over dissipative quantum annealing, finding that this is never the case.

Finally, we turned to dissipative effects in topological adiabatic quantum pumping. Under unitary dynamics, one observes quadratic-in-ω deviations from the quantized value, where ω is the driving frequency; however, we reported that a low-temperature reservoir can decrease such deviations considerably, providing what we called "thermally-assisted Thouless pumping". We analysed this effect in the Floquet framework: the thermal improvement implies a higher population of the lowest-energy coherent Floquet band.

Overall, although our modelling of dissipation is somewhat idealized, it permit-

ted us to reveal basic effects that are very likely to persist in real systems. In particular, it is clear from our results that dissipation can be a *surprisingly good resource* — rather than an obstacle — towards the realization of quantum technologies. However, a deeper understanding of driven-dissipative systems is still needed and much work has to be done in this direction.

In the future, it would be very interesting to focus on more general models, taking into account also disorder and interactions. This is important, for example, in quantum annealing, where solving an optimization problem requires generically to deal with a spin-glass system [27]. The study of dissipation in these settings is, however, a very challenging problem, due to the exponentially-large Hilbert space and the need to compute the full density matrix. Nevertheless, more refined numerical techniques like quantum trajectories [73, 74, 75, 76] and tensor networks [68, 21] can partly serve for this purpose and are definitely worth exploring.

Another intriguing extension of our work would be to model more realistic system-bath couplings, accounting for non-Markovian effects and/or different bath spectral functions (accounting for low-frequency noise, for example [104]). This task requires more advanced and computationally heavy numerical tools [58, 63, 62, 143] that go beyond the standard Bloch-Redfield approach we outlined in Chapter 2.

In this thesis, we have always modelled the bath to reproduce unavoidable dissipation in real systems. However, it would be fascinating to reverse the perspective and engineer the dissipative dynamics to accomplish specific tasks, like preparing quantum states as steady states of open systems. One could, therefore, devise the environment at will, with dissipators that can be fully controlled and even driven in time. This line of research goes under the name of "reservoir engineering" [14, 15, 16].

Finally, another point that is worth exploring is related to topological measures for generically mixed states. Referring to the dissipative topological pumping discussed in Chapter 5, the results at $T = 0$ in Fig. 5.5 showed persistence of charge quantization even in the non-adiabatic regime. It would be very interesting to find a relation between the pumped charge and some other topological measure, such as the Uhlmann phase [142] or the Ensemble Geometric Phase [134].

Appendix A

Correlation functions for harmonic uncorrelated baths

In this appendix, we compute more explicitly the bath correlation functions. To specialize the discussion to the cases studied in this thesis, we assume here that the baths acting on the system are *uncorrelated*. This means that only diagonal terms in the correlation functions can be non-zero, so that $C_{\nu\nu'}(t) = \delta_{\nu,\nu'} C_{\nu\nu}(t)$. We can compute more explicitly Eq. (2.10), to get

$$C_{\nu\nu}(t) = \sum_l \lambda_{l\nu}^2 \Big[\mathrm{e}^{i\omega_{l\nu}t} f_B(\omega_{l\nu}) + \mathrm{e}^{-i\omega_{l\nu}t} \left(f_B(\omega_{l\nu}) + 1 \right) \Big] , \tag{A.1}$$

where $\langle \, \cdot \, \rangle_{\mathrm{eq}} = \mathrm{Tr}\{ \, \cdot \, \hat{\rho}_{\mathrm{B}} \}$ and $f_B(\omega_{l\nu}) = \langle \hat{b}_{l\nu}^\dagger \hat{b}_{l\nu} \rangle_{\mathrm{eq}}$ is the usual Bose distribution function. We can transform the sum into an integral by using the spectral function defined in Eq. (2.5), to write

$$\begin{aligned} C_{\nu\nu}(t) &= \int_0^\infty \mathrm{d}\omega \; J_\nu(\omega) \Big[\mathrm{e}^{i\omega t} f_B(\omega) + \mathrm{e}^{-i\omega t} \left(f_B(\omega) + 1 \right) \Big] = \\ &= \int_0^\infty \mathrm{d}\omega \; J_\nu(\omega) \left[\coth\left(\frac{\hbar\omega}{2k_B T} \right) \cos(\omega t) - i \sin(\omega t) \right] , \end{aligned} \tag{A.2}$$

where in the second expression we have explicitly split the real and imaginary parts. The Fourier transforms of the correlation functions can now be expressed as

$$\gamma_{\nu\nu}(\omega) = \begin{cases} 2\pi \, J_\nu(|\omega|) \, f_B(|\omega|) & \text{for } \omega < 0 \\ 2\pi \, J_\nu(\omega) \left(f_B(\omega) + 1 \right) & \text{for } \omega > 0 \end{cases} \tag{A.3}$$

Notice that, by taking the ratio $\gamma_{\nu\nu}(-\omega)/\gamma_{\nu\nu}(\omega) = \mathrm{e}^{-\beta\hbar\omega}$, all details about the bath spectral function $J_\nu(\omega)$ disappear completely, and the result is essentially a consequence of a detailed balance condition. The limit of Eq. (A.3) for $\omega \to 0$

depends on the details of the spectral function chosen. For the *ohmic* case in Eq. (2.6) we get

$$\gamma_{\nu\nu}(\omega \to 0) = 4\pi\hbar\alpha_\nu \, k_B T \; . \tag{A.4}$$

For the super-ohmic case the limit is zero, while for the sub-ohmic one it is infinity and therefore hard to handle.

A popular belief in the community is that the correlation function of an ohmic bath decays exponentially in time for large temperatures, while it shows a long polynomial decay only at low temperatures. This implies the idea that the Bloch-Redfield QME should be valid only at high temperatures, where it is possible to define a time-scale for the validity of the Markov approximation. We want to prove here that this argument is wrong and cannot invalidate the reliability of the QME at low temperatures. Let us thus have a deeper look into the behaviour of the bath correlation function. Dropping the ν index for simplicity, notice that the imaginary part of $C(t)$ is temperature independent, as can be seen from Eq. (A.2). Therefore, we can extract it from the easy $T = 0$ case,

$$C^{T=0}(t) = \int_0^\infty d\omega J(\omega) \mathrm{e}^{-i\omega t} = 2\alpha(\hbar\omega_c)^2 \frac{\Gamma(s+1)}{(1+i\omega_c t)^{s+1}} \; , \tag{A.5}$$

so that, for $s = 1$, we have

$$\mathrm{Im}\{C(t)\} = \mathrm{Im}\{C^{T=0}(t)\} = -4\alpha(\hbar\omega_c)^2 \frac{\omega_c t}{(1+\omega_c^2 t^2)^2} \; . \tag{A.6}$$

Hence, the imaginary part of $C(t)$ scales as t^{-3} for $t \gg 1/\omega_c$. The bath correlation function, for a generic s in Eq. (2.7), can also be expressed analytically:

$$\begin{aligned} C(t) = \alpha(\hbar\omega_c)^{1-s}(k_B T)^{1+s}\Gamma(s+1) \times \\ \times \left[\zeta\left(s+1, \frac{1+\beta\hbar\omega_c - i\omega_c t}{\beta\hbar\omega_c}\right) + \zeta\left(s+1, \frac{1+i\omega_c t}{\beta\hbar\omega_c}\right)\right] \; , \end{aligned} \tag{A.7}$$

where $\Gamma(x)$ is the Gamma function[1] and

$$\zeta(z,u) = \sum_{n=0}^{\infty} \frac{1}{(n+u)^z} \tag{A.8}$$

is the Hurwitz Zeta function. Fig. A.1 illustrates the behaviour of the real part of $C(t)$ at different bath temperature regimes: we observe a polynomial decay as t^{-2} for all temperatures. A slight signature of exponential decay can be seen only at low

[1] For x integer, the Gamma function gives

$$\Gamma(x+1) = x! \; .$$

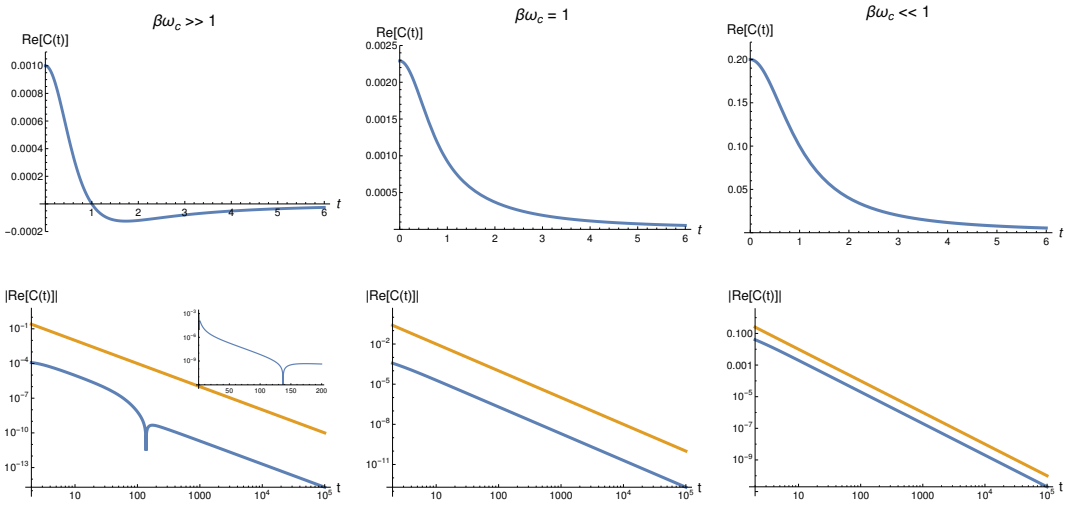

Figure A.1: **First row:** Real part of the bath correlation function *vs* time for different temperature regimes. **Second row:** Log-log plot of the absolute value, to highlight the power law scaling at large times. The orange line represents t^{-2}. In the low temperature case, there is a tiny region with exponential decay around $t = 100$ — as can be seen from the inset in linear-log scale —, but then the power law starts again.

temperature and intermediate times (see the inset in Fig. A.1), making contact with the study in Ref. [77]. Therefore, $C(t)$ decays *polynomially* as t^{-2} for all temperatures and, if the popular belief was correct, the Markovian approximation should never be appropriate and the Bloch-Redfield QME should never give good results! However this is not the case, as we see from our benchmarks in Chapter 3: we give extensive evidence for the reliability of the Bloch-Redfield QME at all temperature regimes.

Appendix B

Dissipative evolution equations for two-level systems

Suppose we have a generic two-level system. Its Hamiltonian, apart from constant energy shifts, can always be written in the Pauli basis as

$$\widehat{H}_{\mathrm{TLS}}(t) = \mathbf{R}(t) \cdot \hat{\boldsymbol{\sigma}} \,, \tag{B.1}$$

i.e. it is described by a real vector $\mathbf{R}(t)$ with three components and $\hat{\boldsymbol{\sigma}}$ is the vector of Pauli matrices. We consider a coupling to one common environment, with interaction Hamiltonian $\widehat{H}_{\mathrm{SB}} = \hat{A} \otimes \hat{B}$ and the operator acting on the system Hilbert space is in a generic direction in pseudo-spin space,

$$\hat{A} = \boldsymbol{\lambda} \cdot \hat{\boldsymbol{\sigma}} \,, \tag{B.2}$$

with $|\boldsymbol{\lambda}| = 1$. For this system, we are going to derive now explicit differential time-evolution equations starting from the Bloch-Redfield QME.

B.1 Adiabatic evolution and RWA

We derive here the evolution equations for an adiabatic evolution, assuming that there is no gap closing throughout the whole dynamics. This holds for all the cases studied in the present work: the Landau-Zener model has a finite gap Δ by definition, while the Rice-Mele model has just one gapless point, but we never explore it during the dynamics we study. Therefore, we can use Eq. (2.50). Neglecting the Lamb shift term, which only renormalizes the frequencies proper of the coherent dynamics in a small fashion, and dropping the time-dependence from the operators for simplicity,

we can write

$$\begin{aligned}\frac{d}{dt}\hat{\rho}_{\rm S} = &-\frac{i}{\hbar}\left[\widehat{H}_{\rm S},\hat{\rho}_{\rm S}\right] + \sum_{ab}\gamma_{abba}\,\langle b|\hat{\rho}_{\rm S}|b\rangle\,|a\rangle\langle a| + \\ &-\frac{1}{2}\sum_{b}\left(\sum_{a}\gamma_{abba}\right)\left(\,|b\rangle\langle b|\,\hat{\rho}_{\rm S} + \text{H.c.}\right) + \sum_{a}\gamma_{aa\bar{a}\bar{a}}\,|a\rangle\langle a|\hat{\rho}_{\rm S}|\bar{a}\rangle\langle\bar{a}|\,,\end{aligned} \tag{B.3}$$

where we remind that $|a\rangle$ is one eigenstate of $\widehat{H}_{\rm S}(t)$ and we denoted with $|\bar{a}\rangle$ its respective opposite eigenstate.

In order to go on with the calculation, it is very convenient to write all the operators in Bloch notation.[1] We will write the time-evolved system state as

$$\hat{\rho}_{\rm S}(t) = \frac{1}{2}\left(\mathbb{1} + \mathbf{r}\cdot\hat{\boldsymbol{\sigma}}\right) \tag{B.4}$$

and the system's eigenstates as

$$|a\rangle\langle a| = \frac{1}{2}\left(\mathbb{1} + \mathbf{r}_a\cdot\hat{\boldsymbol{\sigma}}\right)\,. \tag{B.5}$$

This will be particularly convenient because the ground and excited states of the two-level system in Eq. (B.1), in the notation above, are simply represented by

$$\begin{aligned}\mathbf{r}_{gs} &= -\frac{\mathbf{R}}{E} \equiv -\tilde{\mathbf{R}}\\ \mathbf{r}_{ex} &= +\frac{\mathbf{R}}{E} \equiv +\tilde{\mathbf{R}}\,,\end{aligned} \tag{B.6}$$

where $|\tilde{\mathbf{R}}| = 1$ by construction. There are some generic quantities we have to compute. Let us start with

$$\begin{aligned}|b\rangle\langle b|\hat{\rho}_{\rm S} &= \frac{1}{4}\left(\mathbb{1} + \mathbf{r}_b\cdot\hat{\boldsymbol{\sigma}}\right)\left(\mathbb{1} + \mathbf{r}\cdot\hat{\boldsymbol{\sigma}}\right) = \\ &= \frac{1}{4}\Big[\big(1 + \mathbf{r}_b\cdot\mathbf{r}\big)\mathbb{1} + \big(\mathbf{r} + \mathbf{r}_b + i(\mathbf{r}_b\times\mathbf{r})\big)\cdot\hat{\boldsymbol{\sigma}}\Big]\end{aligned}$$

and, consequently,

$$\langle b|\hat{\rho}_{\rm S}|b\rangle = \text{Tr}\left\{|b\rangle\langle b|\hat{\rho}_{\rm S}\right\} = \frac{1}{2}\big(1 + \mathbf{r}\cdot\mathbf{r}_b\big)\,.$$

[1] The following identity will be extremely useful to carry out the calculations:

$$\left(\mathbf{a}\cdot\hat{\boldsymbol{\sigma}}\right)\left(\mathbf{b}\cdot\hat{\boldsymbol{\sigma}}\right) = \left(\mathbf{a}\cdot\mathbf{b}\right)\mathbb{1} + i\left(\mathbf{a}\times\mathbf{b}\right)\cdot\hat{\boldsymbol{\sigma}}$$

The last term in Eq. (B.3) shows factors like

$$|a\rangle\langle a|\hat{\rho}_{\rm S}|b\rangle\langle b| = \frac{1}{8}\Big[\ \Big(1+(\mathbf{r}_a+\mathbf{r}_b)\cdot\mathbf{r}+\mathbf{r}_a\cdot\mathbf{r}_b+i(\mathbf{r}_a\times\mathbf{r})\cdot\mathbf{r}_b\Big)\mathbb{1}+ \\ +\Big((1+\mathbf{r}_b\cdot\mathbf{r})\mathbf{r}_a+(1+\mathbf{r}_a\cdot\mathbf{r})\mathbf{r}_b+(1-\mathbf{r}_a\cdot\mathbf{r}_b)\mathbf{r}+ \\ +i\,(\mathbf{r}_a\times\mathbf{r}+\mathbf{r}\times\mathbf{r}_b+\mathbf{r}_a\times\mathbf{r}_b)\Big)\cdot\hat{\boldsymbol{\sigma}}\Big]\ ,$$

which simplify considerably if we take $b=\bar{a}$, since this implies $\mathbf{r}_{\bar{a}}=-\mathbf{r}_a$, leading to

$$|a\rangle\langle a|\hat{\rho}_{\rm S}|\bar{a}\rangle\langle\bar{a}| = \frac{1}{4}\Big(\mathbf{r}-(\mathbf{r}_a\cdot\mathbf{r})\mathbf{r}_a+i\,\mathbf{r}_a\times\mathbf{r}\Big)\cdot\hat{\boldsymbol{\sigma}}\ .$$

Finally, the rate terms to be computed are

$$\begin{aligned}\gamma_{abba} &= \frac{\alpha^2}{\hbar^2}\,\gamma(\Delta_{ba})\,\langle a|(\boldsymbol{\lambda}\cdot\hat{\boldsymbol{\sigma}})|b\rangle\langle b|(\boldsymbol{\lambda}\cdot\hat{\boldsymbol{\sigma}})|a\rangle = \\ &= \frac{\alpha^2}{\hbar^2}\,\gamma(\Delta_{ba})\,{\rm Tr}\Big\{|a\rangle\langle a|(\boldsymbol{\lambda}\cdot\hat{\boldsymbol{\sigma}})|b\rangle\langle b|(\boldsymbol{\lambda}\cdot\hat{\boldsymbol{\sigma}})\Big\} = \\ &= \frac{\alpha^2}{\hbar^2}\,\gamma(\Delta_{ba})\,\frac{1}{2}\Big(1-\mathbf{r}_a\cdot\mathbf{r}_b+2\,(\boldsymbol{\lambda}\cdot\mathbf{r}_a)(\boldsymbol{\lambda}\cdot\mathbf{r}_b)\Big)\ ,\end{aligned}$$

$$\begin{aligned}\gamma_{aabb} &= \frac{\alpha^2}{\hbar^2}\,\gamma(0)\,\langle a|(\boldsymbol{\lambda}\cdot\hat{\boldsymbol{\sigma}})|a\rangle\langle b|(\boldsymbol{\lambda}\cdot\hat{\boldsymbol{\sigma}})|b\rangle = \\ &= \frac{\alpha^2}{\hbar^2}\,\gamma(0)\,{\rm Tr}\Big\{(\boldsymbol{\lambda}\cdot\hat{\boldsymbol{\sigma}})|a\rangle\langle a|\Big\}{\rm Tr}\Big\{(\boldsymbol{\lambda}\cdot\hat{\boldsymbol{\sigma}})|b\rangle\langle b|\Big\} = \\ &= \frac{\alpha^2}{\hbar^2}\,\gamma(0)\,(\boldsymbol{\lambda}\cdot\mathbf{r}_a)(\boldsymbol{\lambda}\cdot\mathbf{r}_b)\ .\end{aligned}$$

With all these ingredients ready, one can now compute all the terms appearing in Eq. (B.3). Putting all the pieces together, we can write

$$\dot{\mathbf{r}} = \frac{2}{\hbar}\,\mathbf{R}\times\mathbf{r}-\mathbb{A}^{\rm RWA}_{diss}\cdot\mathbf{r}-\mathbf{b}^{\rm RWA}\ , \tag{B.7}$$

where the first term on the r.h.s. gives the coherent evolution, while the other two cause dissipation effects and look as follows:

$$\mathbb{A}^{\rm RWA}_{diss} = \begin{pmatrix}\gamma_{{\rm D},x} & \gamma_{xy} & \gamma_{xz}\\ \gamma_{xy} & \gamma_{{\rm D},y} & \gamma_{yz}\\ \gamma_{xz} & \gamma_{yz} & \gamma_{{\rm D},z}\end{pmatrix} \tag{B.8}$$

$$\mathbf{b}^{\rm RWA} = \tilde{\mathbf{R}}\,\gamma_{\rm R}\tanh(\beta E)\ , \tag{B.9}$$

where

$$\gamma_{\mathrm{D},i} = \left(\frac{\gamma_\mathrm{R}}{2} + \gamma_\varphi\right) + \tilde{R}_i^2 \left(\frac{\gamma_\mathrm{R}}{2} - \gamma_\varphi\right) \tag{B.10}$$

$$\gamma_{ij} = \tilde{R}_i \tilde{R}_j \left(\frac{\gamma_\mathrm{R}}{2} - \gamma_\varphi\right) \ . \tag{B.11}$$

and we defined the time-dependent rates

$$\gamma_\mathrm{R} = \frac{S_X(2E/\hbar)}{\hbar^2}\Big(1 - (\boldsymbol{\lambda}\cdot\tilde{\mathbf{R}})^2\Big) \ , \tag{B.12}$$

$$\gamma_\varphi = \frac{S_X(0)}{\hbar^2}(\boldsymbol{\lambda}\cdot\tilde{\mathbf{R}})^2 \ , \tag{B.13}$$

which, in a time-independent setting, are the so-called relaxation and pure-dephasing rates, respectively. To write them, we employed the Fourier transform of the symmetrized correlation function, $S_X(\omega) = \gamma(\omega) + \gamma(-\omega)$. For an Ohmic spectral density, the $\gamma(\omega)$ rates are given by Eq.s (A.3) and (A.4).

B.2 Adiabatic evolution without RWA

Here we focus on the Bloch-Redfield QME before applying the RWA, keeping all the non-secular terms that having been neglected in the previous approach.

We have to start from Eq. (2.25), using the second Markov approximation to express the $\widehat{S}(t)$ operator as in Eq. (2.28). It is no more convenient to use the system eigenstates basis, as in Sec. B.1. We express all the operators in Bloch vector notation instead, according to Eq. (B.4). Neglecting all the time-dependence indices for simplicity and defining $|\mathbf{R}| = E$, $\omega = E/\hbar$ and $\tilde{\mathbf{R}} = \mathbf{R}/E$, we can write the free system evolution operator as

$$\widehat{U}_{0\mathrm{S}}(t, t-\tau) \simeq \mathrm{e}^{-i\widehat{H}_\mathrm{S}(t)\tau/\hbar} = \cos(\omega t)\mathbb{1} + \mathbf{u}\cdot\hat{\boldsymbol{\sigma}} \ , \tag{B.14}$$

where $\mathbf{u} \equiv -i\tilde{\mathbf{R}}\sin(\omega t)$. Then, we can express the convoluted operator in Eq. (2.28) as

$$\widehat{S}(t) \simeq \int_0^t d\tau C(\tau)\mathrm{e}^{-i\widehat{H}_\mathrm{S}(t)\tau/\hbar}(\boldsymbol{\lambda}\cdot\hat{\boldsymbol{\sigma}})\mathrm{e}^{i\widehat{H}_\mathrm{S}(t)\tau/\hbar} = \mathbf{s}\cdot\hat{\boldsymbol{\sigma}} \ , \tag{B.15}$$

with $\mathbf{s} = \boldsymbol{\lambda}\,\Gamma_c(2\omega) + (\tilde{\mathbf{R}}\times\boldsymbol{\lambda})\,\Gamma_s(2\omega) + \tilde{\mathbf{R}}(\tilde{\mathbf{R}}\cdot\boldsymbol{\lambda})\,(\Gamma_0 - \Gamma_c(2\omega))$, upon defining $\Gamma_0 = \int_0^\infty d\tau C(\tau)$, $\Gamma_c(\omega) = \int_0^\infty d\tau C(\tau)\cos(\omega\tau)$ and $\Gamma_s(\omega) = \int_0^\infty d\tau C(\tau)\sin(\omega\tau)$. Within this notation, the Bloch-Redfield QME without RWA, Eq. (2.25), looks

$$\begin{aligned}\dot{\mathbf{r}} &= \frac{2}{\hbar}\,\mathbf{R}\times\mathbf{r} - \frac{2\alpha^2}{\hbar^2}\Big\{i(\boldsymbol{\lambda}\times\mathbf{s} - \boldsymbol{\lambda}\times(\mathbf{s}\times\mathbf{r}) + \mathrm{c.c.}\Big\} = \\ &= \frac{2}{\hbar}\,\mathbf{R}\times\mathbf{r} - \frac{2\alpha^2}{\hbar^2}\Big\{i\boldsymbol{\lambda}\times(\mathbf{s}-\mathbf{s}^*) - \boldsymbol{\lambda}\times\big((\mathbf{s}+\mathbf{s}^*)\times\mathbf{r}\big)\Big\} \ .\end{aligned} \tag{B.16}$$

Carrying out the calculation until the end, one eventually gets a differential equation of the form of Eq. (B.7),

$$\dot{\mathbf{r}} = \frac{2}{\hbar}\,\mathbf{R} \times \mathbf{r} - \mathbb{A}_{diss}^{no\ \mathrm{RWA}} \cdot \mathbf{r} - \mathbf{b}^{no\ \mathrm{RWA}} \,, \tag{B.17}$$

where

$$\mathbb{A}_{diss}^{no\ \mathrm{RWA}} = \begin{bmatrix} \tilde{\gamma}_{\mathrm{D},x} & \tilde{\gamma}_{xy} & \tilde{\gamma}_{xz} \\ \tilde{\gamma}_{yx} & \tilde{\gamma}_{\mathrm{D},y} & \tilde{\gamma}_{yz} \\ \tilde{\gamma}_{zx} & \tilde{\gamma}_{zy} & \tilde{\gamma}_{\mathrm{D},z} \end{bmatrix} \,, \tag{B.18}$$

$$\mathbf{b}^{no\ \mathrm{RWA}} = \begin{bmatrix} \gamma_{\mathrm{R}} \\ 0 \\ \gamma_{zx} \end{bmatrix} \tanh(\beta E(t)/2) \,. \tag{B.19}$$

The rates are

$$\tilde{\gamma}_{\mathrm{D},i} = \gamma_{\mathrm{R}} + \gamma_{\varphi} - \tilde{\gamma}_{ii} \,, \tag{B.20}$$

$$\tilde{\gamma}_{ij} = \lambda_j \big(\tilde{R}_i(\tilde{\mathbf{R}} \cdot \boldsymbol{\lambda}) \left(S_X(2E) - S_X(0) \right) - \lambda_i S_X(2E) \big) \,. \tag{B.21}$$

B.3 Evolution equations in the instantaneous system energy eigenbasis

We show here the differential equations used in Ref.s [31, 32] to compute the dynamics of Landau-Zener-like Hamiltonians. In these works, the equations were written in a time-dependent basis, to make contact with previous works [101, 95].

We consider thus a system governed by the Landau-Zener Hamiltonian

$$\widehat{H}_{\mathrm{LZ}}(t) = \frac{\epsilon(t)}{2}\hat{\sigma}_z + \frac{\Delta}{2}\hat{\sigma}_x \,, \tag{B.22}$$

under the influence of a single bath coupled as $\widehat{H}_{\mathrm{SB}} = \hat{A} \otimes \hat{B}$, with

$$\hat{A} = \sin\theta\,\hat{\sigma}_x + \cos\theta\,\hat{\sigma}_z \,. \tag{B.23}$$

We perform a time-dependent rotation on all the operators in the Bloch-Redfield QME, so that

$$\widetilde{H}_{\mathrm{S}}(t) = \hat{R}^{\dagger}(t)\widehat{H}_{\mathrm{S}}(t)\hat{R}(t) = \frac{E(t)}{2}\hat{\sigma}_x \,, \tag{B.24}$$

where $E(t) = \sqrt{\epsilon^2(t) + \Delta^2}$, $\hat{R}(t) = \exp(i\phi(t)\hat{\sigma}_y/2)$ and $\phi(t) = \arctan(\epsilon(t)/\Delta)$. With this choice, relaxation will happen only along the specific $\hat{\sigma}_x$ component, giving the possibility of highlighting more clearly the two time-scales of relaxation and dephasing [85]. Notice that, as a consequence of the time-dependence of the change

of basis, a new term appears in the QME because

$$\begin{aligned}\partial_t\widetilde{\rho}_{\mathrm{S}}(t) &= \partial_t(\hat{R}^\dagger(t)\hat{\rho}_{\mathrm{S}}(t)\hat{R}(t)) = \\ &= \partial_t\hat{R}^\dagger(t)\hat{R}(t)\widetilde{\rho}_{\mathrm{S}}(t) + \widetilde{\rho}_{\mathrm{S}}(t)\hat{R}^\dagger(t)\partial_t\hat{R}(t) + \hat{R}^\dagger(t)\partial_t\hat{\rho}_{\mathrm{S}}(t)\hat{R}(t)\ ,\end{aligned} \tag{B.25}$$

where $\partial_t\hat{R}^\dagger(t)\hat{R}(t) = -i\dot{\phi}(t)\hat{\sigma}_y/2$. Following the same approaches used before without rotation, we can compute the explicit equations from the Bloch-Redfield QME with and without RWA. For both cases, neglecting time dependence indices for simplicity, and using $\widetilde{\rho}_{\mathrm{S}} = (\mathbb{1} + \tilde{\mathbf{r}}\cdot\hat{\boldsymbol{\sigma}})/2$, we can write

$$\partial_t\tilde{\mathbf{r}} = \mathbb{A}_{\mathrm{coh}}\cdot\tilde{\mathbf{r}} - \mathbb{A}_{\mathrm{diss}}\cdot\tilde{\mathbf{r}} + \mathbf{b}\ , \tag{B.26}$$

with the following coherent matrix

$$\mathbb{A}_{\mathrm{coh}} = \begin{bmatrix} 0 & 0 & -\dot{\phi} \\ 0 & 0 & E \\ \dot{\phi} & -E & 0 \end{bmatrix}\ . \tag{B.27}$$

If we employ the RWA, we find

$$\mathbb{A}_{\mathrm{diss}} = \begin{bmatrix} \gamma_{\mathrm{R}} & 0 & 0 \\ 0 & \gamma_{\mathrm{D}} & 0 \\ 0 & 0 & \gamma_{\mathrm{D}} \end{bmatrix}\ , \tag{B.28a}$$

$$\mathbf{b} = \begin{bmatrix} \gamma_{\mathrm{R}} \\ 0 \\ 0 \end{bmatrix} \tanh(\beta E(t)/2)\ . \tag{B.28b}$$

Notice how the purely dissipative dynamics of populations and of coherences are completely decoupled. For a time-independent problem, relaxation would happen only along $\hat{\sigma}_x$, while dephasing would take place only along $\hat{\sigma}_y$ and $\hat{\sigma}_z$, giving rise to classical rate equations. If we instead do not use the RWA, we get

$$\mathbb{A}_{\mathrm{diss}} = \begin{bmatrix} \gamma_{\mathrm{R}} & 0 & -\gamma_{xz} \\ 0 & \gamma_{\mathrm{D}} + \frac{\gamma_{\mathrm{R}}}{2} & 0 \\ \gamma_{zx} & 0 & \gamma_{\mathrm{D}} - \frac{\gamma_{\mathrm{R}}}{2} \end{bmatrix}\ , \tag{B.29a}$$

$$\mathbf{b} = \begin{bmatrix} \gamma_{\mathrm{R}} \\ 0 \\ \gamma_{zx} \end{bmatrix} \tanh(\beta E(t)/2)\ . \tag{B.29b}$$

The time-dependent rate constants corresponding, for a time-independent problem, to the usual "relaxation" γ_{R}, "pure dephasing" γ_φ and "decoherence" γ_{D} rates [85]

are defined as

$$\gamma_{\mathrm{R}}(t) = \frac{\pi}{2\hbar^2} \coth\left(\frac{\beta E(t)}{2}\right) J(E(t)/\hbar)\, \cos^2(\phi(t)+\theta) \tag{B.30a}$$

$$\gamma_{\varphi}(t) = \frac{2\pi\alpha}{\hbar\beta}\, \sin^2(\phi(t)+\theta) \tag{B.30b}$$

$$\gamma_{\mathrm{D}}(t) = \gamma_{\varphi}(t) + \frac{1}{2}\gamma_{\mathrm{R}}(t)\ ; \tag{B.30c}$$

moreover, if we do not employ the RWA, we have the following two extra terms:

$$\gamma_{zx}(t) = -\frac{\pi}{4\hbar^2} \coth\left(\frac{\beta E(t)}{2}\right) J(E(t)/\hbar)\, \sin 2(\phi(t)+\theta) \tag{B.31a}$$

$$\gamma_{xz}(t) = \frac{\pi\alpha}{\hbar\beta}\, \sin 2(\phi(t)+\theta)\ . \tag{B.31b}$$

B.4 Periodic evolution and RWA in the Floquet basis

We proceed here to derive a rate equation for computing the steady state of a dissipative periodically-driven quantum two-level system. This is used in Chapter 5 to compute the steady pumped charge in the dissipative Rice-Mele model. Consider thus the density matrix elements in the Floquet basis as

$$\rho_{ab} \equiv \langle \psi_a(t)|\hat{\rho}_{\mathrm{S}}(t)|\psi_b(t)\rangle \tag{B.32}$$

so that, for a two-level system, ρ_{+-} is the coherence term, while ρ_{--} is one of the two populations. For simplicity, we assume no degeneracies in the differences between quasi-energies and neglect the Lamb-shift Hamiltonian. Starting from Eq. (2.62), we can thus write a QME where coherences and populations are decoupled. Regarding the coherence, we have

$$\dot{\rho}_{+-} = -\frac{1}{2}\Big(\widetilde{\gamma}_{-++-} + \widetilde{\gamma}_{+--+} + \widetilde{\gamma}_{++++} + \widetilde{\gamma}_{----} - 2\widetilde{\gamma}_{++--}\Big)\rho_{+-}\ , \tag{B.33}$$

where it is possible to show that the real part of the coefficient on the r.h.s. is negative [83, 79] so that, eventually, coherences are zero in the steady state. One of the two populations obeys instead the following equation:

$$\dot{\rho}_{--} = \widetilde{\gamma}_{-++-}\rho_{++} - \widetilde{\gamma}_{+--+}\rho_{--}\ , \tag{B.34}$$

which is a rate equation that will eventually reach an equilibrium value. Hence, because $\rho_{++} = 1 - \rho_{--}$, we can very simply evaluate the steady state of the system

by requiring $\dot{\rho}_{--} = 0$, to get

$$\begin{aligned} \rho^{ss}_{--} &= \frac{\widetilde{\gamma}_{-++-}}{\widetilde{\gamma}_{-++-} + \widetilde{\gamma}_{+--+}} \ , \\ \rho^{ss}_{++} &= 1 - \rho^{ss}_{--} \ . \end{aligned} \tag{B.35}$$

Appendix C

Thermal defects density calculation

In this appendix, we compute analytically the equilibrium thermal defects density for an ordered transverse-field Ising chain with a fixed h. To start, recall that the Hamiltonian in Eq. (4.1) conserves the parity of the number of up (or down) spins. As a consequence, the Hilbert space can be partitioned into even and odd parity sectors. This partitioning survives also when moving to the spinless fermions picture, so that we can think the Hamiltonian in Eq. (4.2) as being the *even fermion* block of the total Hamiltonian $\widehat{H}^F_{\text{even}} \oplus \widehat{H}^F_{\text{odd}}$. Observe that, considering $\widehat{H}^F_{\text{even}}$ only, we account for $N/2$ two-level systems, hence a total of $2^{N/2}$ states. Let us, for a moment, assume that we treat these $N/2$ two-level systems in a thermal state at temperature T_b. For a given momentum k, we reduce the basis states to just absence/presence of pairs of opposite momentum and diagonalize the Hamiltonian $\widehat{H}^{(k)}_{\text{S}} = \xi_k \hat{\tau}^z_k + \Delta_k \hat{\tau}^x_k$ to get

$$\widehat{H}^{(k)}_{\text{diag}} = \begin{bmatrix} \epsilon_k & 0 \\ 0 & -\epsilon_k \end{bmatrix} , \tag{C.1}$$

where $\epsilon_k = \sqrt{\xi_k^2 + \Delta_k^2}$. Therefore, the corresponding thermal state is given by

$$\begin{aligned} \hat{\rho}^{(k)}_{\text{therm}} &\equiv \frac{e^{-\beta_b \widehat{H}^{(k)}_{\text{diag}}}}{\text{Tr}\{e^{-\beta_b \widehat{H}^{(k)}_{\text{diag}}}\}} = \\ &= \frac{1}{\text{e}^{\beta_b \epsilon_k} + \text{e}^{-\beta_b \epsilon_k}} \begin{bmatrix} \text{e}^{-\beta_b \epsilon_k} & 0 \\ 0 & \text{e}^{\beta_b \epsilon_k} \end{bmatrix} . \end{aligned} \tag{C.2}$$

This state is expressed in the basis of the eigenstates of $\widehat{H}^{(k)}_{\text{S}}$, which are combinations of the original basis states $|\uparrow\rangle_k \equiv \hat{c}^\dagger_k \hat{c}^\dagger_{-k}|0\rangle$, and $|\downarrow\rangle_k \equiv |0\rangle$. The corresponding creation operators $\hat{\eta}^\dagger_k$, in terms of which $\widehat{H}^{(k)}_{\text{diag}} = \epsilon_k(\hat{\eta}^\dagger_k \hat{\eta}_k - \hat{\eta}_{-k}\hat{\eta}^\dagger_{-k})$, are simply

related to the original fermionic operators by

$$\hat{c}_k = u_k \hat{\eta}_k - v_k \hat{\eta}^\dagger_{-k} \,, \tag{C.3}$$

where $(u_k, v_k) = (\epsilon_k + \xi_k, \Delta_k)/\sqrt{2\epsilon_k(\epsilon_k + \xi_k)}$. Writing the defect density operator $\hat{n}^{(k)}_{\rm def}$ in Eq. (4.9) in terms of the $\hat{\eta}^\dagger_k$, the corresponding expectation value over the thermal state finally reads

$$\begin{aligned} n^{T_b}_{\rm def} &= \frac{1}{N}\sum_{k>0} \mathrm{Tr}\{\hat{n}^{(k)}_{\rm def}\,\hat{\rho}^{(k)}_{\rm therm}\} = \\ &= \frac{1}{N}\sum_{k>0}\Big[1 - y_k\big(1 - 2\,\mathrm{Tr}\{\hat{\eta}^\dagger_k\hat{\eta}_k\hat{\rho}^{(k)}_{\rm therm}\}\big)\Big] = \\ &= \frac{1}{N}\sum_{k>0}\Big[1 - y_k \tanh\big(\beta_b\epsilon_k\big)\Big] \,, \end{aligned} \tag{C.4}$$

where $y_k \equiv (\Delta_k \sin k - \xi_k \cos k)/\epsilon_k$ and $\mathrm{Tr}\{\hat{\eta}^\dagger_k\hat{\eta}_k\hat{\rho}^{(k)}_{\rm therm}\} = f_F(2\beta_b\epsilon_k)$, with $f_F(x) = 1/(1+e^x)$ being the Fermi distribution function. Notice the factor 2 in the Fermi function argument, due to the fact that excitations here consist of two fermions, and cost an energy $2\epsilon_k$. Eq. (C.4) gives the density of defects for a system that thermalizes with a bath at temperature T_b, but can only explore states with pairs of fermions with opposite momenta.

The original problem, however, was a transverse-field Ising chain, and we are evidently making violence to the correct thermodynamics by looking only at the even-fermion sector of the Hilbert space: the counting of states, $2^{N/2}$, as opposed to the 2^N states of the full Hilbert space, is a clear witness of that error. Thinking in terms of the correct approach to the problem, one would immediately realize that the very fact that the fermionic boundary conditions, and hence the required k-vectors, change when the fermionic parity changes, brings a non-trivial "interaction" between fermions, which does not allow for a simple thermodynamical free-fermion calculation. However, one can devise the following shortcut, which should be correct in the thermodynamic limit $N \to \infty$, when the difference in the k-vectors associated to the two parity sectors is negligible. Let us assume that we keep the $N/2$ k-vectors fixed to those selected by the ABC boundary conditions for fermions, but allow also for the *singly occupied* states $\hat{c}^\dagger_k|0\rangle$ and $\hat{c}^\dagger_{-k}|0\rangle$. For each of the $N/2$ values of k, we have 4 states, hence $4^{N/2} = 2^N$ states in total. The Hamiltonian at fixed k, in the basis given by $\{\hat{c}^\dagger_k|0\rangle, \hat{c}^\dagger_{-k}|0\rangle, \hat{c}^\dagger_k\hat{c}^\dagger_{-k}|0\rangle, |0\rangle\}$, is now four-dimensional, and given by

$$\widehat{H}^{(k)}_{\rm full} = \begin{bmatrix} 0 & 0 & 0 & 0 \\ 0 & 0 & 0 & 0 \\ 0 & 0 & \epsilon_k & 0 \\ 0 & 0 & 0 & -\epsilon_k \end{bmatrix} . \tag{C.5}$$

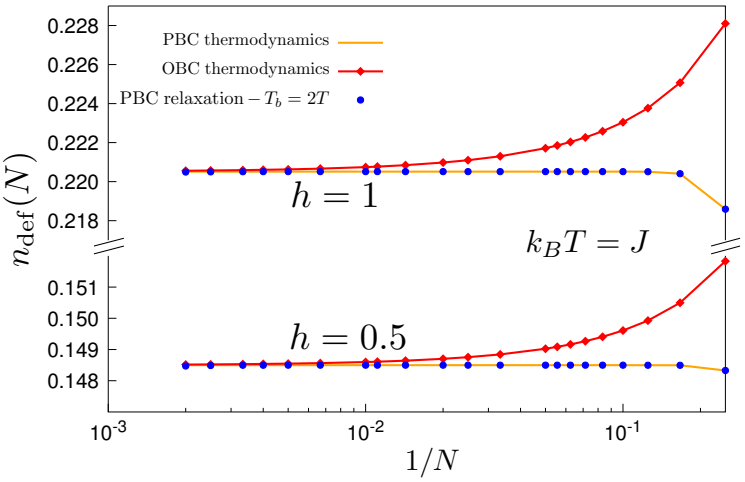

Figure C.1: Thermodynamics of the defects density in the transverse-field Ising chain for $k_BT = J$. The PBC thermodynamics (orange solid lines) is calculated with Eq. (C.7), while the OBC thermodynamics (red solid lines and diamonds) corresponds to Eq. (C.11). The blue solid circles are PBC-QME relaxation dynamics data for $N/2$ two-level systems for $T_b = 2T$.

To get the thermal equilibrium state, we exponentiate $\widehat{H}^{(k)}_{\rm full}$:

$$\hat{\rho}^{(k)}_{\rm full} = \frac{1}{Z_{\rm full}} \begin{bmatrix} 1 & 0 & 0 & 0 \\ 0 & 1 & 0 & 0 \\ 0 & 0 & \mathrm{e}^{\beta\epsilon_k} & 0 \\ 0 & 0 & 0 & \mathrm{e}^{-\beta\epsilon_k} \end{bmatrix}, \tag{C.6}$$

where $Z_{\rm full} = 2 + \mathrm{e}^{-\beta\epsilon_k} + \mathrm{e}^{\beta\epsilon_k}$. Building on this result, we can compute the defect density starting from the second line in Eq. (C.4), but noting that now we have $\mathrm{Tr}\{\hat{\eta}^\dagger_k \hat{\eta}_k \hat{\rho}^{(k)}_{\rm full}\} = f(\beta\epsilon_k)$. Therefore, it follows that

$$n^{\rm full}_{\rm def} = \frac{1}{N} \sum_{k>0} \left[1 - y_k \tanh\left(\frac{\beta\epsilon_k}{2}\right)\right], \tag{C.7}$$

where y_k is defined exactly as before. A comparison of this equation with Eq. (C.4) shows that, restricting to states with only pairs of fermions with opposite momenta, the density of defects at thermal equilibrium corresponds to the true thermodynamic one, provided the temperature of the bath is rescaled by a factor 2, *i.e.* $T = T_b/2$.

Properly speaking, the expression in Eq. (C.7) is exact only in the thermodynamic limit $N \to \infty$. One might wonder how close it describes the equilibrium thermodynamics for a finite value of N. Here, an exact and consistent reference value can be easily obtained for an Ising chain with open boundary conditions (OBC),

where the spectrum does not depend on the fermionic parity. The price to be paid is that the diagonalization is not a trivial k-sum of 2×2 problems. Nevertheless, for a given value of the transverse field h, the problem can be always reduced to an ensemble of N two-level systems. The standard result is then [119, 144]

$$\widehat{H}_{\mathrm{OBC}} = \sum_{m=1}^{N} \tilde{\epsilon}_m \left[\tilde{\eta}_m^\dagger \tilde{\eta}_m - \tilde{\eta}_m \tilde{\eta}_m^\dagger \right] \tag{C.8}$$

where $\tilde{\eta}_m^\dagger$ are the creation operators for the eigenstates with energies $\tilde{\epsilon}_m$, defined as

$$\tilde{\eta}_m = \sum_{i=1}^{N} \left(g_{m,i} \hat{c}_i + h_{m,i} \hat{c}_i^\dagger \right) \tag{C.9}$$

The real coefficients $g_{m,i}, h_{m,i}$, together with the energies $\tilde{\epsilon}_m$, can be computed numerically [119, 144]. The thermal state is thus the normalized matrix exponential of Eq. (C.8):

$$\tilde{\rho}_{\mathrm{therm}}^{(m)} = \frac{1}{\mathrm{e}^{\beta\tilde{\epsilon}_m} + \mathrm{e}^{-\beta\tilde{\epsilon}_m}} \begin{bmatrix} \mathrm{e}^{-\beta\tilde{\epsilon}_m} & 0 \\ 0 & \mathrm{e}^{\beta\tilde{\epsilon}_m} \end{bmatrix} . \tag{C.10}$$

We can finally express the defect density operator in Eq. (4.8) by using the $\tilde{\eta}_m$ operators, and then compute its expectation value on the thermal state (C.10):

$$n_{\mathrm{def}}^{\mathrm{OBC}} = \frac{1}{2} - \frac{1}{N-1} \sum_{m=1}^{N} \left(\tilde{A}_m \, f_F(2\beta\tilde{\epsilon}_m) + \tilde{B}_m \, f_F(-2\beta\tilde{\epsilon}_m) \right) \tag{C.11}$$

with

$$\tilde{A}_m = \sum_{i=1}^{N-1} g_{m,i}(g_{m,i+1} + h_{m,i+1}) \, , \tag{C.12a}$$

$$\tilde{B}_m = \sum_{i=1}^{N-1} h_{m,i}(g_{m,i+1} + h_{m,i+1}) \, . \tag{C.12b}$$

In Fig. C.1 we show the results for the density of defects at $k_B T = J$ versus N, for two different values of the transverse field: the critical value $h = h_c = 1$, and a value in the ferromagnetically ordered phase, $h = 0.5 < h_c$. The plot reports the results obtained by three different approaches: *i)* the PBC formula in Eq. (C.7) (orange solid lines); *ii)* an explicit QME relaxation with $T_b = 2T$ (blue circles); *iii)* the exact OBC evaluation, following Eq. (C.11) (red solid lines and diamonds). Notice that the convergence of the PBC results to the thermodynamic limit is exponentially fast in N, while the OBC data show $1/N$ finite-size scaling corrections. This is illustrated in Fig. C.2, where we show the finite-size scaling of both the PBC data (top) and OBC results (bottom) to the common thermodynamical limit for $k_B T = J$

and $h = 0.5, 1$.

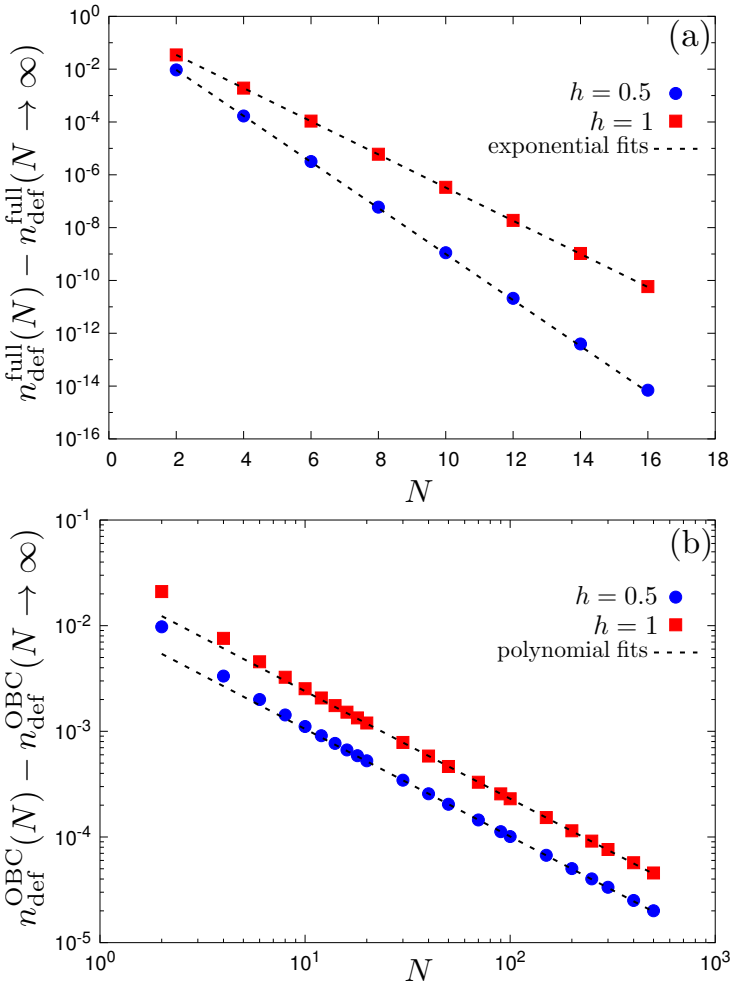

Figure C.2: Difference between density of defects for (a) PBC and (b) OBC and the expected thermal value at the thermodynamic limit, plotted versus the number of sites N, for $h = 0.5, 1$. Panel (a): the scaling is exponential in N. Panel (b): the scaling is polynomial in N; our best fit gives a convergence with $1/N$.

Appendix D

The origin of pumping quantization

In this appendix, we will review the main ingredients that lead to pumping quantization in a periodically-driven non-dissipative non-interacting model [43, 42]. Specifically, we will see that, under specific conditions, the pumped charge in the thermodynamic limit

$$Q = \lim_{L\to\infty} \frac{1}{L} \int_0^\tau \langle\psi(t)|\hat{\mathrm{J}}(t)|\psi(t)\rangle \tag{D.1}$$

is equal to a Chern number and must be therefore quantized. Here, L is the chain length, $|\psi(t)\rangle$ is the time-evolved state and $\hat{\mathrm{J}}(t)$ is the total current operator. Eq. (D.1) is precisely Eq. (5.6) for $m = 1$, computed on a state that remains pure over the whole evolution.

Consider non-interacting electrons subject to a periodic potential, as for the Rice-Mele model in Sec. 5.1. Due to the independence of the particles, we can focus on the single-particle Hamiltonian

$$\widehat{H}_{\mathrm{S}} = \hat{p}^2/2m + \hat{V}(x) \ , \tag{D.2}$$

where $\hat{V}(x)$ is the periodic potential. Its eigenstates are the famous Bloch wavefunctions $|\psi_{nk}\rangle = \mathrm{e}^{ik\hat{x}}|u_{nk}\rangle$, with $\langle x + a|u_{nk}\rangle = \langle x|u_{nk}\rangle$ and a the lattice constant, and k denotes the quasi-particle momentum while n is the band index. A convenient common choice is to work with a Hamiltonian whose eigenstates are the $|u_{nk}\rangle$ states, so that they have the same periodicity of the Hamiltonian. This is achieved by the transformation

$$\widehat{H}_{\mathrm{S}}(k) = \mathrm{e}^{-ik\hat{x}}\, \widehat{H}_{\mathrm{S}}\, \mathrm{e}^{ik\hat{x}} = \frac{(\hat{p} + \hbar k)^2}{2m} + \hat{V}(x) \ . \tag{D.3}$$

Eq. (D.3) gives us the possibility to express the current operator in a rather convenient form,

$$\hat{\mathrm{J}}(k) = \frac{\hat{p} + \hbar k}{m} = \frac{1}{\hbar}\partial_k \widehat{H}_{\mathrm{S}}(k) \ , \tag{D.4}$$

which will turn out to be very useful shortly.

Now, let us require that the ground state of our system is an *insulator* at all the times of our driving, *i.e.* there is a finite gap between the ground and first excited state during the whole dynamics. We then *start from the ground insulating state* at $t = 0$, which can be written as

$$|\Psi(0)\rangle = \prod_{n}^{\text{occ}} \prod_{k}^{\text{BZ}} |u_{nk}\rangle \ , \tag{D.5}$$

and drive the system *adiabatically*, coming back to the initial Hamiltonian after a time τ, the period of the time-evolution. According to the adiabatic theorem [28], the time evolution of the state $|\Psi(0)\rangle$, up to first order in $1/\tau$ and up to a global phase, can be written as $|\Psi(t)\rangle = \prod_n^{\text{occ}} \prod_k^{\text{BZ}} |\psi_{nk}(t)\rangle$, where

$$|\psi_{nk}(t)\rangle = |u_{nk}(t)\rangle + i\hbar \sum_{m\neq n} \frac{|u_{mk}(t)\rangle\langle u_{mk}(t)|\partial_t u_{nk}(t)\rangle}{E_m(t) - E_n(t)} \ , \tag{D.6}$$

with $E_n(t)$ being the eigenvalue of $\widehat{H}_{\text{S}}(k,t)$ corresponding to the eigenstate $|u_{nk}(t)\rangle$.

We can now compute the current corresponding to the time-evolved state $|\Psi(t)\rangle$. At fixed band n and momentum k, up to first order in $1/\tau$, we have

$$\begin{aligned}\langle\psi_{nk}(t)|\hat{\text{J}}(k)|\psi_{nk}(t)\rangle = \langle u_{nk}(t)|\hat{\text{J}}(k)|u_{nk}(t)\rangle + \\ + i\sum_{m\neq n}\left[\frac{\langle u_{nk}(t)|\hat{\text{J}}(k)|u_{mk}(t)\rangle\langle u_{mk}(t)|\partial_t u_{nk}(t)\rangle}{E_m(t) - E_n(t)} - \text{c.c.}\right].\end{aligned} \tag{D.7}$$

The first element on the r.h.s. is

$$\langle u_{nk}(t)|\frac{1}{\hbar}\partial_k \widehat{H}_{\text{S}}(k,t)|u_{nk}(t)\rangle = \frac{1}{\hbar}\partial_k E_n(k,t) \ , \tag{D.8}$$

where the equality follows from the Hellmann-Feynman theorem. Regarding the second term on the r.h.s. of Eq. (D.7), we can use the identity

$$\frac{\langle u_{nk}(t)|\partial_k \widehat{H}_{\text{S}}(k,t)|u_{mk}(t)\rangle}{E_n(k,t) - E_m(k,t)} = \langle \partial_k u_{nk}(t)|u_{mk}(t)\rangle \ , \tag{D.9}$$

together with the fact that $\langle \partial_k u_{nk}(t)|u_{nk}(t)\rangle$ is purely imaginary, to write Eq. (D.7) in a very interesting way:

$$\begin{aligned}\langle\psi_{nk}(t)|\hat{\text{J}}(k)|\psi_{nk}(t)\rangle &= \frac{1}{\hbar}\partial_k E_n(k,t) - i\Big(\langle\partial_k u_{nk}(t)|\partial_t u_{nk}(t)\rangle - \text{c.c.}\Big) = \\ &= \frac{1}{\hbar}\partial_k E_n(k,t) - \mathcal{B}_n(k,t) \ .\end{aligned} \tag{D.10}$$

The quantity $\mathcal{B}_n(k,t) = i\left(\langle\partial_k u_{nk}(t)|\partial_t u_{nk}(t)\rangle - \text{c.c.}\right)$ is the Berry curvature associated to the adiabatic evolution of the state $|u_{nk}(t)\rangle$ [41]. It inherits very intriguing topological properties: indeed, let us now compute the current by summing over all the occupied band indices and integrating over the whole first Brillouin zone. Since the ground state is always a band insulator, the k-derivative of the energies gives null contribution after integration and summation. The pumped charge can thus be expressed as

$$Q = -\sum_n^{\text{occ}} \int_{\text{BZ}} \frac{dk}{2\pi} \int_0^\tau dt \mathcal{B}_n(k,t) \ , \tag{D.11}$$

that is a double integral of a Berry curvature. This is a topological object: it is usually called *Chern number* and it must be an integer [42, 40].

All the above discussion holds under the assumption of independent electrons. However, this result can be recovered even in case of interacting electrons and disorder, provided that the system remains an insulator throughout the whole dynamics, by using the so-called *trick of twisted boundary conditions* [133, 42].

Appendix E

Spectral function parameters for the Rice-Mele model

Let us first focus on how the stationary pumped charge $\overline{Q}$ changes as the interaction α is changed over different orders of magnitude. Fig. E.1(a) shows this for the case of $\tau = 20\hbar/J_0$ and $T = J_0$: we observe that $\overline{Q}$ converges to a finite value for $\alpha \to 0$ and that it remains almost constant for weak enough couplings. Since we want to reproduce the perturbative regimes, for which our approach is valid, we select $\alpha = 0.001$, indicated by the arrow in the plot. One might also choose weaker couplings, but then the number of periods needed to reach stationarity would increase considerably, requiring much longer simulation times.

We turn now to the issue of choosing the cutoff ω_c in the bath spectral function. Generally ω_c is taken to be the largest energy scale of the system, so that the dynamics becomes insensitive to the detail of this parameter. In the present case, since the system energy gap is always of the order of J_0 and we consider temperatures $T \leq J_0$, we require $\hbar\omega_c \gg J_0$. The behavior of $\overline{Q}$ vs the cutoff ω_c, see Fig. E.1(b), shows the range of cutoff frequencies for which we observe a convergence of $\overline{Q}$. We therefore selected $\hbar\omega_c = 1000J_0$. Fig. E.1(b) is also useful to illustrate the effect of some basic dissipation mechanisms. If ω_c is much smaller than the minimum system energy gap, the probability of having jumps between energy levels is negligible and the result tends to become again insensitive to the cutoff value. Then, the only relevant dissipation mechanism comes from pure dephasing, given by γ_φ in Eq. (B.13). Notice however that $\gamma_\varphi \sim T$ and hence it vanishes at $T = 0$. This is consistent with what we observe in Fig. E.1(b) for $\hbar\omega_c \ll J_0$, $\overline{Q}$ is insensitive to the cutoff; moreover, for $T = 0$, we recover precisely the coherent result, pinpointed by the horizontal dashed line.

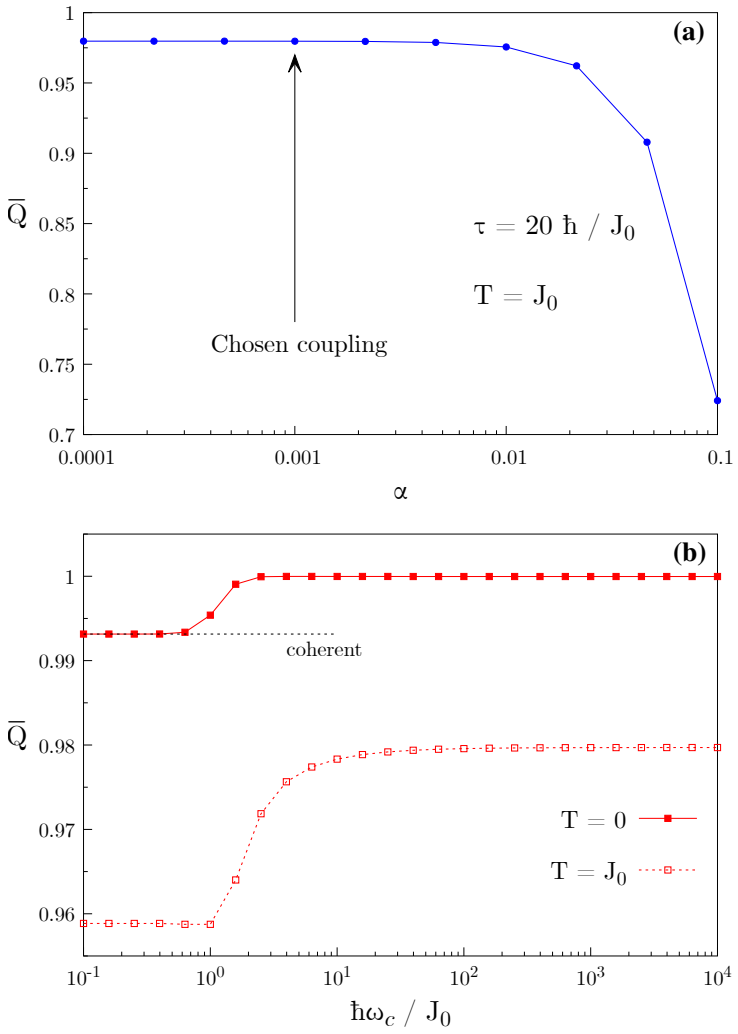

Figure E.1: Scaling of the steady pumped charge $\overline{Q}$ as a function of (a) coupling strenght α and (b) cutoff frequency ω_c, both for fixed $\tau = 20\hbar/J_0$. **Panel (a):** The bath temperature is $T = J_0$. We observe convergence for small enough α, and the arrow points to the value $\alpha = 0.001$, employed for all the results presented in the main text. **Panel (b):** We consider bath temperatures $T = 0, J_0$. The horizontal dashed line indicates the value of $Q_{\rm d}^{\rm coh}$, the pumped charge at stationarity for the corresponding coherent dynamics.

Acknowledgements

I first would like to thank my supervisor Prof. Giuseppe Santoro for guiding me through the intricate world of physics research: I learnt a lot working with him in these years of collaboration.

I want to thank Mary and my parents for their continuous support and for being pillars in my life, on which I can count in every difficult moment.

Then, a special thank goes to the fellows of the office "310": Francesco, Juraj and Jacopo, plus the "CM adopted" Milo. We had a great time together and I would really love this to never end. Many thanks also to my friends of the SISSA volleyball team, both past and present, with whom I enjoyed a lot of moments here. Even when we were losing all the matches, it was a great fun to be all together. There are so many people that I met in these years and that I would like to thank, but it is hard to mention them all... Thanks to all of you, the time spent here in SISSA was fantastic!

Bibliography

[1] D. J. P. MacFarlane A. G. J. and M. G. J., "Quantum technology: the second quantum revolution," *Philosophical Transactions of the Royal Society of London. Series A: Mathematical, Physical and Engineering Sciences*, vol. 361, 2003.

[2] A. Acín, I. Bloch, H. Buhrman, T. Calarco, C. Eichler, J. Eisert, D. Esteve, N. Gisin, S. J. Glaser, F. Jelezko, S. Kuhr, M. Lewenstein, M. F. Riedel, P. O. Schmidt, R. Thew, A. Wallraff, I. Walmsley, and F. K. Wilhelm, "The quantum technologies roadmap: a european community view," *New Journal of Physics*, vol. 20, p. 080201, aug 2018.

[3] "The quantum flagship," *https://qt.eu/*.

[4] I. Buluta and F. Nori, "Quantum simulators," *Science*, vol. 326, p. 108, 2009.

[5] R. P. Feynman, "Simulating physics with computers," *International Journal of Theoretical Physics*, vol. 21, pp. 467–488, Jun 1982.

[6] I. Bloch, "Ultracold quantum gases in optical lattices," *Nature Physics*, vol. 1, no. 1, pp. 23–30, 2005.

[7] R. Blatt and C. F. Roos, "Quantum simulations with trapped ions," *Nature Physics*, vol. 8, pp. 277 EP –, Apr 2012. Review Article.

[8] M. J. Hartmann, F. G. S. L. Brandão, and M. B. Plenio, "Strongly interacting polaritons in coupled arrays of cavities," *Nature Physics*, vol. 2, no. 12, pp. 849–855, 2006.

[9] J. Eisert, M. Friesdorf, and C. Gogolin, "Quantum many-body systems out of equilibrium," *Nature Physics*, vol. 11, pp. 124 EP –, Feb 2015. Review Article.

[10] A. J. Leggett, S. Chakravarty, A. T. Dorsey, M. P. A. Fisher, A. Garg, and W. Zwerger, "Dynamics of the dissipative two-state system," *Rev. Mod. Phys.*, vol. 59, pp. 1–85, Jan 1987.

[11] E. M. Kessler, G. Giedke, A. Imamoglu, S. F. Yelin, M. D. Lukin, and J. I. Cirac, "Dissipative phase transition in a central spin system," *Phys. Rev. A*, vol. 86, p. 012116, Jul 2012.

[12] H. J. Carmichael, "Breakdown of photon blockade: A dissipative quantum phase transition in zero dimensions," *Phys. Rev. X*, vol. 5, p. 031028, Sep 2015.

[13] F. Minganti, A. Biella, N. Bartolo, and C. Ciuti, "Spectral theory of liouvillians for dissipative phase transitions," *Phys. Rev. A*, vol. 98, p. 042118, Oct 2018.

[14] J. F. Poyatos, J. I. Cirac, and P. Zoller, "Quantum reservoir engineering with laser cooled trapped ions," *Phys. Rev. Lett.*, vol. 77, pp. 4728–4731, Dec 1996.

[15] M. Mller, S. Diehl, G. Pupillo, and P. Zoller, "Engineered open systems and quantum simulations with atoms and ions," in *Advances in Atomic, Molecular, and Optical Physics* (P. Berman, E. Arimondo, and C. Lin, eds.), vol. 61 of *Advances In Atomic, Molecular, and Optical Physics*, pp. 1 – 80, Academic Press, 2012.

[16] D. Kienzler, H.-Y. Lo, B. Keitch, L. de Clercq, F. Leupold, F. Lindenfelser, M. Marinelli, V. Negnevitsky, and J. P. Home, "Quantum harmonic oscillator state synthesis by reservoir engineering," *Science*, vol. 347, no. 6217, pp. 53–56, 2015.

[17] F. Verstraete, M. M. Wolf, and J. Ignacio Cirac, "Quantum computation and quantum-state engineering driven by dissipation," *Nature Physics*, vol. 5, pp. 633 EP –, Jul 2009.

[18] S. Diehl, A. Tomadin, A. Micheli, R. Fazio, and P. Zoller, "Dynamical phase transitions and instabilities in open atomic many-body systems," *Phys. Rev. Lett.*, vol. 105, p. 015702, Jul 2010.

[19] C.-E. Bardyn, M. A. Baranov, C. V. Kraus, E. Rico, A. İmamoğlu, P. Zoller, and S. Diehl, "Topology by dissipation," *New Journal of Physics*, vol. 15, p. 085001, aug 2013.

[20] J. C. Budich, P. Zoller, and S. Diehl, "Dissipative preparation of chern insulators," *Phys. Rev. A*, vol. 91, p. 042117, Apr 2015.

[21] H. Weimer, A. Kshetrimayum, and R. Orus, "Simulation methods for open quantum many-body systems," arXiv:1907.07079 (2019).

[22] J. Preskill, "Quantum Computing in the NISQ era and beyond," *Quantum*, vol. 2, p. 79, Aug. 2018.

[23] A. B. Finnila, M. A. Gomez, C. Sebenik, C. Stenson, and J. D. Doll, "Quantum annealing: A new method for minimizing multidimensional functions," *Chem. Phys. Lett.*, vol. 219, p. 343, 1994.

[24] T. Kadowaki and H. Nishimori, "Quantum annealing in the transverse Ising model," *Phys. Rev. E*, vol. 58, p. 5355, 1998.

[25] J. Brooke, D. Bitko, T. F. Rosenbaum, and G. Aeppli, "Quantum annealing of a disordered magnet," *Science*, vol. 284, p. 779, 1999.

[26] G. E. Santoro, R. Martoňák, E. Tosatti, and R. Car, "Theory of quantum annealing of an Ising spin glass," *Science*, vol. 295, p. 2427, 2002.

[27] T. Albash and D. A. Lidar, "Adiabatic quantum computation," *Rev. Mod. Phys.*, vol. 90, p. 015002, 2018.

[28] A. Messiah, *Quantum mechanics*, vol. 2. Amsterdam: North-Holland, 1962.

[29] R. Harris, M. W. Johnson, S. Han, A. J. Berkley, J. Johansson, P. Bunyk, E. Ladizinsky, S. Govorkov, M. C. Thom, S. Uchaikin, B. Bumble, A. Fung, A. Kaul, A. Kleinsasser, M. H. S. Amin, and D. V. Averin, "Probing noise in flux qubits via macroscopic resonant tunneling," *Phys. Rev. Lett.*, vol. 101, p. 117003, Sep 2008.

[30] J. Johansson, M. H. S. Amin, A. J. Berkley, P. Bunyk, V. Choi, R. Harris, M. W. Johnson, T. M. Lanting, S. Lloyd, and G. Rose, "Landau-zener transitions in a superconducting flux qubit," *Phys. Rev. B*, vol. 80, p. 012507, Jul 2009.

[31] L. Arceci, S. Barbarino, R. Fazio, and G. E. Santoro, "Dissipative landau-zener problem and thermally assisted quantum annealing," *Phys. Rev. B*, vol. 96, p. 054301, Aug 2017.

[32] L. Arceci, S. Barbarino, D. Rossini, and G. E. Santoro, "Optimal working point in dissipative quantum annealing," *Phys. Rev. B*, vol. 98, p. 064307, Aug 2018.

[33] M. H. S. Amin, P. J. Love, and C. J. S. Truncik, "Thermally assisted adiabatic quantum computation," *Phys. Rev. Lett.*, vol. 100, p. 060503, Feb 2008.

[34] N. G. Dickson, M. W. Johnson, M. H. Amin, R. Harris, F. Altomare, A. J. Berkley, P. Bunyk, J. Cai, E. M. Chapple, P. Chavez, F. Cioata, T. Cirip, P. deBuen, M. Drew-Brook, C. Enderud, S. Gildert, F. Hamze, J. P. Hilton, E. Hoskinson, K. Karimi, E. Ladizinsky, N. Ladizinsky, T. Lanting, T. Mahon, R. Neufeld, T. Oh, I. Perminov, C. Petroff, A. Przybysz, C. Rich, P. Spear, A. Tcaciuc, M. C. Thom, E. Tolkacheva, S. Uchaikin, J. Wang, A. B. Wilson,

Z. Merali, and G. Rose, "Thermally assisted quantum annealing of a 16-qubit problem," *Nature Communications*, vol. 4, pp. 1903 EP –, 05 2013.

[35] G. E. Santoro and E. Tosatti, "Optimization using quantum mechanics: Quantum annealing through adiabatic evolution," *J. Phys. A: Math. Gen.*, vol. 39, pp. R393–R431, 2006.

[36] V. Bapst, L. Foini, F. Krzakala, G. Semerjian, and Z. F., "The quantum adiabatic algorithm applied to random optimization problems: The quantum spin glass perspective," *Physics Reports*, vol. 523, pp. 127–206, 2013.

[37] M. M. Wauters, R. Fazio, H. Nishimori, and G. E. Santoro, "Direct comparison of quantum and simulated annealing on a fully connected ising ferromagnet," *Phys. Rev. A*, vol. 96, p. 022326, Aug 2017.

[38] A. Fubini, G. Falci, and A. Osterloh, "Robustness of adiabatic passage through a quantum phase transition," *New J. Phys.*, vol. 9, no. 5, p. 134, 2007.

[39] D. J. Thouless, M. Kohmoto, M. P. Nightingale, and M. den Nijs, "Quantized hall conductance in a two-dimensional periodic potential," *Phys. Rev. Lett.*, vol. 49, pp. 405–408, Aug 1982.

[40] M. Z. Hasan and C. L. Kane, "Colloquium: Topological insulators," *Rev. Mod. Phys.*, vol. 82, pp. 3045–3067, Nov 2010.

[41] M. V. Berry, "Quantal phase factors accompanying adiabatic changes," *Proc. R. Soc. Lond. A*, vol. 392, 1984.

[42] D. Xiao, M.-C. Chang, and Q. Niu, "Berry phase effects on electronic properties," *Rev. Mod. Phys.*, vol. 82, pp. 1959–2007, Jul 2010.

[43] D. J. Thouless, "Quantization of particle transport," *Phys. Rev. B*, vol. 27, pp. 6083–6087, May 1983.

[44] M. Lohse, C. Schweizer, O. Zilberberg, M. Aidelsburger, and I. Bloch, "A thouless quantum pump with ultracold bosonic atoms in an optical superlattice," *Nat Phys*, vol. 12, pp. 350–354, 04 2016.

[45] S. Nakajima, T. Tomita, S. Taie, T. Ichinose, H. Ozawa, L. Wang, M. Troyer, and Y. Takahashi, "Topological thouless pumping of ultracold fermions," *Nat Phys*, vol. 12, pp. 296–300, 04 2016.

[46] M. J. Rice and E. J. Mele, "Elementary excitations of a linearly conjugated diatomic polymer," *Phys. Rev. Lett.*, vol. 49, pp. 1455–1459, Nov 1982.

[47] L. Arceci, A. Russomanno, and G. Santoro, "Thermally assisted thouless pumping in the rice-mele model," *arXiv:1905.08808*, 2019.

[48] L. Privitera, A. Russomanno, R. Citro, and G. E. Santoro, "Nonadiabatic breaking of topological pumping," *Phys. Rev. Lett.*, vol. 120, p. 106601, Mar 2018.

[49] G. Lindblad, "On the generators of quantum dynamical semigroups," *Commun. Math. Phys.*, vol. 48, p. 119, 1976.

[50] A. Kossakowski, "On quantum statistical mechanics of non-hamiltonian systems," *Rep. Math. Phys.*, vol. 3, p. 247, 1972.

[51] V. Gorini, A. Kossakowski, and E. C. G. Sudarshan, "Completely positive dynamical semigroups of nlevel systems," *Journal of Mathematical Physics*, vol. 17, no. 5, pp. 821–825, 1976.

[52] G. Schaller, *Open Quantum Systems Far from Equilibrium*, vol. 881. 11 2013.

[53] H.-P. Breuer, E.-M. Laine, J. Piilo, and B. Vacchini, "Colloquium: Non-markovian dynamics in open quantum systems," *Rev. Mod. Phys.*, vol. 88, p. 021002, Apr 2016.

[54] M. Keck, S. Montangero, G. E. Santoro, R. Fazio, and D. Rossini, "Dissipation in adiabatic quantum computers: lessons from an exactly solvable model," *New Journal of Physics*, vol. 19, p. 113029, nov 2017.

[55] A. Nava and M. Fabrizio *arXiv:1905.12029*, 2019.

[56] A. Caldeira and A. Leggett, "Path integral approach to quantum brownian motion," *Physica A: Statistical Mechanics and its Applications*, vol. 121, no. 3, pp. 587 – 616, 1983.

[57] A. Caldeira and A. Leggett, "Quantum tunnelling in a dissipative system," *Annals of Physics*, vol. 149, no. 2, pp. 374 – 456, 1983.

[58] N. Makri, "Numerical path integral techniques for long time dynamics of quantum dissipative systems," *J. Math. Phys.*, vol. 36, no. 5, pp. 2430–2457, 1995.

[59] N. Makri and D. E. Makarov, "Tensor propagator for iterative quantum time evolution of reduced density matrices. i. theory," *J. Chem. Phys.*, vol. 102, no. 11, pp. 4600–4610, 1995.

[60] N. Makri and D. E. Makarov, "Tensor propagator for iterative quantum time evolution of reduced density matrices. ii. numerical methodology," *J. Chem. Phys.*, vol. 102, no. 11, pp. 4611–4618, 1995.

[61] A. W. Chin, A. Rivas, S. F. Huelga, and M. B. Plenio, "Exact mapping between system-reservoir quantum models and semi-infinite discrete chains using orthogonal polynomials," *Journal of Mathematical Physics*, vol. 51, no. 9, p. 092109, 2010.

[62] F. A. Y. N. Schröder and A. W. Chin, "Simulating open quantum dynamics with time-dependent variational matrix product states: Towards microscopic correlation of environment dynamics and reduced system evolution," *Phys. Rev. B*, vol. 93, p. 075105, Feb 2016.

[63] Y. Tanimura and R. Kubo, "Time evolution of a quantum system in contact with a nearly gaussian-markoffian noise bath," *Journal of the Physical Society of Japan*, vol. 58, no. 1, pp. 101–114, 1989.

[64] Y. Tanimura, "Stochastic liouville, langevin, fokkerplanck, and master equation approaches to quantum dissipative systems," *Journal of the Physical Society of Japan*, vol. 75, no. 8, p. 082001, 2006.

[65] A. Redfield, "The theory of relaxation processes," in *Advances in Magnetic Resonance* (J. S. Waugh, ed.), vol. 1 of *Advances in Magnetic and Optical Resonance*, pp. 1 – 32, Academic Press, 1965.

[66] H.-P. Breuer and F. Petruccione, *The Theory of Open Quantum Systems*. Oxford University Press, 2002.

[67] C. Cohen-Tannoudji, J. Dupont-Roc, and G. Grynberg, *Atom-Photon Interactions: Basic Processes and Applications*. John Wiley & Sons, 1992.

[68] D. Jaschke, S. Montangero, and L. D. Carr, "One-dimensional many-body entangled open quantum systems with tensor network methods," *Quantum Science and Technology*, vol. 4, p. 013001, nov 2018.

[69] F. Verstraete, J. J. García-Ripoll, and J. I. Cirac, "Matrix product density operators: Simulation of finite-temperature and dissipative systems," *Phys. Rev. Lett.*, vol. 93, p. 207204, Nov 2004.

[70] M.-D. Choi, "Completely positive linear maps on complex matrices," *Linear Algebra and its Applications*, vol. 10, no. 3, pp. 285 – 290, 1975.

[71] A. Jamiokowski, "Linear transformations which preserve trace and positive semidefiniteness of operators," *Reports on Mathematical Physics*, vol. 3, no. 4, pp. 275 – 278, 1972.

[72] A. H. Werner, D. Jaschke, P. Silvi, M. Kliesch, T. Calarco, J. Eisert, and S. Montangero, "Positive tensor network approach for simulating open quantum many-body systems," *Phys. Rev. Lett.*, vol. 116, p. 237201, Jun 2016.

[73] J. Dalibard, Y. Castin, and K. Mølmer, "Wave-function approach to dissipative processes in quantum optics," *Phys. Rev. Lett.*, vol. 68, pp. 580–583, Feb 1992.

[74] R. Dum, P. Zoller, and H. Ritsch, "Monte carlo simulation of the atomic master equation for spontaneous emission," *Phys. Rev. A*, vol. 45, pp. 4879–4887, Apr 1992.

[75] M. B. Plenio and P. L. Knight, "The quantum-jump approach to dissipative dynamics in quantum optics," *Rev. Mod. Phys.*, vol. 70, pp. 101–144, Jan 1998.

[76] A. J. Daley, "Quantum trajectories and open many-body quantum systems," *Adv. Phys.*, vol. 63, p. 77, 2014.

[77] T. Albash, S. Boixo, D. A. Lidar, and P. Zanardi, "Quantum adiabatic Markovian master equations," *New J. Phys.*, vol. 14, p. 123016, 2012.

[78] M. Grifoni and P. Hänggi, "Driven quantum tunneling," *Physics Reports*, vol. 304, pp. 229–354, 1998.

[79] A. Russomanno, S. Pugnetti, V. Brosco, and R. Fazio, "Floquet theory of cooper pair pumping," *Phys. Rev. B*, vol. 83, p. 214508, 2011.

[80] G. Floquet, "Sur les équations différentielles linéaires à coefficients périodiques," *Annales scientifiques de l'École Normale Supérieure*, vol. 2e série, 12, pp. 47–88, 1883.

[81] J. H. Shirley, "Solution of the schrödinger equation with a hamiltonian periodic in time," *Phys. Rev.*, vol. 138, pp. B979–B987, May 1965.

[82] G. Casati and L. Molinari, ""Quantum Chaos" with Time-Periodic Hamiltonians," *Prog. Theor. Phys. Suppl.*, vol. 98, p. 287, 1989.

[83] S. Kohler, *The interplay of chaos and dissipation in driven quantum systems.* doctoralthesis, Universität Augsburg, 2006.

[84] U. Weiss, *Quantum dissipative systems.* World Scientific, second ed., 1999.

[85] A. Shnirman, Y. Makhlin, and G. Schön, "Noise and decoherence in quantum two-level systems," *Physica Scripta*, vol. T102, pp. 147–154, 2002.

[86] J. Johansson, P. Nation, and F. Nori, "QuTiP: An open-source python framework for the dynamics of open quantum systems," *Computer Physics Communications*, vol. 183, pp. 1760–1772, aug 2012.

[87] J. Johansson, P. Nation, and F. Nori, "QuTiP 2: A python framework for the dynamics of open quantum systems," *Computer Physics Communications*, vol. 184, pp. 1234–1240, apr 2013.

[88] Y. Kayanuma and H. Nakayama, "Nonadiabatic transition at a level crossing with dissipation," *Phys. Rev. B*, vol. 57, pp. 13099–13112, May 1998.

[89] P. Ao and J. Rammer, "Quantum dynamics of a two-state system in a dissipative environment," *Phys. Rev. B*, vol. 43, pp. 5397–5418, Mar 1991.

[90] M. Wubs, K. Saito, S. Kohler, P. Hänggi, and Y. Kayanuma, "Gauging a quantum heat bath with dissipative landau-zener transitions," *Phys. Rev. Lett.*, vol. 97, p. 200404, Nov 2006.

[91] K. Saito, M. Wubs, S. Kohler, Y. Kayanuma, and P. Hänggi, "Dissipative landau-zener transitions of a qubit: Bath-specific and universal behavior," *Phys. Rev. B*, vol. 75, p. 214308, Jun 2007.

[92] D. Zueco, P. Hnggi, and S. Kohler, "Landau–zener tunnelling in dissipative circuit QED," *New Journal of Physics*, vol. 10, p. 115012, nov 2008.

[93] P. Nalbach and M. Thorwart, "Landau-zener transitions in a dissipative environment: Numerically exact results," *Phys. Rev. Lett.*, vol. 103, p. 220401, Nov 2009.

[94] "Competition between relaxation and external driving in the dissipative landauzener problem," *Chemical Physics*, vol. 375, no. 2, pp. 234 – 242, 2010. Stochastic processes in Physics and Chemistry (in honor of Peter Hnggi).

[95] S. Javanbakht, P. Nalbach, and M. Thorwart, "Dissipative landau-zener quantum dynamics with transversal and longitudinal noise," *Phys. Rev. A*, vol. 91, p. 052103, May 2015.

[96] L. D. Landau, "A theory of energy transfer II," *Phys. Z. Sowjetunion*, vol. 2, p. 46, 1932.

[97] C. Zener, "Non-adiabatic crossing of energy levels," *Proc. Royal Soc. A*, vol. 137, p. 696, 1932.

[98] E. C. G. Stueckelberg, "Theorie der unelastischen stsse zwischen atomen," *Helvetica Physica Acta*, vol. 5, no. 369, 1932.

[99] E. Majorana, "Atomi orientati in campo magnetico variabile," *Il Nuovo Cimento (1924-1942)*, vol. 9, pp. 43–50, Feb 1932.

[100] Y. Gefen, E. Ben-Jacob, and A. O. Caldeira, "Zener transitions in dissipative driven systems," *Phys. Rev. B*, vol. 36, pp. 2770–2782, Aug 1987.

[101] P. Nalbach, "Adiabatic-markovian bath dynamics at avoided crossings," *Phys. Rev. A*, vol. 90, p. 042112, Oct 2014.

[102] M. H. S. Amin and D. V. Averin, "Macroscopic resonant tunneling in the presence of low frequency noise," *Phys. Rev. Lett.*, vol. 100, p. 197001, May 2008.

[103] S. Ashhab, "Landau-zener transitions in a two-level system coupled to a finite-temperature harmonic oscillator," *Phys. Rev. A*, vol. 90, p. 062120, Dec 2014.

[104] A. Y. Smirnov and M. H. Amin, "Theory of open quantum dynamics with hybrid noise," *New Journal of Physics*, vol. 20, p. 103037, oct 2018.

[105] M. Demirplak and S. A. Rice, "Adiabatic population transfer with control fields," *The Journal of Physical Chemistry A*, vol. 107, no. 46, pp. 9937–9945, 2003.

[106] M. V. Berry, "Transitionless quantum driving," *Journal of Physics A: Mathematical and Theoretical*, vol. 42, no. 36, p. 365303, 2009.

[107] A. del Campo, M. M. Rams, and W. H. Zurek, "Assisted finite-rate adiabatic passage across a quantum critical point: Exact solution for the quantum ising model," *Phys. Rev. Lett.*, vol. 109, p. 115703, Sep 2012.

[108] S. Suzuki, J.-i. Inoue, and B. Chakrabarti, *Quantum Ising Phases and Transitions in Transverse Ising Models*, vol. 862. 01 2013.

[109] J. Dziarmaga, "Dynamics of a quantum phase transition: Exact solution of the quantum ising model," *Phys. Rev. Lett.*, vol. 95, p. 245701, Dec 2005.

[110] A. Dutta, A. Rahmani, and A. del Campo, "Anti-kibble-zurek behavior in crossing the quantum critical point of a thermally isolated system driven by a noisy control field," *Phys. Rev. Lett.*, vol. 117, p. 080402, Aug 2016.

[111] Z.-P. Gao, D.-W. Zhang, Y. Yu, and S.-L. Zhu, "Anti-kibble-zurek behavior of a noisy transverse-field XY chain and its quantum simulation with two-level systems," *Phys. Rev. B*, vol. 95, p. 224303, Jun 2017.

[112] M. Gong, X. Wen, G. Sun, D.-W. Zhang, D. Lan, Y. Zhou, Y. Fan, Y. Liu, X. Tan, H. Yu, Y. Yu, S.-L. Zhu, S. Han, and P. Wu, "Simulating the kibble-zurek mechanism of the ising model with a superconducting qubit system," *Sci. Rep.*, vol. 6, p. 22667, feb 2016.

[113] D. Patanè, A. Silva, L. Amico, R. Fazio, and G. E. Santoro, "Adiabatic dynamics in open quantum critical many-body systems," *Physical Review Letters*, vol. 101, p. 175701, 2008.

[114] D. Patanè, A. Silva, L. Amico, R. Fazio, and G. E. Santoro, "Adiabatic dynamics of a quantum critical system coupled to an environment: Scaling and kinetic equation approaches," *Physical Review B*, vol. 80, p. 2009, 2009.

[115] P. Nalbach, S. Vishveshwara, and A. A. Clerk, "Quantum kibble-zurek physics in the presence of spatially correlated dissipation," *Phys. Rev. B*, vol. 92, p. 014306, Jul 2015.

[116] V. N. Smelyanskiy, D. Venturelli, A. Perdomo-Ortiz, S. Knysh, and M. I. Dykman, "Quantum annealing via environment-mediated quantum diffusion," *Phys. Rev. Lett.*, vol. 118, p. 066802, Feb 2017.

[117] S. M. Griffin, M. Lilienblum, K. T. Delaney, Y. Kumagai, M. Fiebig, and N. A. Spaldin, "Scaling behavior and beyond equilibrium in the hexagonal manganites," *Phys. Rev. X*, vol. 2, p. 041022, Dec 2012.

[118] S. Sachdev, *Quantum Phase Transitions (Second Edition)*. Cambridge University Press, 2011.

[119] E. Lieb, T. Schultz, and D. Mattis, "Two soluble models of an antiferromagnetic chain," *Annals of Physics*, vol. 16, pp. 407–466, 1961.

[120] P. Pfeuty, "The one-dimensional ising model with a transverse field," *Ann. Phys.*, vol. 57, no. 1, p. 79, 1970.

[121] T. Caneva, R. Fazio, and G. E. Santoro, "Adiabatic quantum dynamics of a random Ising chain across its quantum critical point," *Phys. Rev. B*, vol. 76, p. 144427, 2007.

[122] R. Harris, M. W. Johnson, T. Lanting, A. J. Berkley, J. Johansson, P. Bunyk, E. Tolkacheva, E. Ladizinsky, N. Ladizinsky, T. Oh, F. Cioata, I. Perminov, P. Spear, C. Enderud, C. Rich, S. Uchaikin, M. C. Thom, E. M. Chapple, J. Wang, B. Wilson, M. H. S. Amin, N. Dickson, K. Karimi, B. Macready, C. J. S. Truncik, and G. Rose, "Experimental investigation of an eight qubit unit cell in a superconducting optimization processor," *Phys. Rev. B*, vol. 82, p. 024511, 2010.

[123] M. W. Johnson, M. H. S. Amin, S. Gildert, T. Lanting, F. Hamze, N. Dickson, R. Harris, A. J. Berkley, J. Johansson, P. Bunyk, E. M. Chapple, C. Enderud, J. P. Hilton, K. Karimi, E. Ladizinsky, N. Ladizinsky, T. Oh, I. Perminov, C. Rich, M. C. Thom, E. Tolkacheva, C. J. S. Truncik, S. Uchaikin, J. Wang, B. Wilson, and G. Rose, "Quantum annealing with manufactured spins," *Nature*, vol. 473, pp. 194–198, 2011.

[124] P. Nalbach and M. Thorwart, "Landau-zener transitions in a dissipative environment: Numerically exact results," *Phys. Rev. Lett.*, vol. 103, p. 220401, Nov 2009.

[125] A. Polkovnikov, K. Sengupta, A. Silva, and M. Vengalattore, "Nonequilibrium dynamics of closed interacting quantum systems," *Rev. Mod. Phys.*, vol. 83, p. 863, 2011.

[126] S. Boixo, V. N. Smelyanskiy, A. Shabani, S. V. Isaksov, M. Dykman, V. S. Denchev, M. H. Amin, A. Y. Smirnov, M. Mohseni, and H. Neven, "Computational multiqubit tunnelling in programmable quantum annealers," *Nat. Commun.*, vol. 7, p. 10327, 2016.

[127] J. Dziarmaga, "Dynamics of a quantum phase transition in the random ising model: Logarithmic dependence of the defect density on the transition rate," *Phys. Rev. B*, vol. 74, p. 064416, 2006.

[128] F. Verstraete, J. J. García-Ripoll, and J. I. Cirac, "Matrix Product Density Operators: Simulation of Finite-Temperature and Dissipative Systems," *Phys. Rev. Lett.*, vol. 93, p. 207204, 2004.

[129] M. Zwolak and G. Vidal, "Mixed-State Dynamics in One-Dimensional Quantum Lattice Systems: A Time-Dependent Superoperator Renormalization Algorithm," *Phys. Rev. Lett.*, vol. 93, p. 207205, 2004.

[130] L. Wang, M. Troyer, and X. Dai, "Topological charge pumping in a one-dimensional optical lattice," *Phys. Rev. Lett.*, vol. 111, p. 026802, Jul 2013.

[131] L. Zhou, D. Y. Tan, and J. Gong, "Effects of dephasing on quantum adiabatic pumping with nonequilibrium initial states," *Phys. Rev. B*, vol. 92, p. 245409, Dec 2015.

[132] J. Asbth, L. Oroszlny, and A. Plyi, "A short course on topological insulators: Band-structure topology and edge states in one and two dimensions," *Lecture Notes in Physics*, vol. 919, 2016.

[133] Q. Niu and D. J. Thouless, "Quantised adiabatic charge transport in the presence of substrate disorder and many-body interaction," *Journal of Physics A: Mathematical and General*, vol. 17, pp. 2453–2462, aug 1984.

[134] C.-E. Bardyn, L. Wawer, A. Altland, M. Fleischhauer, and S. Diehl, "Probing the topology of density matrices," *Phys. Rev. X*, vol. 8, p. 011035, Feb 2018.

[135] A. Russomanno, A. Silva, and G. E. Santoro, "Periodic steady regime and interference in a periodically driven quantum system," *Phys. Rev. Lett.*, vol. 109, p. 257201, 2012.

[136] J. H. Shirley, "Solution of schrodinger equation with a hamiltonian periodic in time," *Phys. Rev.*, vol. 138, p. B979, 1965.

[137] J. Hausinger and M. Grifoni, "Dissipative two-level system under strong ac driving: A combination of floquet and van vleck perturbation theory," *Phys. Rev. A*, vol. 81, p. 022117, 2010.

[138] A. Russomanno and G. E. Santoro, "Floquet resonances close to the adiabatic limit and the effect of dissipation," *Journal of Statistical Mechanics: Theory and Experiment*, vol. 2017, p. 103104, oct 2017.

[139] W.-K. Shih and Q. Niu, "Nonadiabatic particle transport in a one-dimensional electron system," *Phys. Rev. B*, vol. 50, no. 16, p. 11902, 1994.

[140] A. Russomanno, A. Silva, and G. E. Santoro, "Linear response as a singular limit for a periodically driven closed quantum system," *Journal of Statistical Mechanics: Theory and Experiment*, vol. 2013, p. P09012, sep 2013.

[141] D. Jaschke, S. Montangero, and L. D. Carr, "One-dimensional many-body entangled open quantum systems with tensor network methods," *Quantum Science and Technology*, vol. 4, p. 013001, nov 2018.

[142] O. Viyuela, A. Rivas, and M. A. Martin-Delgado, "Uhlmann phase as a topological measure for one-dimensional fermion systems," *Phys. Rev. Lett.*, vol. 112, p. 130401, Apr 2014.

[143] D. Suess, A. Eisfeld, and W. T. Strunz, "Hierarchy of stochastic pure states for open quantum system dynamics," *Phys. Rev. Lett.*, vol. 113, p. 150403, Oct 2014.

[144] M. Campostrini, A. Pelissetto, and E. Vicari, "Quantum ising chains with boundary fields," *J. Stat. Mech.*, vol. 2015, no. 11, p. P11015, 2015.